5-13-2016

# Smad4 and Transforming Growth Factor β Regulate the CD8 T Cell Response to Influenza Virus Infection

Yinghong Hu
yinhu@uchc.edu

**Smad4 and Transforming Growth Factor β Regulate the CD8 T Cell Response to Influenza Virus Infection**

Yinghong Hu

University of Connecticut, 2016

Transforming growth factor β (TGFβ) is an immunosuppressive cytokine with multiple functions in the immune system, including regulation of cytotoxic T lymphocytes. This thesis will examine how TGFβ, and the downstream signaling molecule Smad4, alter the CD8 T cell response to infection with different strains of influenza A virus (IAV). Chapter III shows how TGFβ and Smad4 regulate the phenotype, localization and function of antigen-specific CD8 T cells in the lungs. Our data reveal a previously unappreciated role of Smad4 in regulating effector and memory CD8 T cell differentiation independently of TGFβRII. Specifically we find that Smad4 promotes terminal differentiation of KLRG1+ T effector ($T_{EFF}$) cells, a subset that is inhibited by TGFβ. Smad4 and TGFβ also play reciprocal roles in regulation of CD103+ tissue resident memory T ($T_{RM}$) cells and CD62L+ central memory T ($T_{CM}$) cells. Altered expression of multiple homing receptors changes the distribution of antigen-specific CD8 T cells *in vivo*, and therefore impacts viral clearance during primary viral infection and heterosubtypic immunity. Chapter IV explores the mechanism by which Smad4 regulates the CD8 T cell response, by examining the global transcription profile, cellular metabolism and signaling pathways of mutant and wild type CTLs. Our data suggests that Smad4 is activated by a novel pathway to promote terminal differentiation of effector T cells possibly through enhancing IL-12 signaling and T-bet expression, and inhibiting OXPHOS activity. Also, by enhancing T-bet and Eomesodermin, Smad4 may act as a suppressor of CD103 and later promotes re-expression of CD62L. This novel pathway of Smad4 ligand is counter-regulated by TGFβ, possibly by competing for Smad4 with phosphorylated Smad2/3. Our study sheds new light on the signals that regulate the

differentiation and distribution of virus-specific CD8 T cells during IAV infection, which can be utilized to optimize cell-mediated immunity during the design of IAV vaccine.

# Smad4 and Transforming Growth Factor β Regulate the CD8 T Cell Response to Influenza Virus Infection

Yinghong Hu

B.S., China Agricultural University, China, 2008

M.S., Fudan University, China, 2011

A Dissertation

Submitted in Partial Fulfillment of the

Requirements for the Degree of

Doctor of Philosophy

at the

University of Connecticut

2016

APPROVAL PAGE

Doctor of Philosophy Dissertation

Smad4 and Transforming Growth Factor β Regulate the CD8 T Cell Response to Influenza Virus Infection

Presented by

Yinghong Hu, B.S., M.S.

Major Advisor _____
Linda S. Cauley, Ph.D.

Associate Advisor _____
Stefan Brocke, M.D., Ph.D.

Associate Advisor _____
Anthony Vella, Ph.D.

University of Connecticut
2016

**ACKNOWLEDGEMENTS**

Foremost, I would like to express my deepest gratitude to my advisor, Dr. Linda Cauley, for all her effort and support throughout my Ph.D. study. With her patient guidance I were able to not only learn a broad spectrum of scientific knowledge and skills, but also acquire a better understanding on how to design and conduct research independently. This dissertation would not have been possible without her helpful instructions.

I would also like to thank my committee members, Dr. Stefan Brocke and Dr. Anthony Vella, who had been closely following the progress of my project and provided me with helpful advices. I also appreciate all their insightful comments on my thesis. I also want to thank my external reader, Dr. Edward Usherwood, who specifically travelled to UCHC to attend my defense and provided me with important feedbacks on my thesis.

I would also like to express my appreciation for all the former and current members of Dr. Cauley's lab, Jenny Suarez-Ramirez, Young-Tae Lee, Tao Wu, Brian Roberts, and Keith Bouchard, for all their help, suggestion and friendship. I would also like to thank members of Dr. Anthony Vella's lab for helping me with the Seahorse XF Flux Analyzer. I also appreciate all the help from members of Dr. Kamal Khanna's lab. I also want to thank Dr. Michael Bevan for the dLck-Cre TGFβRII$^{flox/flox}$ mice, Dr. Beth Garvy for the Smad4$^{flox/flox}$ mice and Dr. Susan Kaech for the collaboration on this project.

I would also like to thank the FACS facility led by Dr. Evan Jellison, for all the help and suggestions on my flow cytometry and cell sorting experiments. I also want to thank the CCAM facility and animal facility for their assistance to my research. I am also very grateful for all the help and support from the faculty and administrators of the immunology department.

Finally I really appreciate all the help from my family members and friends. I would like to specially thank my parents who are always there to give me unconditional love and support.

## TABLE OF CONTENTS

**ABBREVIATIONS**

2-DG: 2-Deoxy-D-glucose

AMP: Adenosine monophosphate

AMPK: AMP-activated protein kinase

AP4: Activating enhancer binding protein 4

APC: Antigen presenting cell

ATP: Adenosine triphosphate

Bcl: B cell lymphoma

BFA: Brefeldin A

Blimp-1: B lymphocyte-induced maturation protein-1

BM: Bone marrow

BMP: Bone morphogenic protein

BPTES: Bis-2-(5-phenylacetamido-1,3,4-thiadiazol-2-yl)ethyl sulfide

BrdU: Bromodeoxyuridine

CCR7: C-C chemokine receptor 7

CD11a: Integrin $\alpha_L$

CD62L: L-selectin

CD103: Integrin $\alpha_E\beta_7$

CFSE: Carboxy fluorescein diacetate succinimidyl ester

c-Myc: Cellular myc

CPT1α: Carnitine palmitoyl transferase 1α

CTL: Cytotoxic T lymphocyte

DC: Dendritic cells

dpi: Days post infection

ECAR: Extracellular acidification rate

EEC: Early effector cell

EMT: Epithelial to mesenchymal transition

Eomes: Eomesodermin

EpCAM: Epithelial cell adhesion molecule

ERK: Extracellular signal-regulated kinase

ETC: Electron transport chain

Etomoxir: 2-[6-(4-Chlorophenoxy)hexyl]-oxirane-2-carboxylic acid

FACS: Fluorescence-activated cell sorting

FAO: Fatty acid oxidation

FAS: Fatty acid synthesis

FCCP: Carbonyl cyanide-4-(trifluoromethoxy)-phenylhydrazone

Fox: Forkhead box transcription factor

Glc: Glucose

Gln: Glutamine

GLS: Glutaminase

GSEA: Gene set enrichment analysis

GTP: Guanosine triphosphate

HA: Hemagglutinin

HEV: High endothelial venule

HIF1α: Hypoxia induced factor 1α

IAV: Influenza A virus

IFN-I: Type I interferon

IFN-γ: Interferon-gamma

Ig: Immunoglobulin

IL: Interleukin

ILN: Inguinal lymph node

i.n.: intranasal

IPA: Ingenuity pathway analysis

i.v.: intravenous

JNK: c-Jun N terminal kinase

KLR: Killer cell lectin-like receptor

LKB1: Liver kinase B1

LM: Listeria Monocytogene

LXR: Liver X receptor

M: Matrix protein

MAPK: Mitogen-activated protein kinase

MHCI: Major histocompatibility complex class I molecule

MLN: Mediastinal lymph node

MPEC: Memory precursor effector cell

mTOR: Mammalian target of rapamycin

NA: Neuraminidase

NK: Natural killer cell

NP: Nucleoprotein

NS: Nonstructural protein

OCR: Oxygen consumption rate

OVA: Ovalbumin

OXPHOS: Oxidative phosphorylation

p: phosphorylated

PA: Polymerase acidic protein

PB: Polymerase basic protein

PDK1: Phosphoinositide-dependent kinase 1

PDHK: Pyruvate dehydrogenase kinase

PFA: Paraformaldehyde

PI3K: Phosphoinositide-3-kinase

PPAR: Peroxisome proliferator-activated receptor

RNA-Seq: RNA sequencing

S6: Ribosomal protein S6

SARA: Smad anchor for receptor activation

Smad: Sma and Mad-related transcription factor

SRC: Spare respiratory capacity

STAT: Signal transducer and activator of transcription

TAK1: TGF-β-activated kinase 1

TCA: Tricarboxylic acid

$T_{CM}$: Central memory CD8 T cell

TCR: T-cell antigen receptor

$T_{EM}$: Effector memory CD8 T cell

$T_{EFF}$: Effector CD8 T cell

TFAM: Mitochondrial transcription factor A

TGFβ: Transforming growth factor β

Th: T helper cell

TNF: Tumor necrosis factor

TRAF6: TNF receptor-associated factor 6

Treg: regulatory T cell

TRM: Tissue-resident memory CD8 T cell

UK5099: 2-Cyano-3-(1-phenyl-1H-indol-3-yl)-2-propenoic acid

**LIST OF FIGURES**

# CHAPTER I

# INTRODUCTION

## 1. Influenza virus and human disease

Infection with Influenza A virus (IAV) is a leading cause of respiratory disease-associated morbidity and mortality. Worldwide, these viruses result in about 3 to 5 million cases of severe illness, and about 250,000 to 500,000 deaths annually. In the United States, there are around 300,000 hospitalizations with more than 40,000 deaths each year (1;2). In addition to the seasonal epidemics, global pandemics occur when new strains of IAVs cause widespread infection and high mortality rates as people have little pre-existing immunity (3;4). Elderly people are at particularly high risk for complications during IAV epidemics, with nearly 60 percent hospitalizations being among people 65 years or older (5). Other vulnerable groups include young children, pregnant women and people with chronic disease or a weakened immune system (6). The symptoms of seasonal influenza infection are characterized by high fever, cough, headache, muscle and joint pain, sore throat and runny nose. Most adults recover from the infection within 1-2 weeks. The mortality is usually driven by two different mechanisms (7;8). Some IAVs are highly pathogenic and induce the release of large quantities of inflammatory cytokines in the lungs, leading to local vascular leakage and alveoli damage (9). Other less pathogenic viruses can induce a transient period of immune suppression that facilitates secondary bacterial infections in the respiratory tract (10).

IAVs belong to the Orthomyxoviridae family of enveloped viruses with a segmented genome comprised of single-strand, negative-sense RNA. The 8 RNA segments encode 11 proteins, including hemagglutinin (HA), neuraminidase (NA), and matrix protein M2, which are embedded in the viral envelop (11). Inside the envelope are the matrix protein M1, and complexes of nucleoprotein (NP) and RNA polymerase proteins. The subunits are polymerase acidic protein (PA), polymerase basic proteins 1 and 2 (PB1 and PB2), and PB1-F2 which is encoded by an alternate reading frame within the PB1 gene. There are also two non-structural proteins (NS1 and NS2) (11;12). HA enables the binding of the viral particles to sialic-acid groups on the

surface of host cells and subsequent endocytosis. The low pH environment inside the endosome induces a conformational change which mediates the fusion of the viral HA and opens a pore in the endosomal membrane. The M2 protein is part of a pH activated ion channel which enables the internal acidification of the influenza virion and the release of viral RNPs into the cytoplasm (13;14). Importantly, HA is synthesized as a precursor molecule which must be cleaved by extracellular proteases that are expressed in specialized cells in the human respiratory tract (15). Viral RNP is then transported into the nucleus where the negative-sense viral RNA is used as a template to transcribe messenger RNA (mRNA) for the production of viral proteins, and complementary RNA (cRNA) which is the genome of new viral RNAs. The nascent viral proteins and RNAs are then packaged into particles and budded from host cells (16). NA is essential for the release of newly synthesized virions from cell surface by cleaving sialic acid groups that are bound to HA (17).

## 2. Protection by the adaptive immune response

### A. Humoral immunity

Most licensed influenza vaccines confer protection against clinical disease by targeting the humoral immune response (12;18). Antibodies that are specific for HA provide immediate protection at mucosal sites by neutralizing infectivity, whereas NA-specific antibodies restrict viral dissemination by preventing the release of new virions. The viral coat proteins undergo constant genetic mutation to escape the host immune response. High mutation rates are characteristic of RNA viruses and cause antigen drift. In addition, re-assortment of the segmented genome can occur during co-infection of two different strains and produce a re-assorted strain which is referred to as an antigenic shift (12). Antibodies to the coat proteins are used to identify different serotypes. Currently, 18 HA (H1-H18), and 11 NA serotypes (N1-N11) have been recorded (19). Currently most antibody-based vaccines are unable to provide

protection against multiple serotypes of IAV, and therefore require constant reformulation to target new strains, leading to huge economic burden as well as substantial failure rates (1).

**B. Cellular immunity**

CD8 T cells play an active role in viral clearance, by directly eliminating infected epithelial cells (20). Importantly, some CD8 T cells are specific for epitopes derived from internal viral proteins that are highly conserved between different strains (21), and can therefore provide immunity between serologically distinct strains known as heterosubtypic immunity (22;23). The goal of my study is to explore whether these CTLs can provide lasting protection against multiple serotypes after vaccination.

**i. Effector CD8 T cell differentiation**

Naïve antigen-specific CD8 T cells persist at low frequencies and must circulate around the body to provide comprehensive surveillance of different lymphoid organs, where cognate antigen is presented to T cells by professional antigen presenting cells (APCs)(24). When naïve CD8 T cells recognize cognate antigen and become activated, they undergo rapid clonal expansion and differentiate into effector ($T_{EFF}$) cells which can produce cytokines such as interferon-γ (IFN-γ), tumor-necrosis factor (TNF) or interleukin 2 (IL-2). Most CD8 T cells also gain lytic function and express molecules such as granzymes and perforin (25).

During infection the pool of activated CTLs becomes highly heterogeneous in terms of phenotypic markers (26;27). The IL-7 receptor α chain (CD127), and killer cell lectin-like receptor G1 (KLRG-1) are often used to distinguish $T_{EFF}$ cell subsets (28;29). Activated CD8 T cells downregulate CD127 and proliferate into the early effector cells (EECs, KLRG-$1^{lo}$CD$127^{lo}$). During clonal expansion some $T_{EFF}$ cells upregulate KLRG-1 and acquire a terminally differentiated phenotype (KLRG-$1^{hi}$CD$127^{lo}$). Many of these CTLs undergo apoptosis after the infection is cleared. A subset of $T_{EFF}$ cells can re-express CD127 and acquire a memory

precursor phenotype that is KLRG-1$^{lo}$CD127$^{hi}$, indicating that they can further differentiate into long-lived memory cells. Nevertheless, it should be noted that neither KLRG-1 nor CD127 is sufficient or necessary to determine the fate decisions of $T_{EFF}$ cells (30;31). The heterogeneity of the $T_{EFF}$ cell population has been further examined at single-cell level. Some studies suggest that the fate of $T_{EFF}$ cells is determined by asymmetric distribution of surface and intracellular molecules during the first cell division (32). Others suggest TCR affinity determines whether CD8 T cells undergo symmetric or asymmetric cell division and thus controls the phenotype of the daughter cells (33). However, studies using single-cell transfer or 'DNA-barcoding' show that individual cells bearing the same TCR can yield progeny cells with disparate fates, and exhibit highly diverse abilities to proliferate and give rise to progeny with heterogeneous phenotypic markers (34-37).

The plasticity of $T_{EFF}$ cell differentiation underscores the importance of extrinsic signals which can come from a variety of sources including antigen stimulation (signal 1), co-stimulation (signal 2) and inflammatory cytokines (signal 3). Studies show that the abundancy and duration of available antigens are not only in proportion to the magnitude of clonal expansion, but also affect memory differentiation of $T_{EFF}$ cells (38;39). A high frequency of naïve CD8 T cell precursors (40;41), or activation of naïve T cells during a late stage of infection (42), typically leads to decreased expansion and preferential differentiation towards a memory phenotype.

Costimulatory molecules play important roles during different stages of the CD8 T cell response, including activation, expansion, and memory formation (43;44). The interactions between CD28 and CD80/CD86 during priming are crucial for the generation of a successful effector CD8 T cell response, especially for T cells with low affinity receptors (45). Costimulation through CD28, CD27, 4-1BB and OX40 promotes survival by increasing the expression of anti-apoptotic molecules (46). For instance, incorporation of 4-1BB into a vaccine vector increased the numbers of antigen-specific CD8 T cells in mice after IAV infection and prolonged the duration

of protection, by promoting the survival of activated CD8 T cells (47). Costimulatory signals also contribute to the generation of memory CD8 T cells in variety of infection models (45). For instance, a recent study demonstrates that NP-specific CD8 T cells are able to receive a signal via CD27 by interacting with CD70-bearing dendritic cells (DCs) at late stage after primary infection, which facilitate the development of memory cells with high proliferative capacity (48).

The milieu of pro-inflammatory cytokines that are produced upon innate immune recognition of pathogen-associated molecular patterns (PAMPs) can also influence the properties of developing CD8 $T_{EFF}$ cells (49). IL-12, IFNγ, type I IFN or IL-27 can augment the expansion as well as the contraction of $T_{EFF}$ cells, by increasing the ratio of terminally differentiated cells to memory precursors (29;50). Recent studies also show that IL-1 can significantly increase clonal expansion and augment the effector functions of antigen-specific CD8 T cells (51). In addition, autocrine IL-2 production is essential for $T_{EFF}$ cell expansion, differentiation and survival. Studies show that some $T_{EFF}$ cells which maintain high expression of the high-affinity IL-2 receptor α chain (CD25) undergo extensive proliferation and become terminally differentiated, while $T_{EFF}$ cells with low expression of CD25 preferentially become memory cells (52;53).

**ii. Circulating memory CD8 T cells**

A majority of $T_{EFF}$ cells undergo apoptosis as the pathogen is cleared. This process is determined by the balance between pro-survival molecules such as B-cell lymphoma 2 (Bcl-2) or myeloid cell leukemia 1 (Mcl-1), and pro-apoptotic molecules such as Bim or Noxa. Activation of downstream effector molecules caspase-3 and -7 can also be regulated by the external signals that are received by $T_{EFF}$ cells (54;55). Contraction of the CD8 T cell response leaves small numbers of long-lived memory CD8 T cells which rely on IL-7 and IL-15 for survival and homeostatic turnover (45). A key feature of these memory cells is their ability to respond rapidly to re-encounter of antigen by acquiring effector functions and generating secondary $T_{EFF}$ cells.

Antigen-specific memory cells persist at higher frequencies than naïve CD8 T cells, and mount more robust secondary responses after reinfection (56).

The memory CD8 T cell pool can be divided into different subsets based on their phenotype, function and location. There are two broad subsets of memory CD8 T cells in the circulation which are central memory T ($T_{CM}$) cells and effector memory ($T_{EM}$) cells (57). The lineage decisions between $T_{CM}$ and $T_{EM}$ cells can be regulated by early signals such as antigen availability, costimulation and cytokines (58). $T_{CM}$ cells have high expression of CD62L and CCR7 which facilitate the homing to secondary lymphoid organs, while $T_{EM}$ cells lacking these two markers are predominantly found in peripheral tissues (59). Transmigration of $T_{CM}$ cells into the peripheral lymph nodes is mediated by interactions between CD62L and peripheral node addressin (PNAd) on high endothelial venules (HEVs), which enables the tethering and rolling of T cells along HEVs (60). CCR7 then engages with HEV-associated chemokines such as CCL21, which leads to the activation of lymphocyte function-associated antigen 1 (LFA-1) on T cells. The interaction between LFA1 with intercellular adhesion molecules (ICAMs) on the HEVs results in firm arrest of T cells and their transmigration into the lymph node parenchyma. Functionally, $T_{CM}$ cells have greater proliferative potential and produce IL-2 upon recall, whereas $T_{EM}$ cells constitutively display effector functions such as cytotoxicity (59). Conversion can occur between these two subsets during memory development and maintenance (59). Importantly, a recent study used adoptive transfer of individual cells to show that $T_{CM}$ cells have self-renewal capacity, as well as multipotency to generate phenotypically diverse progeny across serial adoptive transfers and repeated infections (60).

**iii. Tissue-resident memory CD8 T cells**

In addition to the two subsets of circulating memory CD8 T cells, recent studies identified a third population of virus-specific memory CD8 T cells that locate in peripheral tissues and do not re-

enter circulation. These CTLs remains at the site of potential re-infection, such as a mucosal tissue, and are therefore referred to as tissue resident memory T ($T_{RM}$) cells (61;62). Large numbers of $T_{RM}$ cells are generated in the lungs after local, but not systemic, IAV infection (63). Microarray analysis revealed a core transcriptional signature of this population that is distinct from $T_{CM}$ or $T_{EM}$ cells (64). Most $T_{RM}$ cells are characterized by their high expression of the activation marker CD69 and $\alpha_E\beta_7$ integrin CD103, but are devoid of CD62L and CCR7 expression. Studies have shown that $T_{RM}$ cells develop from the KLRG-$1^{lo}$ subset of $T_{EFF}$ cells in response to tissue-derived signals, such as the cytokine transforming growth factor β (TGFβ) (64). This thesis will address the role of TGFβ in the generation and/or maintenance of $T_{RM}$ cell population.

Previous studies have shown that TGFβ controls the expression of CD103 on $T_{RM}$ cells and therefore promotes interactions with E-cadherin expressed on epithelial cells, which is important for retention in mucosal tissues (65-68). The role of prolonged presentation of cognate antigen after acute infection remains controversial, and may promote the differentiation and/or maintenance of $T_{RM}$ cells in the lung (65;69), but is not required in the intestine or skin (70;71). IL-15 also plays a role in the formation and survival of $T_{RM}$ cells in the skin (64). In addition, downregulation of Krüppel-like Factor 2 (KLF2) and its target, the receptor for sphingosine 1-phosphate (S1P1), is mediated by TGFβ, IL-33 and TNF via the phospophatidylinositol-3-OH kinase (PI3K)/Akt pathway, which prevents the egress of lymphocytes from inflamed tissues and is necessary for the development of $T_{RM}$ cells (72).

Several studies have shown that $T_{RM}$ cells mediate critical protection against local challenge in different tissues including the lungs (73-75). These cells are poised in the tissues to provide frontline defenses during the earliest phase of re-infection, by rapidly recognizing and killing pathogens, or recruiting other types of immune cells. A study from our lab has shown that $T_{RM}$ cells play a crucial role in heterosubtypic immunity against IAV infections by decreasing viral

load (90). The recruitment of circulating memory CD8 T cells to the lungs is not necessary for protection, but it enables the replenishment of different subsets of cells in the memory compartment (90). On the other hand, a recent study showed that re-challenge of $T_{RM}$ cells can quickly induce an anti-viral state locally in the skin or female reproductive tract (FRT) after re-challenge (74;75). These cells can induce the expression of vascular cell adhesion molecule-1 (VCAM-1) on vascular endothelium by secreting IFN-γ upon re-activation, which promotes the recruitment of circulating memory CD8 T cells and B cells. Also, cytokines such as TNF and IL-2 are produced by activated $T_{RM}$ cells to facilitate DC maturation and natural killer (NK) cells activation.

Although virus-specific CD8 T cells can provide cross-protection between different IAVs, eliciting memory populations with the properties that are required for immunity is a major challenge for vaccination. Optimal protection requires a combination of circulating memory CD8 T cells, which move through the bloodstream to migrate around the body, as well as $T_{RM}$ cells which mount rapid responses to reinfection by remaining near the site of inoculation (Figure 1-1). The goal of my work is to identify signaling molecules that influence CD8 T cell differentiation and the production of heterogeneous memory populations which provide heterosubtypic immunity, including $T_{RM}$ cells.

Figure 1-1

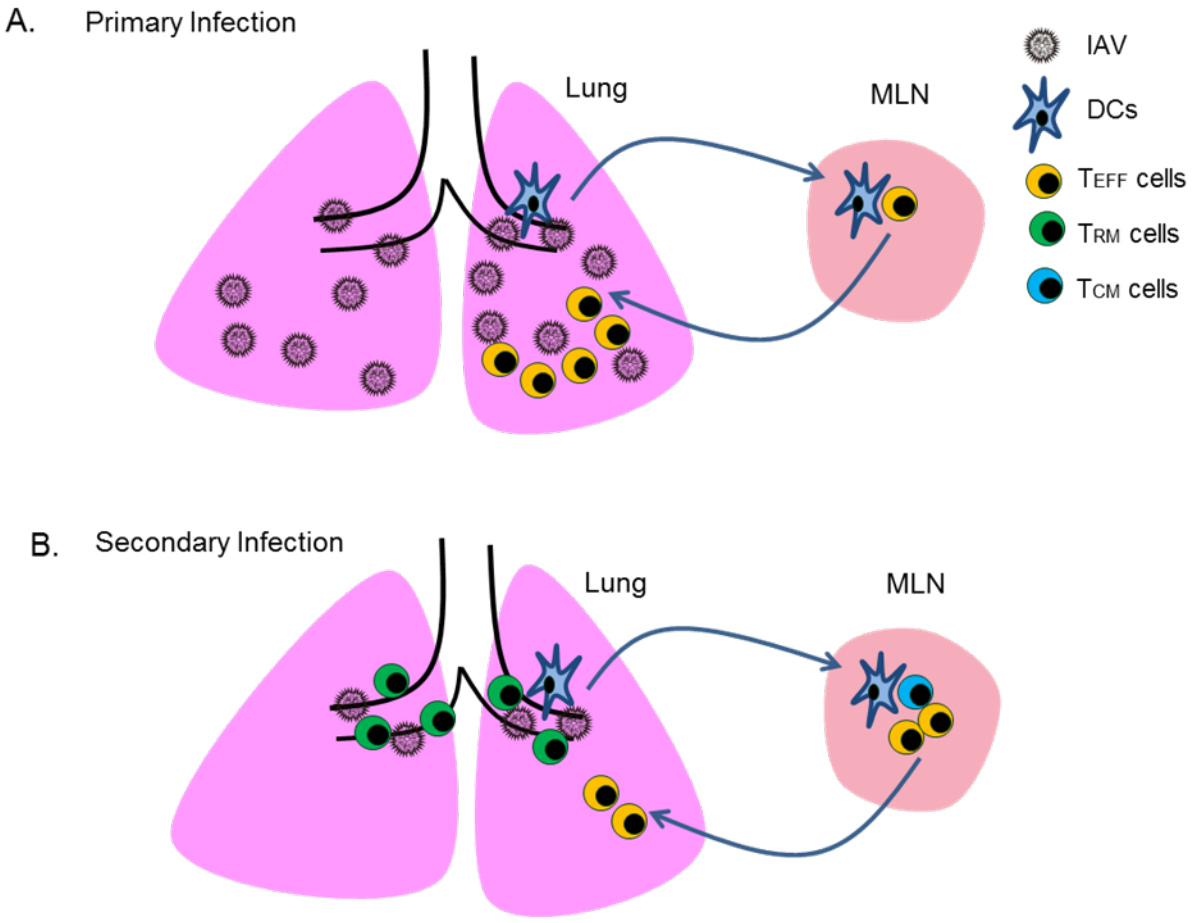
A.
Primary Infection
Lung
MLN
IAV
DCs
TEFF cells
TRM cells
TCM cells
B.
Secondary Infection
Lung
MLN

**Figure 1-1 Different subsets of virus-specific CTLs participate in heterosubtypic immunity.**

**A.** During primary IAV infection, dendritic cells (DCs) migrate from the infected lungs to the mediastinal lymph node (MLN). Naïve CD8 T cells recognize their cognate antigen which is presented by DCs. Upon activation, virus-specific CD8 T cells undergo clonal expansion and differentiate into $T_{EFF}$ cells which migrate into the lungs and kill infected epithelial cells. Since several days pass before $T_{EFF}$ cells arrive in the lung, some virus can reach the alveoli and cause pathology. Residual CTLs remain in the lungs after viral clearance and become $T_{RM}$ cells.

**B.** Upon secondary challenge, $T_{RM}$ cells are located in the airways and rapidly kill newly infected epithelial cells. Since the virus is rapidly cleared from the airways, low viral titers reach the alveoli. Some $T_{CM}$ are reactivated in the MLN, but very few nascent $T_{EFF}$ cells enter lungs and cause mild pathology

# CHAPTER II

# ANIMALS, MATERIALS AND METHODS

**Mice**

C57BL/6 mice were purchased from Charles River (Wilmington, MA). Smad4$^{flox/flox}$ mice were obtained from Dr. Garvy (University of Kentucky), which were crossed with mice that express Cre-recombinase under the control of the distal Lck (dLck) promoter (SKO) (74), as well as OTI TCR transgenic mice (75). The dLck-Cre TGFβRII$^{flox/flox}$ mice (TKO) were generously supplied Dr. M. Bevan (University of Washington). The mice with two mutations, dLck-Cre Smad4$^{flox/flox}$ TGFβRII$^{flox/flox}$ mice (ST-DKO), were generated by cross-breeding. Mice were housed at University of Connecticut Health Center in accordance with institutional guidelines.

**Viral and Bacterial infections**

Virus stocks were grown in fertilized chicken eggs and titers determined as described previously. Mice were anesthetized by ketamine/Xylazine and were infected with $10^3$ plaque-forming unites (PFU) of X31-OVA (H3N2 serotype) or WSN-OVA$_1$ (H1N1 serotype) by intranasal (i.n.) inoculation. For secondary infection, primed mice were challenged with $5x10^3$ PFU of WSN-OVA$_1$ or X31-OVA i.n.

**Mixed bone marrow chimeras**

Lethally irradiated mice (1000 rads) were reconstituted with $5x10^6$ bone marrow cells from congenically marked mutant and control mice (1:1 ratio). To eliminate radio-resistant cells 200μg anti-CD8 antibodies (2.43) were given by i.v. injection 2 days after transfer. Mice were maintained for 6-8 weeks before IAV infection.

**Transfer experiments**

Naïve CD8 T cells from donor mice were sorted for low CD44 expression. Recipient mice received mixed populations of congenically marked mutant and/or wild type donor cells (mixed 1:1, $10^4$ cells total). For proliferation assays, donor cells were labeled with 10 μM CFSE

(carboxyfluorescein diacetate succinimidyl ester) at 37°C for 8 minutes before transfer. Recipient mice received $10^6$ donor cells 2 days before IAV infection.

**Sample preparation for flow analysis**

Single-cell suspensions were made from spleens and lymph nodes, with red blood cells lysed with triammonium chloride (TAC). Lungs were digested with 150 U/ml collagenase (Life Technologies) in RPMI medium 1 mM $MgCl_2$, 1 mM $CaCl_2$, and 10% fetal bovine serum (FBS) and enriched by 44/67% Percoll gradients. Washed lymphocytes were stained with anti-CD8 and $NP_{366-374}$ H2-$D^b$ tetramers for 1 hour at room temperature. The staining of all other surface markers was done at 4°C for 30 minutes. Fluorochrome-conjugated antibodies against the following antigens were used for flow cytometry: CD8α (53-6.7), CD45.1 (104), CD45.2 (A20), KLRG-1 (2F1), CD127 (A7R34), CD44 (IM7), CD69 (H1.2F3), CD103 (2E7), CD62L (MEL-14), CD25 (PC61). CCR7 expression was analyzed using CCL19 conjugated to human Ig and Alexa Fluor 488-conjugated anti-human IgG (Life Technologies). For intravascular staining mice were injected with 3mg anti-CD8β antibodies in 300μL PBS and sacrificed 5 min later. Caspase activity was measured with Vybrant FAM Caspase-3 and -7 Assay Kits (Invitrogen). For assessment of mitochondrial membrane potential, cells were incubated in complete growth medium for 15 minutes at 37 °C with 100 nM MitoTracker Orange CMTMRos (Invitrogen), followed by washing with cold PBS and staining of surface markers. Samples were run on a LSR-II flow cytometer (BD) and analyzed with Flowjo software (Tree Star Inc.).

**Intracellular Staining and Phospho-flow**

For cytokine analysis, lymphocytes were incubated with SIINFEKL peptide (1μg/ml) in the presence of Brefeldin A for 5 hours at 37°C and analyzed with Cytofix/Cytoperm Kit (BD Pharmingen). For BrdU analysis, BrdU was injected intraperitoneally (1mg in 200μl PBS), and lymphocytes were analyzed 3–6 hours later using a BrdU kit (BD Pharmingen). The Foxp3

staining buffer set (eBioscience) was used for intracellular staining of transcription factors using antibodies to T-bet (eBio4B10), Eomes (Dan11mag), Bcl-2 (3F11) (eBioscience).

Phospho-flow analysis were performed directly *ex vivo* using spleens that were harvested from recipient mice at indicated time points and mashed in 2% paraformaldehyde (PFA). Fixed cells were permeabilized with ice-cold 100% methanol and stained with antibodies against p-S6 Ser235/236 (Cell Signaling Techonologies). For *in vitro* stimulation, splenocytes were harvested from recipient mice and rested in tissue culture media with 1% FBS for 3 hours. The cells were stimulated with 2ng/ml IL-12 p70 (Biolegend) for 1 hour or 5ng/ml IL-2 (eBioscience) for 30 minutes. After fixation with 2% PFA cells and permeabilization with methanol, cells were stained with anti-p-S6 Ser235/236, and anti-p-STAT4 Tyr693 or anti-pSTAT5 Tyr694 antibodies (BD Pharmingen).

**Confocal microscopy**

Tissues were fixed with 1% PFA and stained with biotinylated Abs to epithelial cell adhesion molecule (EpCAM) or B220. After washing the cells were stained with streptavidin–Pacific Orange (Life Technologies) and a cocktail of antibodies including PE-conjugated anti-CD45.1 (eBioscience), anti-CD103 Alexa Fluor 647 (BioLegend), KLRG1 Alexa Fluor 488 (BD Pharmingen), and CD31 Pacific Blue (Life Technologies). Images were recorded on a Zeiss LSM 780 confocal microscope with the Zeiss ZEN 2012 digital imaging suite and an inverted Axio Observer Z1 with argon diode, and HeNe lasers using Plan-Neofluar 310/numerical aperture 0.5 and 320/numerical aperture 0.5 objectives. Imaris suite (Bitplane) was used for background subtraction and colocalization.

**RNA-Seq and bioimformatics**

C57BL/6 mice received mixed populations of $10^4$ CD45.1 OTI-WT and CD45.1.2 OTI-SKO cells (1:1 ratio) by trail vein injection and were infected with X31-OVA 2 days later. Splenocytes were

harvested at 6 dpi from a total of 9 mice, and were pooled into 3 samples. CD45.1+ donor cells were positively enriched by biotinylated anti-CD45.1 antibody (Biolegend) and anti-biotin Microbeads (Miltenyi Biotec) on autoMACS machine. The enriched cells were stained with antibodies against CD45.1, CD45.2, CD44, CD8, CD127, KLRG-1, and CD103 before sorting on a FACSAria II (BD). RNA was extracted from sorted cells with an RNAeasy Plus Mini Kit according to the manufacturer's protocol (Qiagen).

RNA samples were sent to Otogenetics Cooperation for RNA-Sequencing. The data sets were analyzed with Tophat2 mapping (DNAnexus). Expression levels were measured with Cuffilinks software (DNAnexus) and differential expression analysis was done with Cuffdiff software (DNAnexus). Genes with transcriptional changes over two folds ($Log_2$ fold change >1 or <-1, $p<0.05$, false discovery rate<0.05) were selected for Ingenuity pathway analysis (Qiagen) and Gene set enrichment analysis (Broad Institute). Heatmaps were generated by Gene E software (Broad Institute).

**Metabolic Assays**

B6 mice recieved $10^5$ or $10^6$ donor cells 2 days before infection with x31-OVA. Lymphocytes were harvested from the mediastinal lymph nodes (MLNs) at 3.5dpi or spleens at 6dpi and 8dpi. Donor cells were positively enriched using biotinylated anti-CD45.1 antibody and anti-biotin microbeads. The enriched cells were stained with CD45.1, CD45.2, CD44, CD8, CD127, KLRG-1, and CD103 antibodies and sorted on a FACSAria II. CD45.1+ donor cells were positively enriched by biotinylated anti-CD45.1 antibody (Biolegend) and anti-biotin Microbeads (Miltenyi Biotec) on autoMACS machine. The enriched cells were stained with antibodies against CD45.1, CD45.2, CD44, CD8, CD127, KLRG-1, and CD103 before sorting on a FACSAria II (BD).

For extracellular flux assays, sorted cells were seeded at $2x10^5$ cells per well on Cell-Tak (Corning) coated 96-well plates, and rested for 1 hour at 37°C without CO2. Oxygen

consumption rate (OCR) and extracellular acidification rate (ECAR) were measured on XF-96 Extracellular Flux Analyzer (Seahorse Biosciences). Briefly, mito stress tests were done in DMEM containing 2mM glutamine, 1mM sodium pyruvate and 25mM glucose. OCR was measured under basal conditions and in response to 4μM oligomycin, 0.5μM fluorocarbonyl cyanide phenylhydrazone (FCCP) and 0.5μM rotenone/antimycin A. 200μM Etomoxir, 50μM BPTES or 50μM UK5099 (Sigma) was used as inhibitors of oxidative phosphorylation. Glycolysis stress tests were done in glucose- and pyruvate-free DMEM. ECAR was measured in response to 10mM glucose, 4μM oligomycin and 50mM 2-DG during the assay.

**Statistical analysis**

Experiments were repeated 2 or 3 times using 3-5 animals per group. Statistical significance was determined using an unpaired two-tailed Student t test. Comparisons that were used to generate p values are indicated by horizontal lines in the figures. A p value<0.05 was considered statistically significant.

# CHAPTER III

# DEFINING THE ROLE OF TGFβ AND SMAD4 DURING $T_{RM}$ CELL FORMATION, CELL MIGRATION AND IMMUNITY

**Abstract**

Although heterogeneous populations of memory CD8 T cells participate in immunity against IAV infection, the signaling pathways that are responsible for this heterogeneity are poorly defined. An important regulatory pathway for activated CTLs is controlled by TGFβ, which reduces the numbers of terminally differentiated $T_{EFF}$ cells in infected tissues and is required for CD103 expression on $T_{RM}$ cells. When genetically-modified mice were used to prevent expression of the TGFβ receptor on activated CTLs during IAV infection, increased numbers of KLRG1+ $T_{EFF}$ cells collected in the infected lungs, while $T_{RM}$ cells were absent during the late stage of the response. To define which signaling pathway is required for CD103 expression on $T_{RM}$ cells, we performed similar experiments with CTLs lacking the downstream signaling intermediate Smad4. We found that Smad4 was required for the formation of KLRG1+ $T_{EFF}$ cells, while $T_{CM}$ cells had no requirement for TGF-β. A large population of CTLs showed signs of arrested development in the absence of Smad4, including aberrant CD103 expression. Imaging studies showed that these signaling pathways alter the distribution of virus-specific memory CD8 T cells in the lungs, but do not affect cytokine production. Smad4-deficency caused slightly delayed viral clearance after primary IAV infection, but was not required for protective immunity upon reinfection with another strain. Our data show that TGFβ and Smad4 are required for normal differentiation of multiple subsets of virus-specific CTLs, including KLRG1+ $T_{EFF}$ cells, CD62L+ $T_{CM}$ cells and CD103+ pulmonary $T_{RM}$ cells.

## Introduction

TGFβ is a cytokine with multiple functions, including regulation of immune cells (76). A latent precursor must be cleaved by proteases in the tissue matrix to release an active 25-kDa peptide which is capable of receptor binding (77). TGFβ can also be activated by the NA enzymes of some viruses and is produced in large quantities in the lungs during IAV infection (78). A published study showed that some highly pathogenic H5N1 strains of IAV do not activate latent TGFβ very effectively and that ectopic expression of TGFβ prolonged the survival of H5N1-infected mice (79). These data suggest that TGFβ may play a role in protecting the host from IAV pathogenesis.

TGFβ is a suppressive cytokine and master regulator of diverse populations of immune cells, including DCs, NK cells and macrophages. In addition, TGFβ inhibits proliferation of B and T cells and can induce apoptosis (80). Other important functions include roles in inducing IgA class switching (81) and regulating CD4 T cell differentiation (80). TGFβ suppresses the formation of Th1 and Th2 subsets and promotes Th17 development by inducing RORγt and suppressing expression of Eomesodermin (Eomes) (82). In addition, TGFβ is crucial for the induction of the Forkhead box p3 (Foxp3) gene during development of regulatory T (Treg) cells (83;84).

How TGFβ regulates the CD8 T cell response is less well defined, but recent studies have shown that naïve CD8 T cells undergo enhanced proliferation in a lymphopenic environment and acquire an activated $CD44^{hi}CD62L^{lo}$ phenotype when the TGFβ receptor (TGFβRII) is not expressed (85). During *Listeria Monocytogene* infection, TGFβRII deficiency resulted in the selective accumulation of KLRG1+ $T_{EFF}$ cells (86). In addition, TGFβ induces expression of $\alpha e\beta 7$ integrin (CD103) which is essential for the generation and/or residence of $T_{RM}$ cells in the lungs, thus indicating a role in protection (64-66). In this thesis we examined the role of TGFβ

during tissue localization of anti-viral CTLs and protective immunity to IAV infection. We also focus on the intracellular signaling molecule Smad4, which acts downstream of the receptors for multiple members of the TGFβ cytokine family.

**Smad-dependent TGFβ signaling pathways**

The TGFβ receptor is comprised of two subunits (TGFβRI and TGFβRII), which are serine/threonine kinases (87). Ligand binding brings TGFβRII in close association with TGFβRI, allowing phosphorylation and signal transduction via multiple pathways (88). The canonical signaling pathways are mediated by Sma and Mad-related (Smad) transcription factors, which are well-studied in cancer (87) and the immune system (80). Eight Smad proteins have been identified in vertebrates, including the multiple receptor activated Smad proteins (i.e. Smad1, 2, 3, 5, and 8), which form complexes with a shared adaptor (Smad4), as well as two inhibitory Smads (Smad6 and 7) which can prevent signal transduction (87;89). At the basal state, R-Smads are predominantly located in the cytoplasm and use cytoplasmic anchors to interact with the Smad Anchor for Receptor Activation (SARA). The adaptor protein Smad4 is evenly distributed throughout the cells and constantly transported between the cytoplasm and nucleus. In response to activation, the TGFβ receptor phosphorylates R-Smad2 and R-Smad3, which dissociate from SARA and bind to Smad4 for translocation into nucleus. The phosphorylated Smad proteins form complexes which attach to Smad-binding elements (SBE) in the promoters of the target genes. DNA binding is mediated by a β-hairpin structure at the N-terminal Mad-homology 1(MH1) domain that is conserved in Smad4 and all R-Smad proteins. Transcriptional activity depends on interactions with other transcription factors, which enable high affinity binding to DNA in selected target genes. Also, depending on these associated co-factors, the complexes either recruit coactivators, such as p300 and cAMP-response element-binding protein (CREB) binding protein (CBP), or corepressors such as histone deacetylases (HDACs). Such interactions are crucial for the diverse functions of TGFβ. When R-Smads are

dephosphorylated in the nucleus, they dissociate from Smad4 and are exported to the cytoplasm for another round of signal transduction. Smad4 is not always required for transcriptional activity of the Smad complex. In Smad4-deficient cancer cells TGFβ treatment can induce translocation of pSmad2/3 into the nucleus, though such complexes do not have transcriptional activity (90). Another transcription factor, transcriptional intermediatory factor 1γ (TIF1γ), can also bind to phosphorylated Smad2/3 in hematopoietic cells and is involved in erythrocyte differentiation (91). Development for invariant natural killer T cells (iNKTs) are controlled by at different stages by Smad4 and TIF1γ (92). A recent study revealed that TIF1γ antagonizes Smad signaling by mono-ubiquitinating Smad4 which causes dissociation of the Smad2/3/4 complex (93).

**Smad-independent TGFβ signaling**

TGF-β receptor can also signal through a variety of pathways that are independent of Smad proteins, which have been extensively studied in other cell types, yet little is known about their functions in immune cells (87;94). TGFβ can activate various branches of mitogen-activated protein kinase (MAPK) pathways, including Erk, c-Jun N terminal kinases (JNKs) and p38 (95). Phosphorylated TGFβ receptors recruit Grb2/Sos and Ras to activate the Raf/MEK/Erk cascade, which is essential for epithelial to mesenchymal transition (EMT) (96). Binding of TNF receptor-associated factor 6 (TRAF6) to activated TGFβ receptors induces the lysine-63 (K63)-linked polyubiquitination of TRAF6, which recruits TGF-β-activated kinase 1 (TAK1) to activate JNKs, or p38 via MKK4 or MKK3/MKK6 respectively. These pathways are important for TGFβ-induced apoptosis and EMT (97;98). The phosphatidylinositol 3-kinase (PI3K)/Akt pathway can also be activated by the TGFβ receptor (99), and contributes to TGFβ-driven EMT. The mechanism may require mammalian target of rapamycin (mTOR) activity, which is a key regulator of protein synthesis (100). The PI3K/Akt/mTOR pathway antagonizes Smad-mediated effects via various mechanisms. For example, Akt activation protects cancer cells from TGF-β-induced growth

arrest and apoptosis (101). In addition, TGFβ can activate small Rho-like GTPases including Rho-A and Cdc42, which promotes the formation of actin stress fibers and dissolution of tight junctions during the EMT (102). These Smad-independent TGFβ signaling pathways are poorly understood in the immune system.

This thesis explores to the role of TGFβ and Smad4 during the contraction of the KLRG-1+ $T_{EFF}$ response in the lungs and/or induction of CD103 expression on $T_{RM}$ cells (103). Using flow cytometry and fluorescence microscopy, we compared the phenotypes and locations of effector and memory CD8 T cells when TGFβRII or Smad4 were absent. In addition, we examined the role of TGFβ and Smad4 in heterosubtypic immunity by comparing host survival after primary and secondary IAV infections.

**Major goals for chapter 3:**

**Aim 1.1** To determine whether TGFβRII or Smad4 deficiency alters the phenotypes and/or functional properties of virus-specific CD8 T cells after IAV infection

**Aim 1.2** To determine whether Smad4-dependent and -independent TGFβ signaling impacts the localization of virus-specific CD8 T cells after IAV infection

**Aim 1.3** To examine whether TGFβRII or Smad4 is required for protective immunity

## Results

*TGF-β suppresses terminal differentiation of KLRG1+ $T_{EFF}$ cell.*

Genetically-modified mice were used to determine how TGF-β alters the CTL response to IAV infection. Chimeric mice were made with mixed bone marrow cells from dLck-Cre TGFβRII$^{flox/flox}$ (TKO) mice (85) and their WT littermates (lacking Cre or flox sites). This approach ensures that mutant and WT CTLs are exposed to identical concentrations of antigen and inflammation during infection. After eight weeks the secondary lymphoid organs contained approximately equal numbers of WT and TKO CD8+ T cells. Large percentages of the TKO cells expressed CD44 at high levels and downregulated CD62L, including KLRG-1 expression on some cells (Figure 3-1A). This phenotype was consistent with enhanced homeostatic proliferation after radiation (85).

To analyze the CTL response to viral infection, chimeric mice were infected with X31-OVA and analyzed for NP-specific CTLs by MHC class I tetramer analysis. There were larger numbers of TKO cells in the lungs and spleens 10 days post infection (dpi), as compared to the controls (Fig. 3-1B). Consistent with the literature (65;86), our phenotypic data showed that high frequencies of TKO cells expressed KLRG1, whereas CD103+ cells were almost completely absent (Fig. 3-1C). These data suggest that KLRG1+ $T_{EFF}$ cells and $T_{RM}$ cells respond to TGF-β in very different ways after IAV infection.

*TGF-β suppresses cell proliferation during the $T_{EFF}$ response.*

Because some CD8 T cells were non-specifically activated in the irradiated mice, we performed adoptive transfer experiments with donor cells from OTI TCR transgenic mice that express an antigen receptor that is specific for the SIINFEKL peptide from the chicken ovalbumin (OVA) gene (107). Donor cells from OTI-TKO and wild type littermates were sorted for low CD44 expression. The recipient animals received mixed populations of congenically marked OTI-TKO

and OTI-WT cells 48 hrs before infection. The kinetic studies show that large numbers of KLRG1+ $T_{EFF}$ cells accumulated in the lungs and spleens in the absence of TGF-β regulation (Figure 3-2A).

To determine whether the phenotypic variation was due to altered cell proliferation, donor cells from OTI-WT and OTI-TKO mice were labeled with Carboxyfluorescein succinimidyl ester (CFSE) before transfer. The mice were infected with X31-OVA and analyzed by flow cytometry 3.5 dpi (Fig. 3-2B). Other recipients were given a single injection of BrdU on 6, 8, or 10 dpi and donor CTLs were analyzed 3–6 h later (Fig. 3-2C). The CFSE analysis showed no difference in cell division 3.5 dpi (Fig. 3-2B), and the CTLs from each group of mice incorporated BrdU at very similar rates 6 dpi (Fig. 3-2C). At later time points the percentages of BrdU+ CTLs in the OTI-TKO population were much higher than the OTI-WT cells (Fig. 3-2C). These studies show that the virus-specific CTLs underwent prolonged proliferation in the absence of TGF-β regulation. Similar levels of activated caspases-3/7 (Fig. 3-2D) and pro-survival molecule Bcl-2 were detected in the transferred cells (Fig. 3-2E), which indicated that TGF-β did not substantially alter cell survival.

Similar to the tetramer+ CTLs from chimeric mice, CD103 was absent on OTI-TKO cells 30 dpi (Fig. 3-3A). Only small percentages (and numbers) OTI-TKO cells expressed CD69 in the lungs (Figure 3-3A and 3-3B hatched shading), indicating limited production of pulmonary $T_{RM}$ cells without CD103. In contrast, a substantial proportion of the OTI-WT cells co-expressed CD103 with CD69 in the lungs, indicating that some $T_{RM}$ cells were present 30dpi (Figure 3-3A, Figure 3-3B black shading). These experiments confirm that TGF-β plays a critical role in the development and/or maintenance of pulmonary $T_{RM}$ cells.

*Most long-lived KLRG1+ CTLs remain in the vasculature*

We have shown that activated CTLs express altered homing receptors in the absence of TGF-β regulation, including the formation of a large KLRG1+ subset. Because the distribution of virus-specific memory CD8 T cells in the lungs is very important for immunity (61), we used confocal microscopy to compare the distribution of OTI-TKO and OTI-WT cells during the recovery from IAV infection (Fig. 3-4A). Naive CD8 T cells ($CD44^{lo}$) were sorted from congenically marked OTI-TKO and OTI-WT mice and transferred to separate recipients. The recipient mice were infected with X31-OVA 48hrs later and the lungs were analyzed by confocal microscopy 10 and 30 dpi, to compare the distribution of transferred CTLs in each group (Figure 3A). Low magnification images show the tissue structure (left panels) with transferred cells shown in blue. CTLs in the marked sub-regions (white boxes) are shown at higher magnification with (i) KLRG1 and (ii) CD103 expression, identified using the co-localization function of the Imaris™ software (white color). EpCAM-specific antibodies were used to define the outer margins of the large airways (marked with red dashed lines in panels on the right side). Large numbers of OTI-TKO cells and some OTI-WT cells expressed KLRG1 during the acute stage of the infection and were located in the tissue surrounding the alveoli (middle column). In contrast, substantial numbers of CTLs from OTI-WT mice expressed CD103 in the airways after the contraction of the $T_{EFF}$ cell response (right column).

Substantial numbers of OTI-TKO cells expressed KLRG1 30dpi, indicating that some terminally differentiated CTLs maintained the capacity for long-term survival (Figure 3-2). These long-lived KLRG1+ CTLs universally expressed CD11a at high levels (Figure 3-4B), showing that they did not reach the lumen of the airways, where high concentrations of host proteases cleave CD11a from the cell surface (104). We further examined where these phenotypically distinct subsets of CTLs were located after infection, using injected antibodies for intravascular staining (105). Congenically marked donor cells were transferred 48 h before infection with X31-OVA. On the

days shown, antibodies to CD8β were given by i.v. injection 5 min before sacrifice. Secondary staining with anti-CD8a was used to identify CTLs in the tissues. This study showed that some KLRG1+ CTLs from both OTI-TKO and OTI-WT mice were protected from the injected antibodies 8 dpi (Figure 3-4C, top row), and therefore entered the lung parenchyma during acute viral infection (106). In contrast, very few KLRG1+ CTLs were protected from the injected antibodies 40 dpi (Figure 3-4C, bottom row), indicating that "terminally differentiated" CTLs were poorly equipped for long-term survival in peripheral tissues. A small number of 'blood-resident' memory CD8 T cells maintained KLRG1 expression 40 dpi.

Previous studies have shown that IAV infection induces long lived CTLs that express CD103 in the lungs, which is a marker of $T_{RM}$ cells (61;63). CD69 is another marker for $T_{RM}$ cells which is not regulated by TGF-β (70). Vascular staining showed that a substantial population of OTI-WT CTLs co-expressed CD103 together with CD69 in the lung parenchyma and were therefore $T_{RM}$ cells (Figure 3-4D). In contrast, only small percentages of OTI-TKO cells were located in the lung parenchyma (7%) and very few expressed CD69 (1.75% of total). The frequencies of CTLs that expressed CD69 in the bloodstream were similar between TKO and WT populations (Figure 3-4D). Taken together, our data show that pulmonary $T_{RM}$ cells require TGF-β during prolonged residence in the lungs.

*Smad4 is required for the formation of KLRG1+ $T_{EFF}$ cells*

To determine whether TGFβ regulates CTL response through Smad-dependent or Smad-independent signaling pathways, we used mice with T cell-specific deletion of Smad4 (dLck-Cre $Smad4^{flox/flox}$)(107). Chimeric mice were made with mixed bone marrow cells from SKO mice and littermates as WT controls. Naïve CD8 T cells from both SKO and WT donors largely maintained a $CD44^{lo}CD62L^{hi}$ resting phenotype and lacked KLRG1 8 weeks after transfer (Figure 3-5A). This contrasted with the TKO CTLs which become activated during the

reconstitution after irradiation (Figure 3-1A). Additional mice were infected with IAV and analyzed by MHCI tetramer staining. Similar numbers of NP-specific CTLs were derived from the SKO and WT donor cells 10dpi and 20dpi after IAV infection (Figure 3-5B). Interestingly, very few SKO CTLs expressed KLRG1, whereas large percentages of CTLs expressed CD103 in the lungs and spleen (Figure 3-5C). This showed that anti-viral CTLs developed reciprocal phenotypes when the TGFβ receptor, or its downstream signaling molecule Smad4, were absent.

To examine whether the kinetics of the $T_{EFF}$ response were regulated through Smad4, recipient mice received mixed populations of $CD44^{lo}$ OTI-SKO and OTI-WT cells 48 hrs before IAV infection and flow analysis was used to monitor the numbers of transferred cells at different times after infection. There was very little difference in the total numbers of OTI-SKO and OTI-WT cells at all time points, yet very few KLRG1+ cells were generated in the absence of Smad4 (Figure 3-6A). We also found no difference in cell proliferation by CFSE-dilution 3.5dpi, or BrdU incorporation 6-10dpi (Figure 3-6B, Figure 3-6C). Therefore, the Smad4-deficient CTLs did not undergo prolonged proliferation and terminal differentiation after IAV infection, which was in complete contrast to the response of CTLs lacking the TGFβ receptor. The OTI-SKO and OTI-WT cells expressed activated caspases-3/7 (Figure 3-6D) and pro-survival molecule Bcl-2 (Figure 3-6E) at similar levels indicating that there was no substantial difference in cell death.

*Pulmonary $T_{RM}$ cells form normally in absence of Smad4*

We next investigated whether Smad4 was required for formation of $T_{RM}$ cells, using CD69 and CD103 expression. Despite the fact that CD103 was widely expressed without Smad4, similar frequencies and numbers of OTI-SKO and OTI-WT cells co-expressed CD69 with CD103 in the lungs 30 dpi (Figure 3-7A, Figure 3-7B black shading). This result indicates that, although TGF-β plays a critical role in the formation of pulmonary $T_{RM}$ cells, Smad4 is not required.

To determine whether Smad4 deletion altered migration of pulmonary CTLs, we used confocal microscopy to compare the distribution of OTI-SKO and OTI-WT cells in the lungs after IAV infection (Figure 3-8A). Images of the lungs showed similar distributions of OTI-SKO and OTI-WT cells 10dpi and 30dpi. Substantial numbers of OTI-SKO cells also expressed CD103 in the airways after the contraction of the $T_{EFF}$ cell response (right columns), indicating normal development/maintenance of pulmonary $T_{RM}$ cells. Flow analysis also showed that most OTI-SKO cells expressed CD11a at high levels 30dpi, confirming that they did not enter lumen of the airways (Figure 3-8B).

We next used intravascular staining to determine which cells were located inside the blood vessels. Similar frequencies of OTI-SKO and OTI-WT cells were found in the blood and tissues (Figure 3-8C, Figure 3-8D). Some OTI-WT cells expressed CD103 in the lung parenchyma (Figure 3-8C), but not in the spleens (Figure 3-8D) or blood (Figure 3-8C, Figure 3-8D). In contrast, CD103 was widely expressed on the OTI-SKO cells, which were equally distributed inside and outside of the blood vessels (Figure 3-8C, Figure 3-8D). Similar numbers of OTI-WT and OTI-SKO cells expressed CD69 together with CD103 in the lung parenchyma (Figure 3-8C). These data indicate that aberrant CD103 expression is not sufficient to increase the size of the $T_{RM}$ population in the lungs.

*Smad4 is required for differentiation of central memory T cells*

Since some OTI-SKO cells were located in the blood stream, we also analyzed the transferred cells for markers of circulating memory CD8 T cells. Flow analysis showed that large numbers of OTI-SKO cells expressed CD103 in the spleen 30 dpi, but lacked CD62L expression indicating that they were not typical central memory T ($T_{CM}$) cells (Figure 3-9A, Figure 3-9B). Yet OTI-SKO cells expressed CCR7, which is another marker of $T_{CM}$ cells, at similar levels as compared to OTI-WT cells (Figure 3-9C, Figure 3-9D). Because $T_{CM}$ cells require CD62L to

access resting lymph nodes via HEVs (108), we analyzed the distribution of transferred cells inside the secondary lymphoid organs by confocal imaging (Figure 3-9E). Substantial populations of OTI-WT and OTI-TKO cells were distributed in the cortex of the inguinal lymph nodes 30 dpi, whereas there were only a few OTI-SKO cells at this location. Still, small populations of OTI-SKO cells, which lacked CD62L, were found in the inguinal lymph nodes by imaging (Figure 3-9E), indicating that normal CCR7 expression on OTI-SKO cells enabled inefficient transendothelial migration in HEVs when CD62L is absent. Therefore Smad4 also plays an important role in the development of $T_{CM}$ cells.

*Smad4 has a TGFβ-independent role in the CD8 T cell response*

Since our data show that TGFβ and Smad4 play very different roles in CD8 T cell differentiation, we further investigated which pathway was dominant. To address this question, we crossed OTI-TKO and OTI-SKO mice to produce progeny lacking both Smad4 and the TGFβ receptor (called OTI-STDKO). Recipient mice received mixed populations of congenically marked donor cells from OTI-STDKO mice and wild type littermates 48h before x31-OVA infection. A kinetic study showed decreased numbers of KLRG1+ OTI-STDKO $T_{EFF}$ cells as compared to OTI-WT cells in lungs and spleens after IAV infection (Figure 3-10A). No difference in cell proliferation was observed either by CFSE dilution or BrdU incorporation between the OTI-WT and OTI-STDKO cells (Figure 3-10B, Figure 3-10C). These results are in contrast to the experiments with CTLs from TGFβRII deficient mice which underwent late proliferation and transitioned to a terminally differentiated KLRG1+ phenotype (Figure 3-2). Thus, these experiments showed that the mutation in Smad4 was dominant and that the CTL response is regulated by a mechanism that does not require the TGFβ receptor.

Because CD103 was widely expressed on SKO cells, we also examined whether TGFβRII was required for CD103 expression when Smad4 was absent. Naïve OTI-WT cells express CD103

which is downregulated upon activation. A small number of OTI-WT cells began to re-express CD103 in the lungs 8dpi, and the size of this subset gradually increased by memory time points, indicating the development of pulmonary $T_{RM}$ cells (Figure 3-11A). Naive OTI-SKO and OTI-STDKO cells expressed CD103 at slightly higher levels than the OTI-WT cells (Figure 3-11A), which was downregulated during TCR stimulation. The OTI-SKO and OTI-STDKO cells both re-expressed CD103 by 6dpi in the lungs and spleens (Figure 3-11A). Some CTLs expressed CD69 together with CD103 indicating that normal numbers of pulmonary $T_{RM}$ cells developed when both TGFβRII and Smad4 were absent (Figure 3-11B). In addition large numbers of OTI-STDKO cells expressed CD103 without CD69 in lungs and spleens (Figure 3-11B). Although TGFβ is critical for CD103 expression and development of $T_{RM}$ cells (64;66;85), these data showed that widespread re-expression of CD103 on OTI-SKO and OTI-STDKO cells, did not require the TGFβ receptor and suggests that Smad4 be a suppressor of CD103 expression.

We also determined whether Smad4 regulates CD62L expression independently of TGFβRII. While high frequencies of OTI-STDKO cells aberrantly expressed CD103 in the spleens and ILNs, very CTLs re-expressed CD62L, while CCR7 expression not undisrupted (Figure 3-11C). Therefore, the OTI-STDKO cells had a similar phenotype to OTI-SKO cells, which suggests that Smad4 has a TGFβRII-independent role in effector and memory CD8 T cell differentiation.

*Delayed viral clearance by Smad4-deficient CTLs after primary infection*

Experiments with a dominant-negative form of TGFβRII have shown that TGFβ can inhibit cytokine production by antigen-specific CD8 T cells (23). We also compared the effector functions of OTI-WT, OTI-TKO, and OTI-SKO cells after *in vitro* stimulation. Each cell population produced large quantities of IFN-γ and TNF after peptide stimulation, confirming that they were functional $T_{EFF}$ cells, despite the differences in CD103 and KLRG-1 expression (Figure 3-12).

To determine whether TGFβ or Smad4 deletion altered immunity against IAVs, mice were infected with a sub-lethal dose of IAVs, and re-challenged with a serologically distinct strain 30 days after primary infection. Similar changes in body weight showed that the TKO mice recovered from primary IAV infection with similar kinetics as WT animals. In contrast, the SKO mice recovered from infection with delayed kinetics (Figure 3-13A&B). The ST-DKO mice showed a similar pattern of weight loss and recovery as SKO mice (Figure 3-13E). Since KLRG1+ CTLs enter the lung parenchyma during acute IAV infection (Figure 3-4), these results indicate that KLRG1+ $T_{EFF}$ cells may participate in viral clearance.

*Smad4 is not required for protection after recall*

Members of our laboratory previously examined heterosubtypic immunity in WT mice and demonstrated that pulmonary $T_{RM}$ cells are crucial for protection during the recall response, while nascent $2^{nd}$ $T_{EFF}$ cells play very little role (61). The protective effects of the $T_{RM}$ cells were evident from early viral clearance and reduced pathogenesis in the lungs (61). To analyze whether TGFβRII or Smad4 play a role in heterosubtypic immunity, separate groups of TKO, SKO and WT mice were infected with X31-OVA (H3N2 serotype) and weighed daily. and the mice were re-challenged 30 days later with WSN-$OVA_1$ (H1N1 serotype). The order of infections was reversed for some experiments. Although the TKO mice underwent similar weight loss as WT mice during primary infection (Figure 3-13A), they recovered slightly slower than the WT group during the recall response (Figure 3-13C). This result was consistent with deficient development of CD103+ $T_{RM}$ cells in these mice. Additional mice will be analyzed for viral titers. In contrast the SKO and ST-DKO mice underwent more severe weight loss and recovered slower than WT mice during primary infection, but no deficit in protective immunity was observed during secondary infection (Figure 3-13D, Figure 3-13F). This result is consistent with normal $T_{RM}$ cell development in the SKO and STDKO mice and an important role in heterosubtypic immunity.

## Discussion

TGF-β is an important regulatory factor for peripheral CD8 T cells, which suppresses responses to self-antigens and prevents autoimmune disease (85). This cytokine also plays a critical role in cell-mediated immunity in mucosal tissues, where virus-specific CTLs use TGFβ-dependent adhesion molecules for local migration. A variety of signaling intermediates act downstream of the TGF-β receptor, including Smad2 and Smad3, which are chaperoned into the nucleus by Smad4 (87). This pathway is involved in differentiation of Th1 cells and production of IgA Abs (81;109), but it is not known to play a major role in CD8 T cell differentiation. In other situations Smad4 chaperones Smad1/5/8 into the nucleus after activation by the receptor for bone morphogenic proteins (BMPs); however, these pathways have not been fully analyzed in immune cells (110). Additional pathways that respond to the TGF-β receptor without involving Smad proteins use MAPKs, Rho-like GTPases, or PI3K as signaling intermediates leading to phosphorylation of Akt/S6/Foxo1/3a (76;80). At this time it is not clear which pathways support cell-mediated immunity and CD103 expression on pulmonary $T_{RM}$ cells.

Our studies add an important piece to the puzzle by showing that Smad4 is not required for the development of CD103+CD69+ $T_{RM}$ cells in the lung, but is required for normal differentiation of multiple subsets of circulating CD8 T cells that use the bloodstream to move around the body. The Smad4-dependent subsets include KLRG1+ $T_{EFF}$ cells, which proliferate extensively in response to cytokine costimulation (29;51), as well as $T_{CM}$ cells which use CD62L to access resting lymph nodes between recurrent infections (55). Substantial numbers of Smad4-deficient CTLs survived the contraction of the $T_{EFF}$ cell response and lacked CD62L, but expressed CCR7 together with CD103, which are not characteristics of effector memory CD8 T cells. This phenotype likely explained why few Smad4-deficient CTLs were found in resting lymph nodes.

There are several potential explanations for the abnormal phenotype of the Smad4-deficient CD8 T cells: 1). It is possible that receptor-activated Smad2/3 proteins can function without Smad4; 2). TGFb signaling via Smad-independent signaling pathways may be enhanced in the absence of Smad4; 3). Smad4 may operate in other signaling pathways which do not require TGFb. Candidate ligands for the unknown pathway might include bone morphogenic proteins or activins. We were able to exclude the first two possibilities by generating CTLs that are deficient for both Smad4 and TGFβRII. The STDKO CTLs developed a similar phenotype as SKO CTLs during IAV infection, which confirms that Smad4 can regulate CD8 T cells independently of TGFβRII. This unknown pathway may be activated by an environmental signal that we refer to as "Smad4 ligand". The reciprocal phenotypes of TKO and SKO CTLs may result from the competition for Smad4, or possible interactions between the TGFβ and Smad4 ligand pathways.

Epithelial cells are an important site of viral replication and release large quantities of infectious virus into the lungs. Irreparable damage can occur when the virus reaches the alveoli and causes severe pulmonary effusion (111). Most $T_{RM}$ cells were embedded in the walls of the large airways, which is an ideal position for controlling viral replication. Although TGF-β plays a minor role in viral clearance during primary infection with mildly pathogenic strains of IAV, deficient generation of $T_{RM}$ cells in the absence of TGFβ had a more serious impact on heterosubtypic immunity, when pulmonary $T_{RM}$ cells provide frontline defenses in the lungs. On the other hand, KLRG1+ cells were dependent on Smad4, which could enter into the lung parenchyma during the acute phase of infection and may participate in viral clearance. Nevertheless, normal recovery of Smad4-deficient mice upon re-challenge confirmed that pulmonary $T_{RM}$ cells can reduce viral burdens with little assistance from nascent $2^{nd}$ $T_{EFF}$ cells generated from circulating memory cells.

In summary, data in this chapter reveal a previously unknown role for Smad4 signaling in the regulation of effector and memory differentiation of CD8 T cells, which is independent of the

TGFβ receptor (Figure 3-14). Smad4 does not regulate the effector functions of CTLs, but is required for the terminal differentiation of KLRG-1+ $T_{EFF}$ cells, by a process that can be inhibited by TGFβ. Smad4 is dispensable for the TGFβ-mediated development of CD103+ $T_{RM}$ cells, which are crucial for protective immunity. We found that Smad4 suppresses aberrant CD103 expression on CTLs in lymphoid organs, and is essential for the development of CD62L+ $T_{CM}$ cells, which were mostly absent from the resting lymph nodes when Smad4 was not expressed. Collectively, these findings provide important insights into the signals that control the distribution of virus-specific CTLs inside the lungs during IAV infection.

Figure 3-1

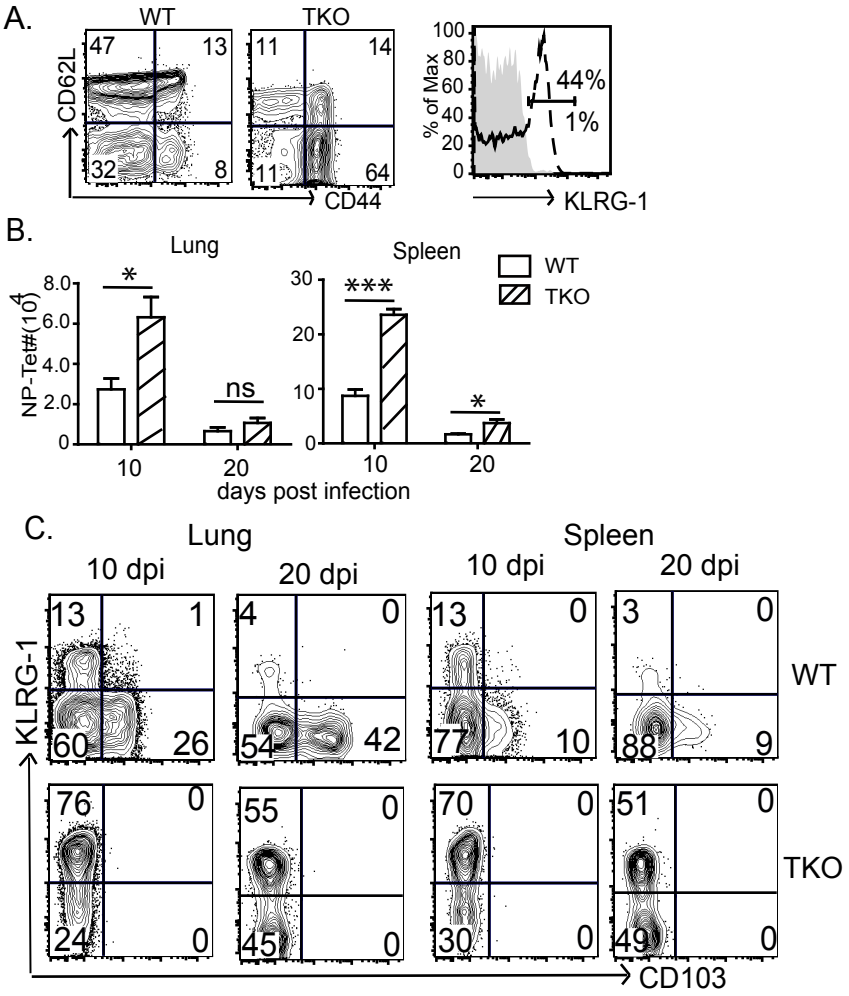
A.
WT
TKO
CD62L
CD44
47
13
32
8
11
14
11
64
% of Max
KLRG-1
44%
1%
B.
Lung
Spleen
WT
TKO
NP-Tet#(10^4)
*
ns
***
*
days post infection
C.
Lung
Spleen
10 dpi
20 dpi
KLRG-1
CD103
WT
TKO

**Figure 3-1. Anti-viral CTLs are regulated by TGF-β**

Chimeric mice were made with mixed bone marrow cells from TKO mice and WT littermates. Plots are representative of two independent experiments with n = 3-4/group.

**(A)** Contour plots show CD44 and CD62L expression on CD8 T cells in peripheral blood of naïve mice 8 weeks after reconstitution. The histogram shows percentages of KLRG1+ within the CD8 gate. TKO (dashed line) and WT (gray fill) are shown.

**(B)** Tetramer analysis was used to calculate the numbers of NP-specific CTLs in the lungs and spleens of chimeric mice after infection with X31-OVA. Donor cells from TKO mice (hatched) and wild type littermates (white). Mean ± SD, *p <0.05, ***p < 0.005.

**(C)** Gated populations of NP-specific CTLs were analyzed for KLRG1 and CD103 expression.

Figure 3-2

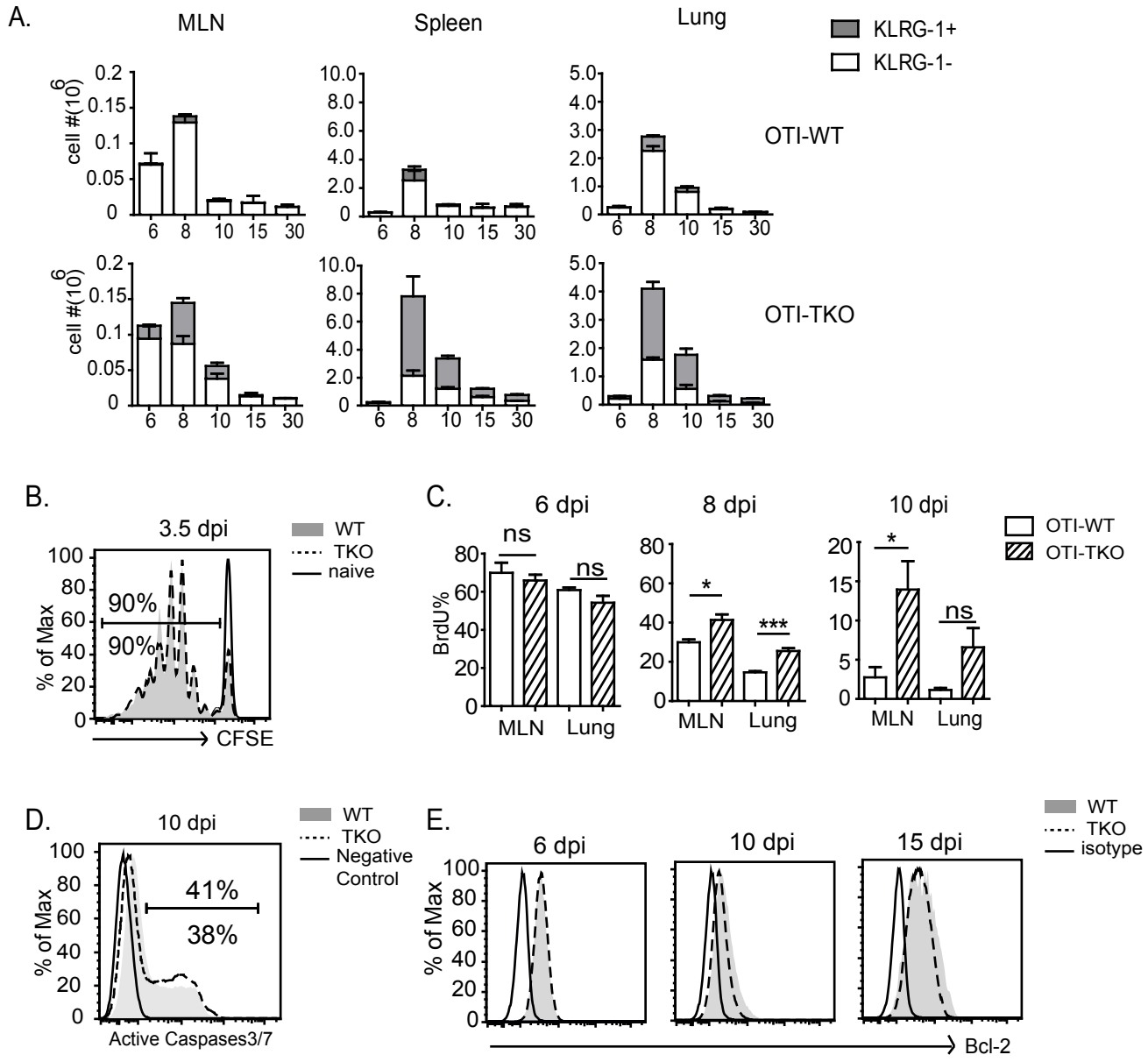
A.
MLN
Spleen
Lung
KLRG-1+
KLRG-1-
cell #(10^6)
OTI-WT
OTI-TKO
B.
3.5 dpi
WT
TKO
naive
90%
90%
% of Max
CFSE
C.
6 dpi
8 dpi
10 dpi
OTI-WT
OTI-TKO
BrdU%
ns
*
***
MLN
Lung
D.
10 dpi
WT
TKO
Negative Control
41%
38%
% of Max
Active Caspases3/7
E.
6 dpi
10 dpi
15 dpi
WT
TKO
isotype
% of Max
Bcl-2

**Figure 3-2. TGF-β suppresses terminal differentiation of KLRG1+ $T_{EFF}$ cells by preventing prolonged cell proliferation**

Congenically marked OTI-WT and OTI-TKO cells were sorted for low CD44 expression and labeled with CFSE-dye before transfer to C57BL/6 recipients. The mice were infected with X31-OVA and BrdU was injected on the days shown. Data are representative of 2 or 3 independent experiments (n = 3-4/group).

**(A)** Bar graphs show the total numbers of transferred cells, including the KLRG1+ subset (gray shading). Mean ± SD. Statistical comparisons are shown in **Table 3-1**.

**(B)** Overlaid histograms show CFSE-dilution 3.5 dpi. OTI-WT (gray fill), TKO (dashed line), and uninfected (solid line).

**(C)** Transferred cells were analyzed 3 hrs (6 dpi) or 6 hrs (8 dpi and 10 dpi) after BrdU injection. Percentages of BrdU+ cells within gated populations of OTI-WT (white bars) and OTI-TKO (hatched bars). Mean ± SD. *p <0.05, ***p < 0.005.

**(D)** Overlaid histograms show gated donor cells analyzed for activated caspase-3/7. OTI-WT (gray fill), OTI-TKO (dashed line), and unstained (solid line).

**(E)** Gated populations of transferred cells were analyzed for Bcl2 expression. OTI-WT (gray fill), OTI-TKO (dashed line), and isotype control (solid line).

Figure 3-3

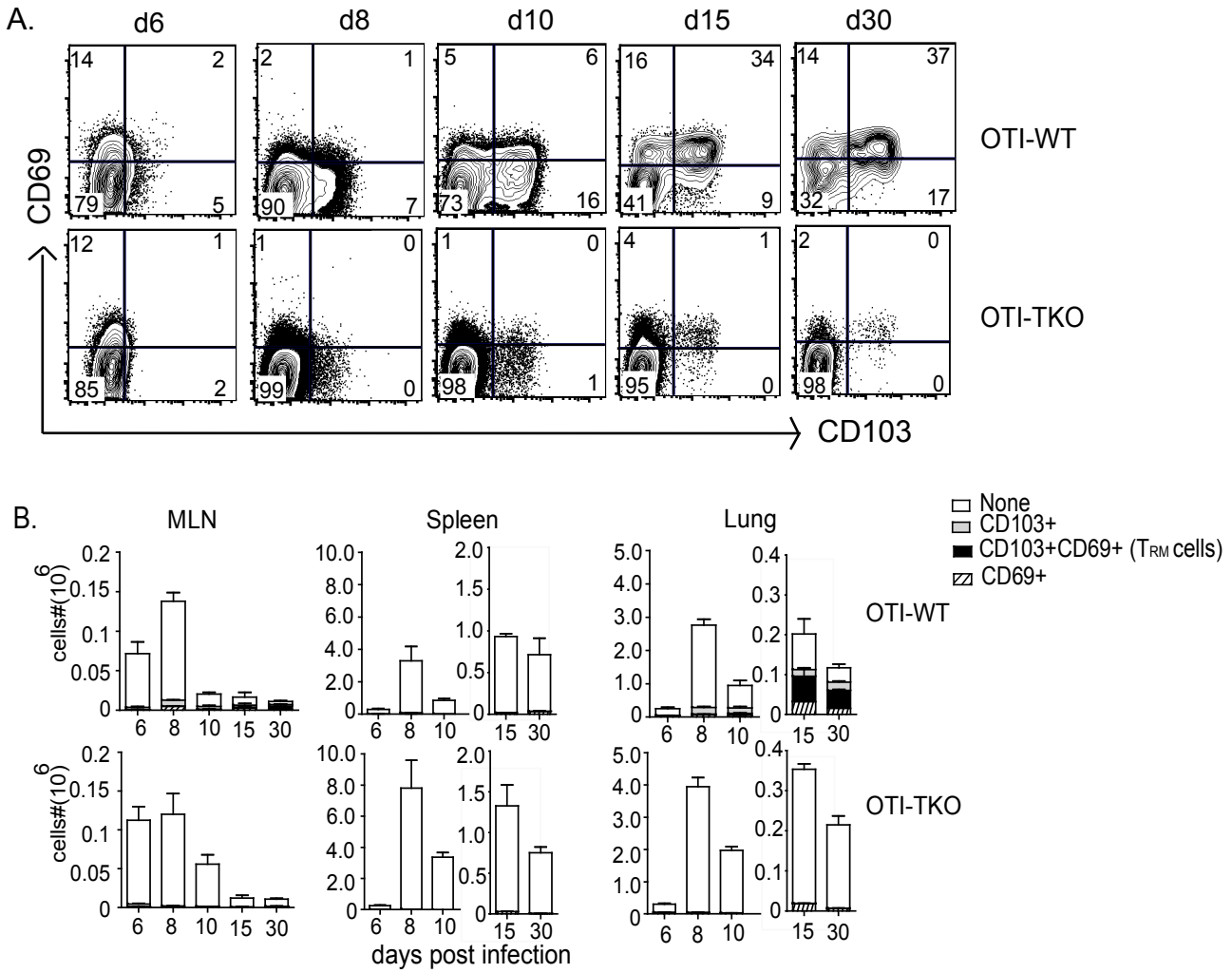
A.
d6
d8
d10
d15
d30
CD69
CD103
OTI-WT
OTI-TKO
14
2
79
5
2
1
90
7
5
6
73
16
16
34
41
9
14
37
32
17
12
1
85
2
1
0
99
0
1
0
98
1
4
1
95
0
2
0
98
0
B.
MLN
Spleen
Lung
None
CD103+
CD103+CD69+ (TRM cells)
CD69+
cells#(10^6)
OTI-WT
OTI-TKO
days post infection

**Figure 3-3. Pulmonary $T_{RM}$ cells require the TGFβ receptor for CD103 expression**

Congenically marked OTI-WT and OTI-TKO cells were sorted for low CD44 expression and transferred to C57BL/6 mice before X31-OVA infection (n = 3-4/group). Three independent experiments gave similar results.

**(A)** CD103 and CD69 expression on donor cells in the lungs.

**(B)** The total numbers of transferred cells were divided into subsets of CD69+ (hatched), CD69+CD103+ (black shading, $T_{RM}$ cells), CD103+ (gray shading), or no markers (white). Bars show means ± SD. Statistical comparisons are shown in **Table 3-2**.

Figure 3-4

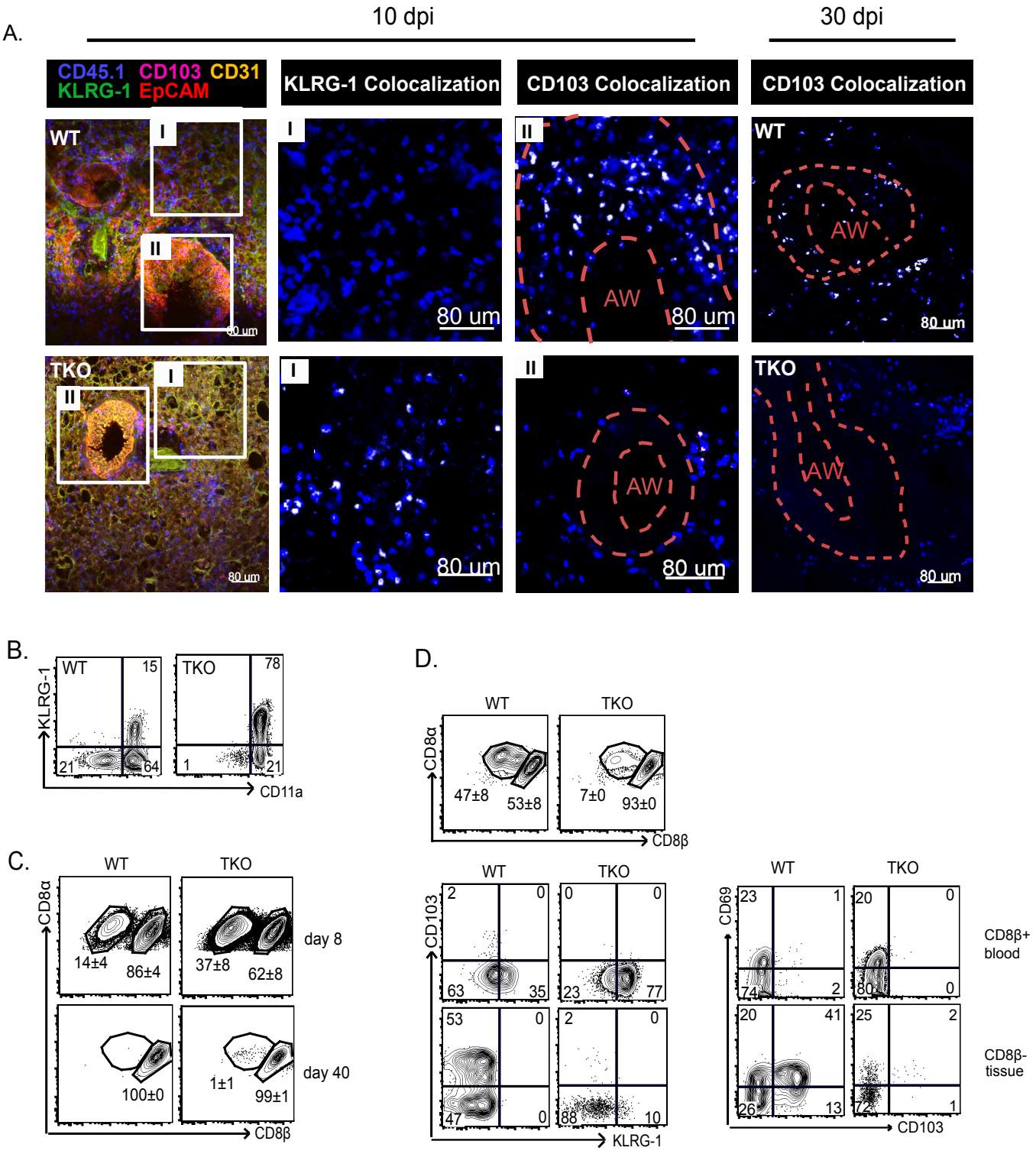
A.
10 dpi
30 dpi
CD45.1 CD103 CD31
KLRG-1 EpCAM
KLRG-1 Colocalization
CD103 Colocalization
CD103 Colocalization
WT
TKO
I
II
AW
80 um
B.
KLRG-1
CD11a
WT
TKO
15
78
21
64
1
21
C.
CD8α
CD8β
WT
TKO
14±4
86±4
37±8
62±8
day 8
100±0
1±1
99±1
day 40
D.
CD8α
CD8β
47±8
53±8
7±0
93±0
CD103
KLRG-1
63
35
23
77
53
47
2
88
10
CD69
CD103
74
2
80
20
41
26
13
25
72
1
CD8β+
blood
CD8β-
tissue

**Figure 3-4. KLRG1+ CTLs persist in the vasculature.**

**(A)** Congenically marked OTI-WT (top) or OTI-TKO (bottom) were sorted for low CD44 expression and transferred to C57BL/6 mice before X31-OVA infection. Lung tissue was stained with antibodies to EpCAM to identify the large airways (red), CD31 for blood vessels (yellow), CD45.1 for transferred cells (blue), KLRG1 (green), and CD103 (magenta). Z-stack images were recorded at original magnification X20 (scale bars, 80 mm). Subregions show **(I)** colocalization between CD45.1 and KLRG1 or **(II)** colocalization between CD45.1 and CD103. Representative data from n = 3/group; two experiments gave similar results.

**(B)** Lungs were harvested 30 dpi and transferred cells were analyzed for CD11a and KLRG1 expression. Two experiments gave similar results (n=3-4/group).

**(C&D)** OTI-WT and OTI-TKO were sorted for low CD44 expression and transferred to C57BL/6 mice before X31-OVA infection. On the days indicated antibodies to CD8β were used for intravascular staining. Two experiments gave similar results (n = 3–4/group).

**(C)** Gated populations of KLRG1+ CTLs were divided into CD8β+ (blood) and CD8β- (tissue resident) subsets.

**(D)** After Intravascular staining the CD8β+ and CD8β- subsets were further analyzed for KLRG1 and CD103 expression (left) or CD69 and CD103 expression (right) 40dpi.

Figure 3-5

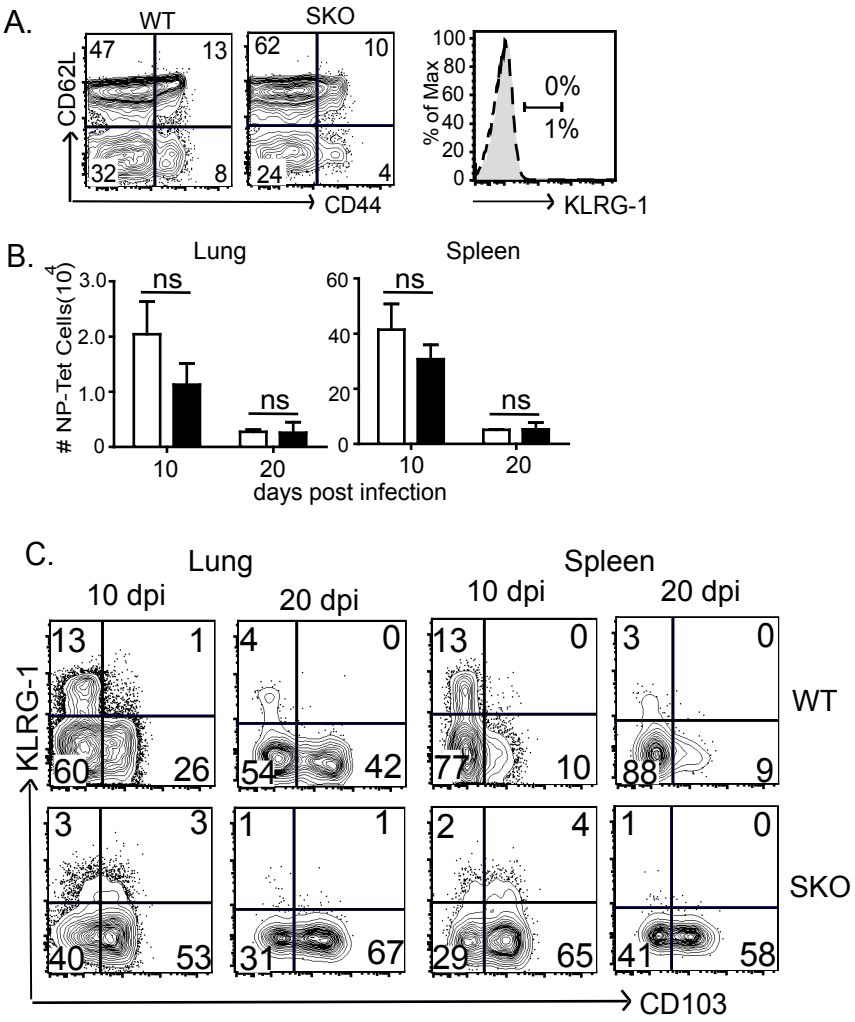
A.
WT
SKO
CD62L
CD44
47
13
32
8
62
10
24
4
% of Max
KLRG-1
0%
1%
B.
Lung
Spleen
# NP-Tet Cells(10^4)
ns
days post infection
C.
Lung
Spleen
10 dpi
20 dpi
KLRG-1
CD103
WT
SKO
13
1
60
26
4
0
54
42
77
10
3
9
88
40
53
31
67
29
65
41
58

**Figure 3-5. CTLs have reciprocal phenotypes in the absence of TGF-βRII or Smad4**

Chimeric mice were made with mixed bone marrow cells from SKO mice and WT littermates.

**(A)** Contour plots show CD8 T cells in peripheral blood of uninfected mice analyzed for CD44 and CD62L expression. The histogram shows that KLRG1 was not expressed. SKO (dashed line) and WT (gray fill) are shown. Plots are representative of two independent experiments with n = 3–4 animals/group.

**(B)** Chimeric mice were infected with X31-OVA and analyzed by MHCI tetramer analysis. Bar graphs show total numbers of NP-specific CTLs in the lungs and spleens. SKO (black) and littermates (white) are shown. Mean ± SD, *p <0.05, ***p < 0.005.

**(C)** Gated populations of NP-specific CTLs were analyzed for KLRG1 and CD103 expression.

Figure 3-6

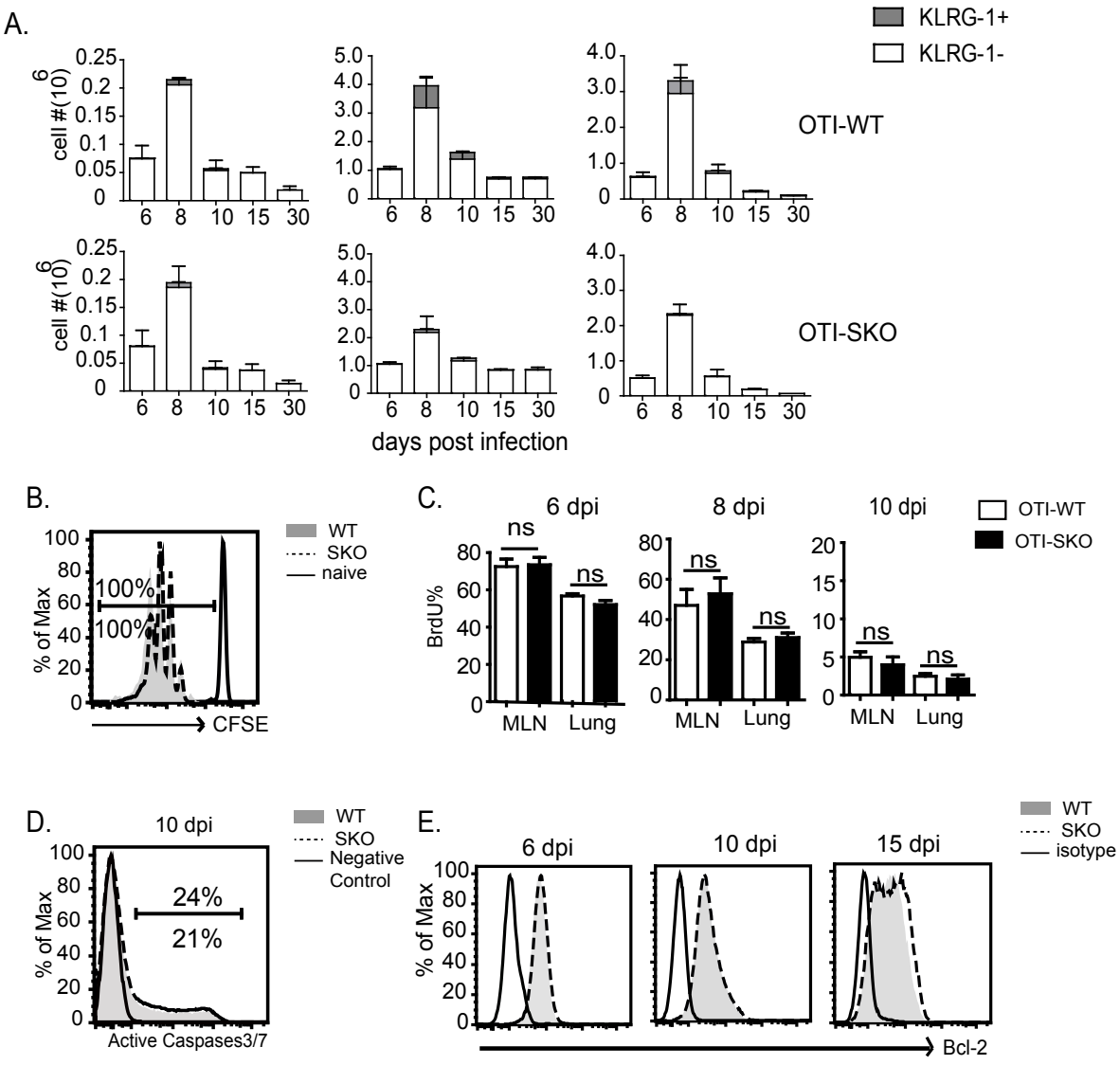
A.
KLRG-1+
KLRG-1-
cell #(10)^6
OTI-WT
OTI-SKO
days post infection
B.
WT
SKO
naive
% of Max
100%
100%
CFSE
C.
6 dpi
8 dpi
10 dpi
OTI-WT
OTI-SKO
BrdU%
ns
MLN
Lung
D.
10 dpi
WT
SKO
Negative Control
% of Max
24%
21%
Active Caspases3/7
E.
6 dpi
10 dpi
15 dpi
WT
SKO
isotype
% of Max
Bcl-2

**Figure 3-6. Smad4 is required for terminal differentiation of KLRG1+ $T_{EFF}$ cells**

Congenically marked OTI-WT and OTI-SKO cells were sorted for low CD44 expression and labeled with CFSE before transfer to C57BL/6 mice. 48hrs later the mice were infected withX31-OVA infection. Some animals were injected with BrdU on the days shown. n = 3–4 animals/group. Two or three independent experiments gave similar results.

**(A)** Bar graphs show total number of transferred CTLs, including the KLRG1+ subset (gray shading). Means (± SD). Statistical comparisons are shown in **Table 3-1**.

**(B)** Donor cells were analyzed for CFSE dilution 3.5 dpi. OTI-WT (gray fill), SKO (dashed line), and uninfected (solid line).

**(C)** Percentages of BrdU+ cells within gated populations of OTI-WT (white bars) and OTI-SKO (black bars). Means ± SD, *p <0.05, ***p < 0.005.

**(D)** Overlaid histograms show gated donor cells analyzed for activated caspase-3/7. OTI-WT (gray fill), OTI-SKO (dashed line), and unstained (solid line).

**(E)** Gated populations of transferred cells were analyzed for Bcl2 expression. OTI-WT (gray fill), OTI-SKO (dashed line), and isotype control (solid line).

Figure 3-7

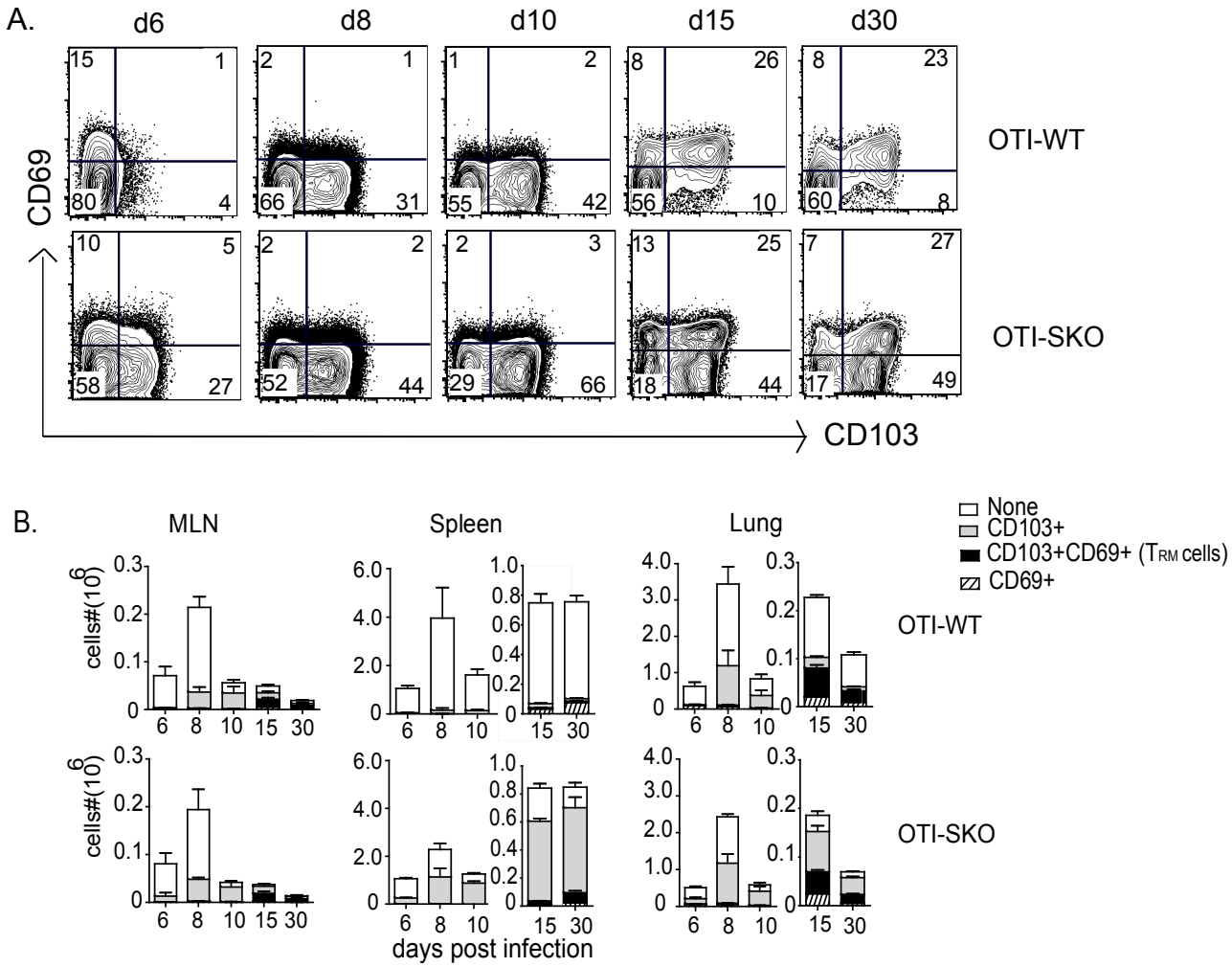
A.
d6
d8
d10
d15
d30
CD69
CD103
OTI-WT
OTI-SKO
15 1 80 4
2 1 66 31
1 2 55 42
8 26 56 10
8 23 60 8
10 5 58 27
2 2 52 44
2 3 29 66
13 25 18 44
7 27 17 49
B.
MLN
Spleen
Lung
None
CD103+
CD103+CD69+ (TRM cells)
CD69+
cells#(10^6)
days post infection
OTI-WT
OTI-SKO

**Figure 3-7. Pulmonary $T_{RM}$ cells form in the absence of Smad4.**

Congenically marked OTI-WT and OTI-SKO cells were sorted for low CD44 expression and transferred to C57BL/6 mice before X31-OVA infection. (n = 3–4 animals/group). Three independent experiments gave similar results

**(A)** CD103 and CD69 expression on donor cells in the lungs.

**(B)** Total numbers of transferred CTLs were subdivided into subsets of CD69+ (hatched), CD69+CD103+ (black shading = $T_{RM}$ cells), CD103+ (gray shading), or no markers (white). Means ± SD. Statistical comparisons are shown in **Table 3-2**.

Figure 3-8

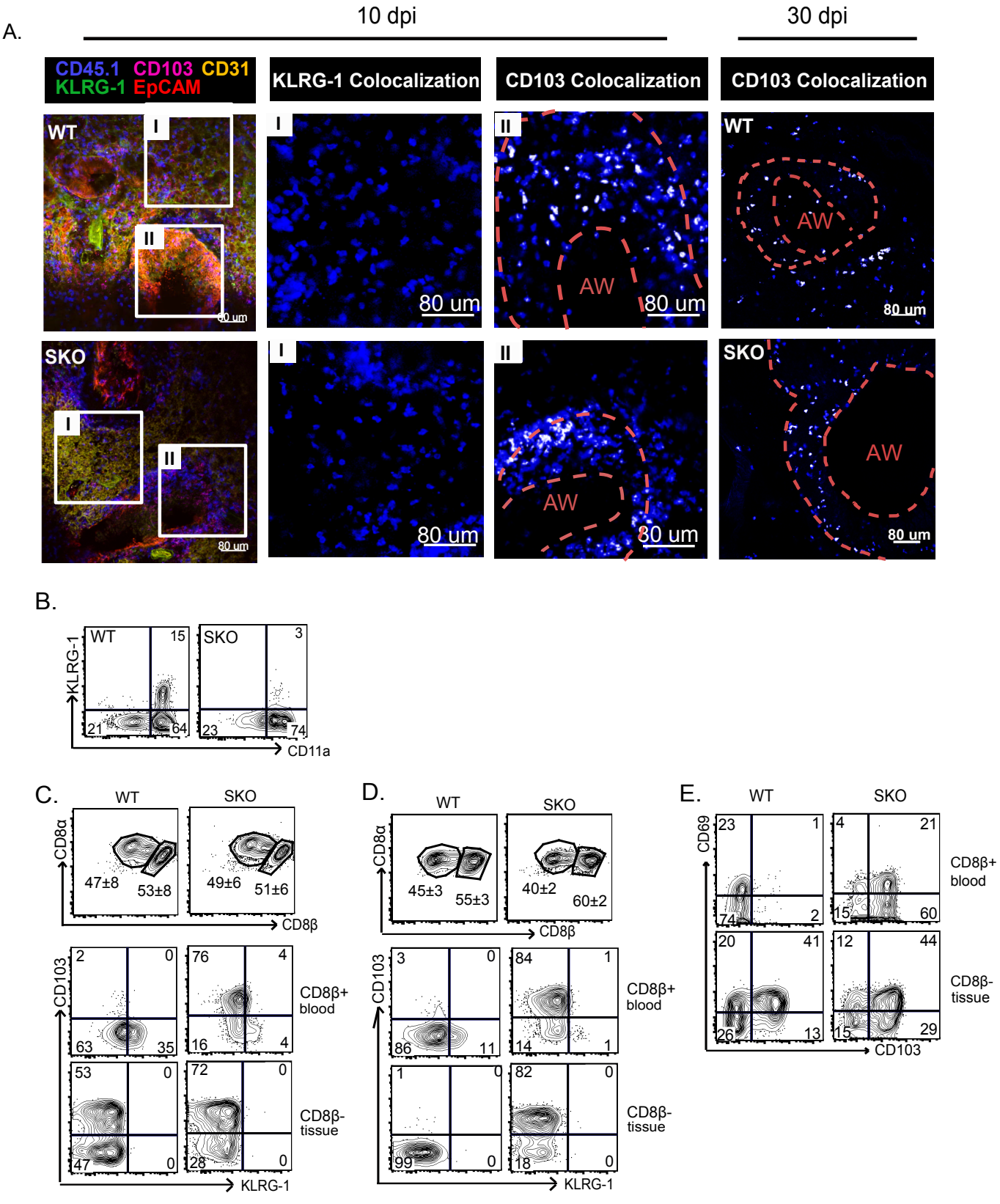
A.
10 dpi
30 dpi
CD45.1 CD103 CD31
KLRG-1 EpCAM
KLRG-1 Colocalization
CD103 Colocalization
CD103 Colocalization
WT
SKO
I
II
AW
80 um
B.
WT
SKO
KLRG-1
CD11a
15
3
21
64
23
74
C.
WT
SKO
CD8α
CD8β
47±8
53±8
49±6
51±6
CD103
CD8β+ blood
CD8β- tissue
KLRG-1
2
0
63
35
76
4
16
4
53
0
47
0
72
0
28
0
D.
WT
SKO
CD8α
CD8β
45±3
55±3
40±2
60±2
CD103
CD8β+ blood
CD8β- tissue
KLRG-1
3
0
86
11
84
1
14
1
1
0
99
0
82
0
18
0
E.
WT
SKO
CD69
CD103
CD8β+ blood
CD8β- tissue
23
1
74
2
4
21
15
60
20
41
26
13
12
44
15
29

**Figure 3-8. Smad4-deficient CTLs are widely distributed inside the lungs.**

Congenically marked OTI-WT (top) or OTI-SKO cells (bottom) were sorted for low CD44 expression and transferred to C57BL/6 mice before X31-OVA infection.

**(A)** Lung tissue was stained with antibodies to EpCAM to identify the large airways (red), CD31 for blood vessels (yellow), CD45.1 for transferred cells (blue), KLRG1 (green), and CD103 (magenta). Z-stack images were recorded at original magnification X20 (scale bars, 80 mm). The subregions show **(I)** colocalization between CD45.1 and KLRG1 or **(II)** colocalization between CD45.1 and CD103. Representative images from n=3/group. Two experiments gave similar results.

**(B)** Lungs were harvested 30 dpi and gated populations of OTI-SKO and OTI-WT cells were analyzed for CD11a and KLRG1 expression; n=3-4/group. Two experiments gave similar results.

**(C-E)** Intravascular staining was used to identify CTLs that were circulating in the blood stream. The transferred cells were divided into CD8β+ and CD8β- subsets and analyzed for KLRG1 and CD103 expression in **(C)** lungs and **(D)** spleens or **(E)** CD69 and CD103 expression in lungs. Representative data are from n = 3-4/group. Two experiments gave similar results.

Figure 3-9

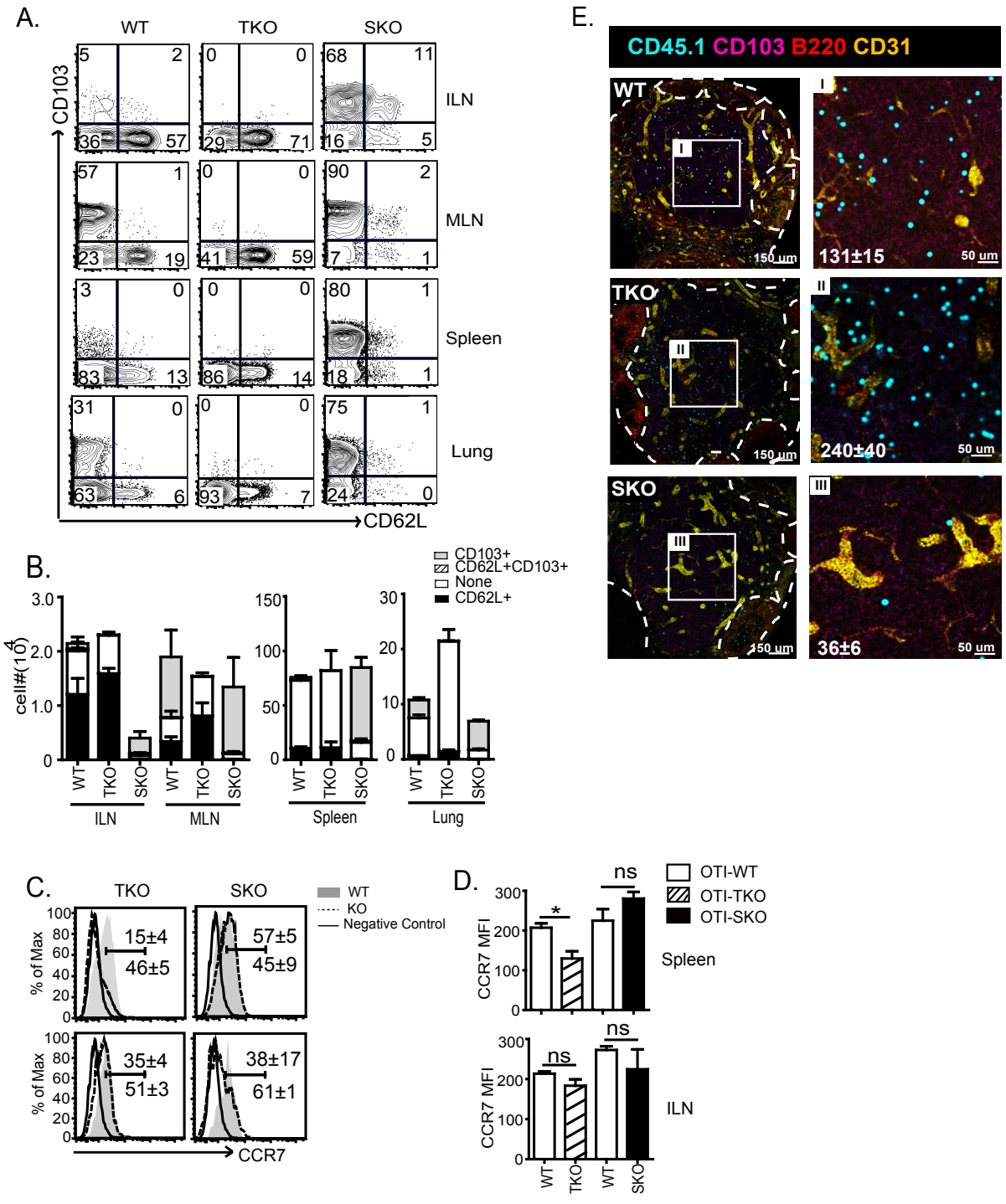
A.
WT
TKO
SKO
CD103
CD62L
ILN
MLN
Spleen
Lung
B.
CD103+
CD62L+CD103+
None
CD62L+
cell#(10^4)
WT
TKO
SKO
ILN
MLN
Spleen
Lung
C.
TKO
SKO
WT
KO
Negative Control
% of Max
15±4
46±5
57±5
45±9
35±4
51±3
38±17
61±1
CCR7
D.
OTI-WT
OTI-TKO
OTI-SKO
CCR7 MFI
ns
*
Spleen
ILN
E.
CD45.1 CD103 B220 CD31
WT
TKO
SKO
131±15
240±40
36±6
150 um
50 um

**Figure 3-9. Smad4 is required for CD62L expression and entry into resting lymph nodes**

Congenically marked OTI-WT, OTI-TKO, and OTI-SKO cells were sorted for low CD44 expression and transferred to C57BL/6 mice before X31-OVA infection. Representative data from n=3-4/group. Two experiments gave similar results.

**(A)** CD62L and CD103 expression on gated OTI-WT, OTI-TKO, and OTI-SKO cells 30 dpi. Dot plots show representative data from 3-4 animals per group. Three independent experiments gave similar results.

**(B)** Numbers of CD62L+ $T_{CM}$ (black), CD62L- (white), CD62L+CD103+ (hatched), and CD62L-CD103+ transition (gray fill) cells 30 dpi. Mean ± SD. Statistical comparisons are shown in **Table 3-3**.

**(C)** Overlaid histograms show CCR7 expression on OTI-WT (gray fill), OTI-SKO or OTI-TKO (dashed line), and isotype control (solid line).

**(D)** Mean fluorescence intensity for CCR7 staining. OTI-TKO (hatched), SKO (black), and littermates (white). *$p < 0.05$.

**(E)** Inguinal lymph nodes were imaged 20 dpi. CD31 (yellow), CD45.1 (blue), B220 (red), CD103 (magenta). **(I-II)** Subregions (white boxes) show enlarged images of transferred CTLs, with the total numbers of cells in the field (means ± SD; n=3). Z-stack images were recorded at original magnification 310.

Figure 3-10

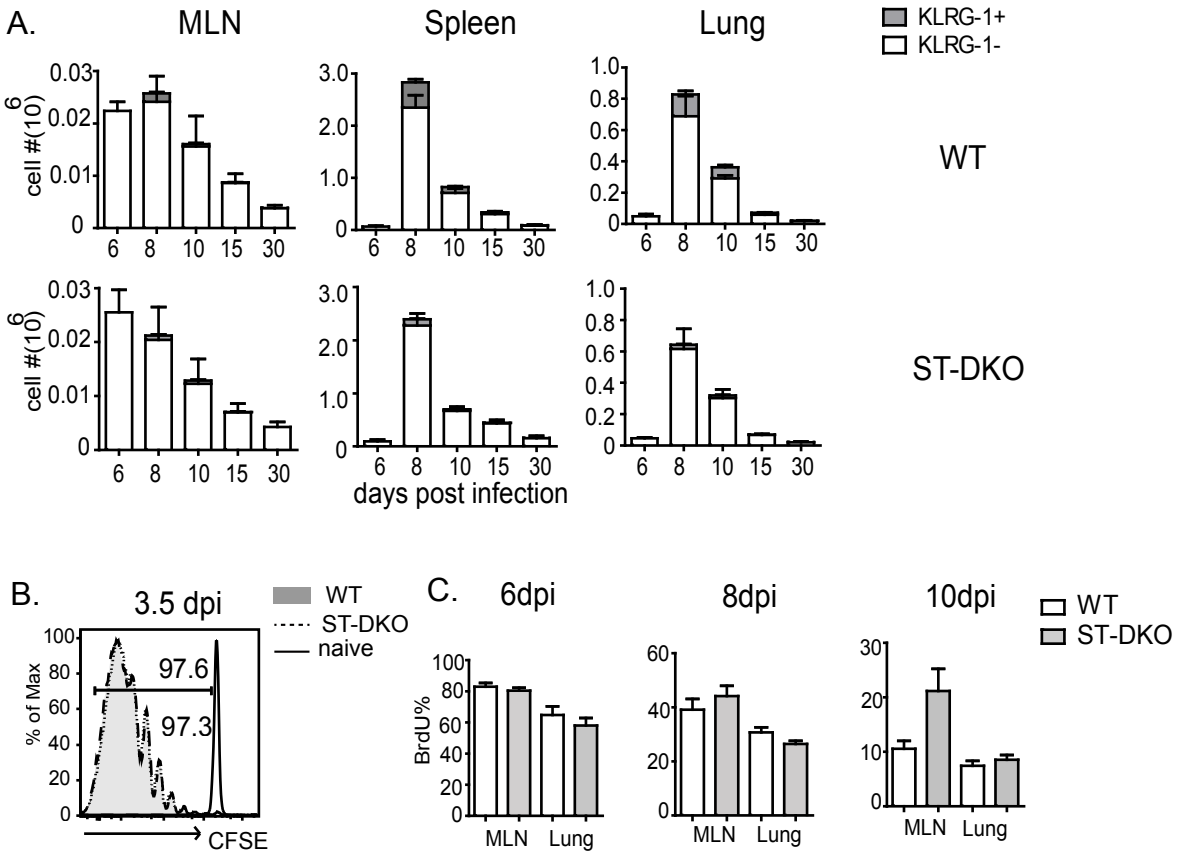
A.
MLN
Spleen
Lung
KLRG-1+
KLRG-1-
WT
ST-DKO
cell #(10)6
days post infection
B.
3.5 dpi
WT
ST-DKO
naive
% of Max
97.6
97.3
CFSE
C.
6dpi
8dpi
10dpi
BrdU%
MLN
Lung

**Figure 3-10. The Smad4-deficient CTLs are not regulated by the TGFβ receptor.**

Congenically marked OTI-WT and OTI ST-DKO cells were sorted for low CD44 expression and transferred to C57BL/6 mice before X31-OVA infection. Data are representative of n=4/group.

**(A)** Numbers of KLRG1+ CTLs (gray shading) and KLRG1- CTLs (white) among donor populations. Mean ± SD.

**(B)** Donor cells were labeled with CFSE-dye and transferred to recipient mice 48 hrs before IAV infection. OTI-WT (Gray fill) and OTI ST-DKO (dashed line) cells were analyzed for CFSE dilution 3.5 dpi (n=4/group), with donor cells in uninfected recipients as control (solid line).

**(C)** BrdU was injected on the days shown, and donor cells were analyzed between 3 and 6 h later. Percentages of BrdU+ cells within gated populations of OTI-WT (white bars) and OTI ST-DKO cells (grey bars). Means ± SD.

Figure 3-11

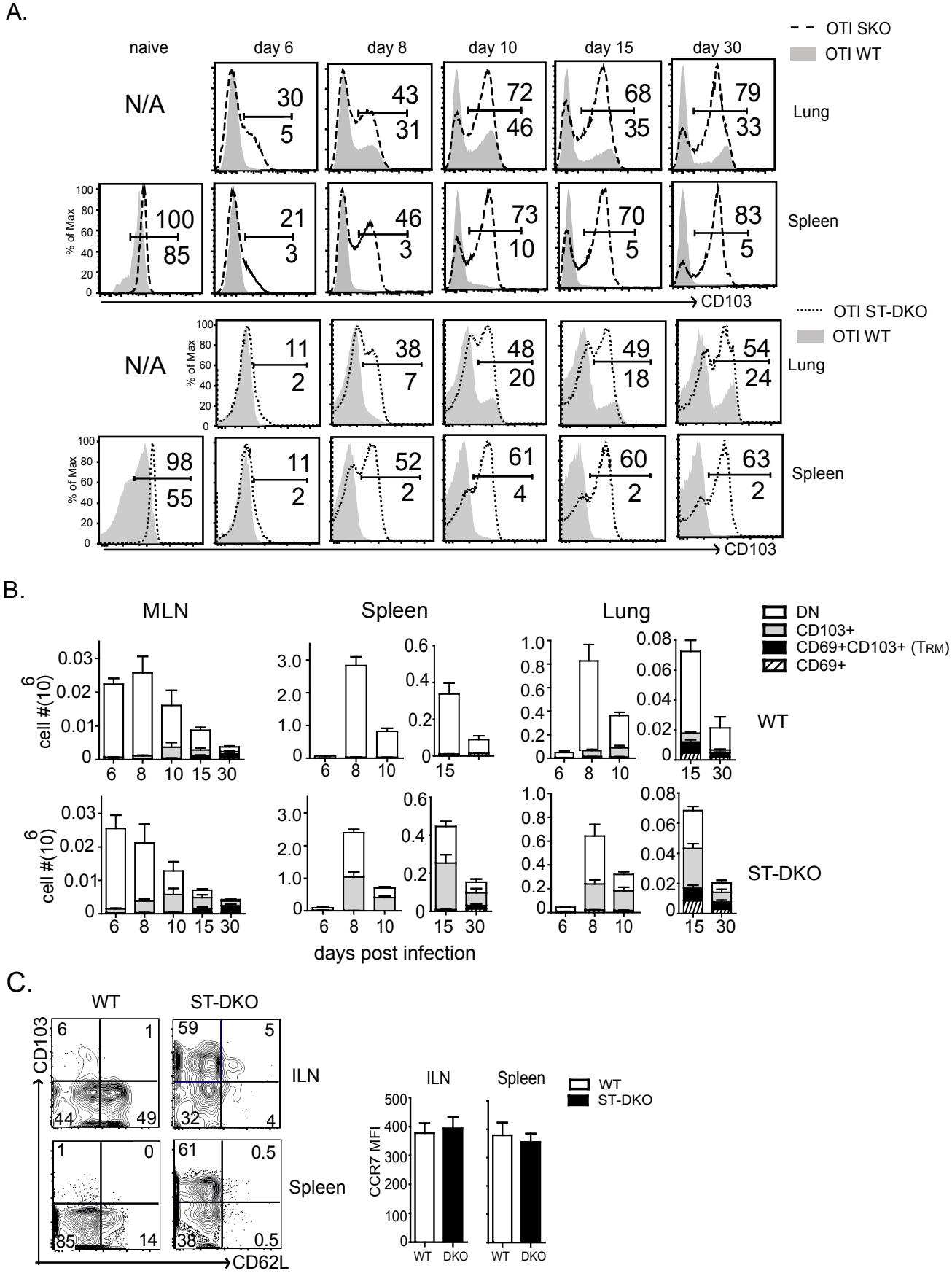
A.
naive
day 6
day 8
day 10
day 15
day 30
OTI SKO
OTI WT
N/A
30
5
43
31
72
46
68
35
79
33
Lung
100
85
21
3
46
3
73
10
70
5
83
5
Spleen
% of Max
CD103
OTI ST-DKO
OTI WT
N/A
11
2
38
7
48
20
49
18
54
24
Lung
98
55
11
2
52
2
61
4
60
2
63
2
Spleen
B.
MLN
Spleen
Lung
DN
CD103+
CD69+CD103+ (TRM)
CD69+
cell #(10)6
WT
ST-DKO
days post infection
C.
WT
ST-DKO
CD103
CD62L
ILN
Spleen
6
1
44
49
59
5
32
4
1
0
85
14
61
0.5
38
0.5
CCR7 MFI
WT
DKO

**Figure 3-11. Smad4 acts as a suppressor of CD103 expression**

OTI-WT, OTI-SKO, and OTI ST-DKO cells were sorted for low CD44 expression and transferred to C57BL/6 mice 48 h before infection with X31-OVA. Data were representative of n=4/group.

**(A)** Kinetics of CD103 expression on OTI-WT (grey shade), OTI-SKO (dashed line, top) and OTI ST-DKO (dotted line, bottom) cells.

**(B)** Bar graphs show total numbers of transferred cells, including subsets of CD69+ (hatched), CD69+CD103+ (black shading, $T_{RM}$ cells), CD103+ (gray shading), or no markers (white). Means ± SD.

**(C)** CD62L and CD103 expression on gated OTI-WT and OTI ST-DKO cells 30 dpi. Bar graphs show mean fluorescence intensity for CCR7 staining on OTI-WT (white) and OTI ST-DKO(black) cells.

Figure 3-12

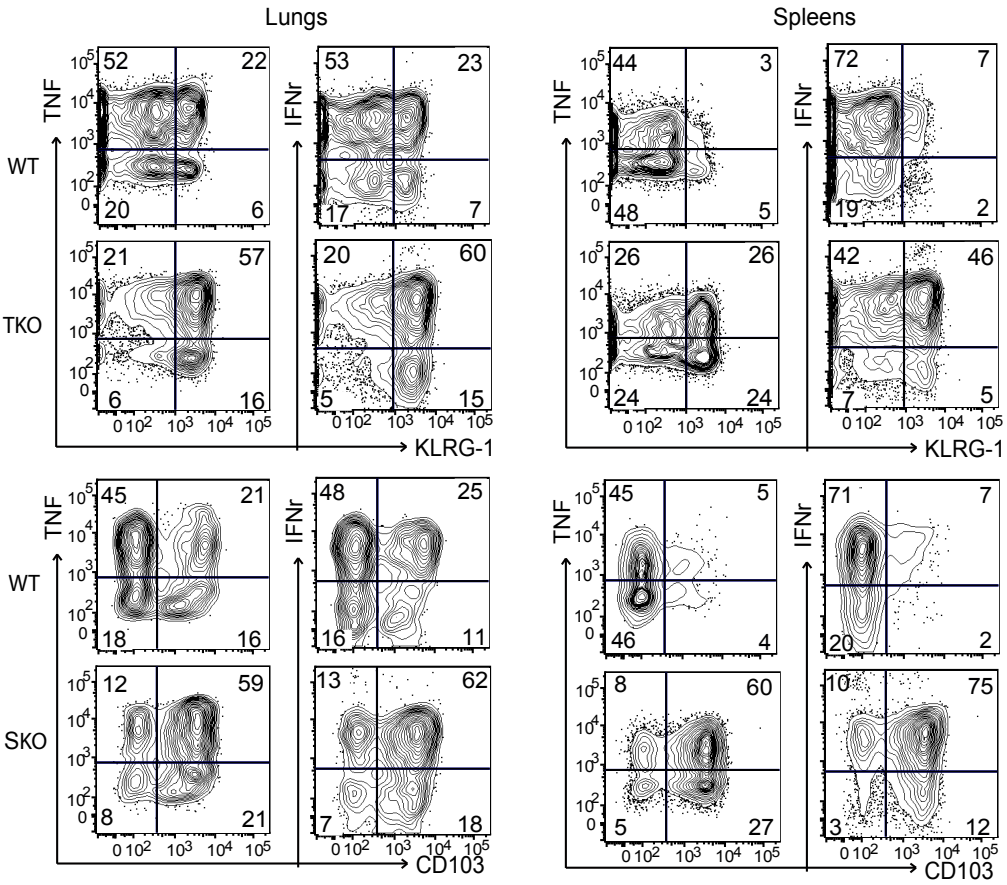
Lungs
Spleens
TNF
IFNr
WT
TKO
SKO
KLRG-1
CD103
52
22
20
6
53
23
17
7
21
57
6
16
20
60
5
15
44
3
48
5
72
7
19
2
26
26
24
24
42
46
7
5
45
21
18
16
48
25
16
11
12
59
8
21
13
62
7
18
45
5
46
4
71
7
20
2
8
60
5
27
10
75
3
12

**Figure 3-12. TGFβ or Smad4 did not alter cytokine production of CTLs**

Congenically marked OTI-WT, OTI-TKO and OTI-SKO cells were sorted for low CD44 expression and transferred to C57BL/6 mice before X31-OVA infection. Lymphocytes were isolated from the lungs 40 dpi and stimulated with SIINFEKL peptide for 5 hrs in the presence of Brefeldin A. Numbers show percentages of donor cells producing IFNγ and TNFα within the KLRG1 and CD103 subsets. Two experiments gave similar results with n=3-4/group.

Figure 3-13

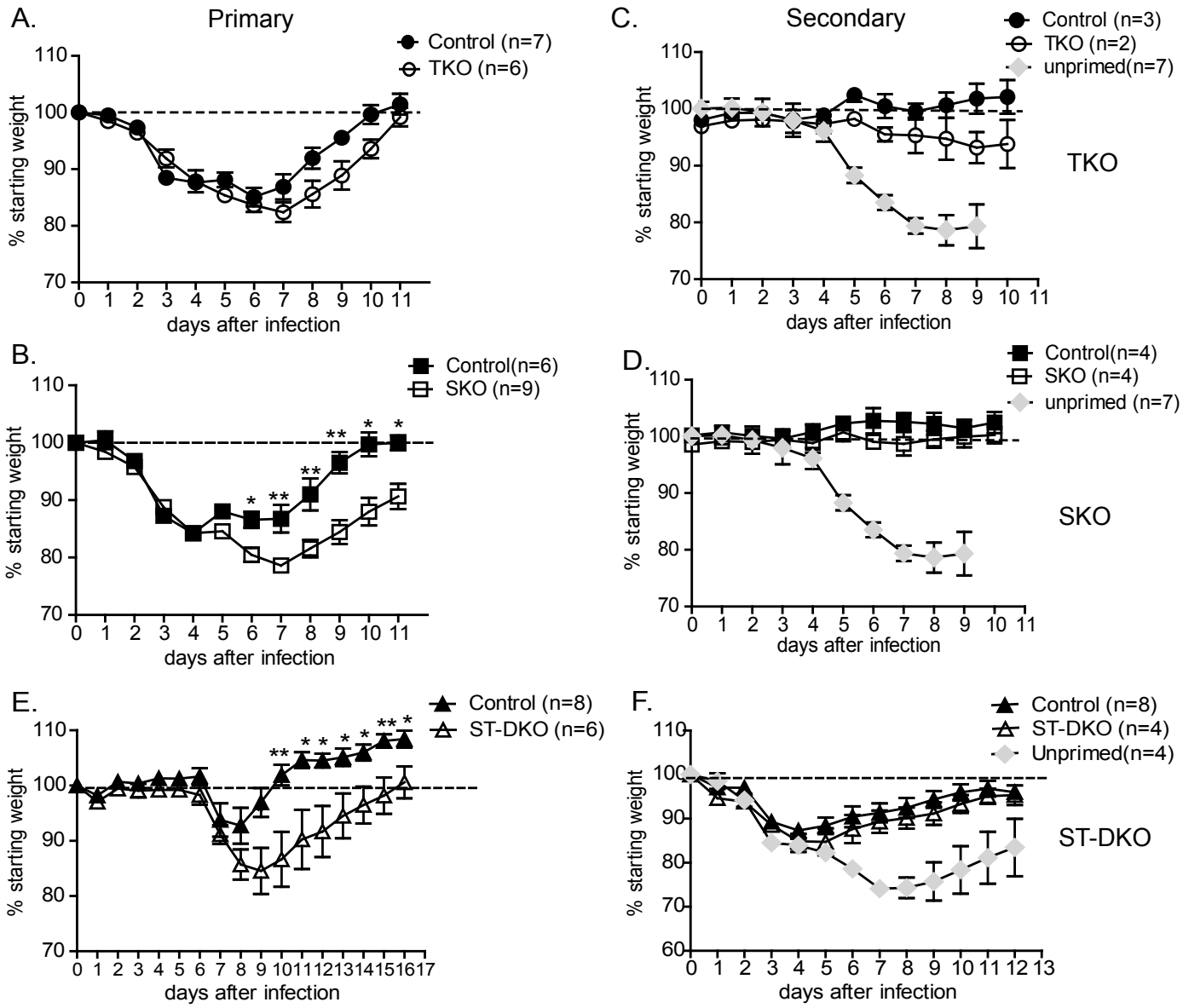
A.
Primary
Control (n=7)
TKO (n=6)
% starting weight
days after infection
B.
Control(n=6)
SKO (n=9)
% starting weight
days after infection
C.
Secondary
Control (n=3)
TKO (n=2)
unprimed(n=7)
TKO
% starting weight
days after infection
D.
Control(n=4)
SKO (n=4)
unprimed (n=7)
SKO
% starting weight
days after infection
E.
Control (n=8)
ST-DKO (n=6)
% starting weight
days after infection
F.
Control (n=8)
ST-DKO (n=4)
Unprimed(n=4)
ST-DKO
% starting weight
days after infection

**Figure 3-13. Smad4 is required for viral clearance during primary infection but not heterosubtypic immunity**

Genetically-modified mice and wild type litter mates were given a sublethal dose of IAV intranasally (i.n.) and weighed daily. 30 dpi after primary infection groups of mice were re-challenged with a heterosubtypic strain of IAV i.n. and weighed daily. The graphs show reduction in body weight as percentage of starting weight. Combined data from two independent experiments are shown. *p <0.05, **p < 0.01.

**(A&B)** Weight loss during primary infection with X31-OVA ($10^3$pfu).

**(A)** TKO = open circle (n=7), littermate controls = black circle (n=6).

**(B)** SKO = open square (n=9), littermate controls = black square (n=6)

**(C&D)** Weight loss during Secondary infection. Mice were primed with X31-OVA ($10^3$pfu) and challenged 30dpi with WSN-$OVA_1$ ($5x10^3$pfu). Naive mice were primed with WSN-$OVA_1$ (5000pfu) as controls.

**(C)** TKO = open circle (n=2), littermate controls = black circle (n=3). Unprimed control = grey square (n =7).

**(D)** SKO = open square (n=4), littermate controls = black square (n=4). Unprimed control = grey square (n =7).

**(E&F)** Weight loss by mice lacking both TGFβ receptor and Smad4 (STDKO). Mice were primed with WSN-$OVA_1$ ($10^3$pfu) and challenged 30dpi with X31-OVA ($5x10^3$pfu).

**(E)** Weight loss during primary infection. ST-DKO = open triangle (n=6), littermate controls = black triangle (n =8).

**(F)** Weight loss during secondary infection. ST-DKO = open triangle (n=4), littermate controls = black triangle (n=8). Naïve mice were infected with 5000pfu X31-OVA as control. Unprimed = grey square (n =4).

Figure 3-14

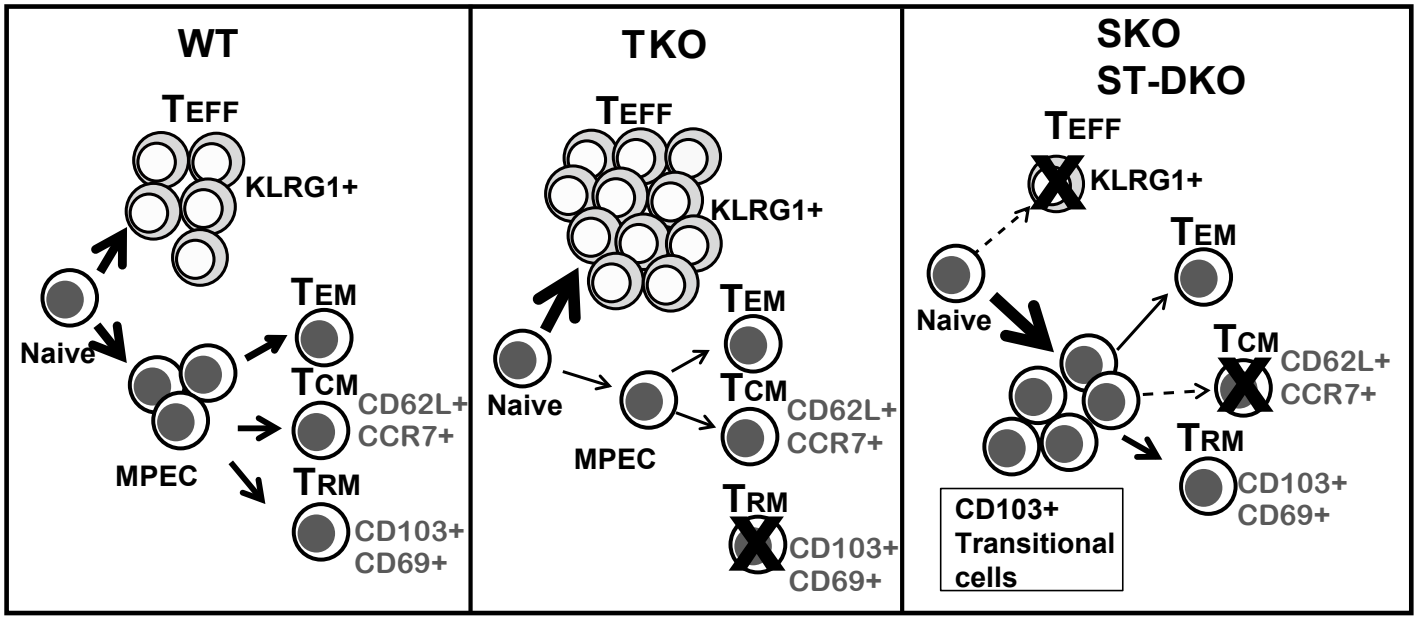
WT
TEFF
KLRG1+
Naive
TEM
TCM
CD62L+
CCR7+
MPEC
TRM
CD103+
CD69+
TKO
TEFF
KLRG1+
TEM
Naive
TCM
CD62L+
CCR7+
MPEC
TRM
CD103+
CD69+
SKO
ST-DKO
TEFF
KLRG1+
TEM
Naive
TCM
CD62L+
CCR7+
TRM
CD103+
CD69+
CD103+
Transitional
cells

**Figure 3-14. Model illustrating the roles of Smad4 and TGFβ during the differentiation of virus-specific CTLs.**

Left panel, Normal CD8 T cells give rise to mixed populations KLRG1+ $T_{EFF}$ cells, CD103+ $T_{RM}$ cells, and circulating memory CD8 T cells. Middle panel, TGF-β signaling reduces the numbers of terminally differentiated $T_{EFF}$ cells and is essential for $T_{RM}$ development. Right panel, Smad4 dependent signaling is required for terminal differentiation of virus-specific $T_{EFF}$ cells and $T_{CM}$ cells.

Table 3-1

OTI-TKO vs. OTI-WT

MLNs

| | KLRG1+ | KLRG1- |
|---|---|---|
| 6d | *** | ns |
| 8d | ** | ns |
| 10d | * | ns |
| 15d | * | ns |
| 30d | *** | ns |

Spleens

| | KLRG1+ | KLRG1- |
|---|---|---|
| 6d | * | ns |
| 8d | * | ns |
| 10d | *** | * |
| 15d | *** | ns |
| 30d | *** | ns |

Lungs

| | KLRG1+ | KLRG1- |
|---|---|---|
| 6d | *** | ns |
| 8d | *** | ** |
| 10d | ** | ns |
| 15d | *** | ns |
| 30d | *** | ns |

**Table 3-1. Statistical comparisons for Figure 3-2.**

An unpaired two-tailed Student's t test was used to compare the numbers of OTI-WT and OTI-TKO after transfer and IAV infection based on expression of KLRG1 (ns = not significant;* $P < 0.05$; ** $P < 0.01$; *** $P < 0.005$). Red lettering indicates larger numbers of mutant CTLs and blue lettering indicates larger numbers of WT CTLs.

Table 3-2

OTI-TKO vs. OTI-WT

MLNs

| | DN | CD103+ | CD69+CD103+ | CD69+ | Total |
|---|---|---|---|---|---|
| 6d | ns | ns | ns | ns | ns |
| 8d | ns | *** | *** | * | ns |
| 10d | * | * | * | ns | ns |
| 15d | ns | ns | ns | ns | ns |
| 30d | * | ns | ns | ns | ns |

Spleens

| | DN | CD103+ | CD69+CD103+ | CD69+ | Total |
|---|---|---|---|---|---|
| 6d | ns | ns | ns | ns | ns |
| 8d | ns | * | ** | ns | ns |
| 10d | *** | ** | *** | ** | *** |
| 15d | ns | *** | ns | ns | ns |
| 30d | ns | * | ns | * | ns |

Lungs

| | DN | CD103+ | CD69+CD103+ | CD69+ | Total |
|---|---|---|---|---|---|
| 6d | ns | * | ns | ns | ns |
| 8d | * | ** | *** | ** | * |
| 10d | ** | ** | ** | * | ns |
| 15d | ** | * | * | ns | ns |
| 30d | ** | *** | *** | * | ** |

**Table 3-2. Statistical comparisons for Figure 3-3.**

An unpaired two-tailed Student's t test was used to compare the numbers of OTI-WT and OTI-TKO after transfer and IAV infection based on expression of CD69 and CD103 (ns = not significant;* P < 0.05; ** P <0.01; *** P < 0.005). Red lettering indicates larger numbers of mutant CTLs and blue lettering indicates larger numbers of WT CTLs.

Table 3-3

OTI-SKO vs. OTI-WT

MLNs

| | KLRG1+ | KLRG1- |
|---|---|---|
| 6d | ns | ns |
| 8d | ns | ns |
| 10d | ns | ns |
| 15d | ns | ns |
| 30d | ns | ns |

Spleens

| | KLRG1+ | KLRG1- |
|---|---|---|
| 6d | ns | ns |
| 8d | * | ns |
| 10d | * | ns |
| 15d | * | ns |
| 30d | *** | ns |

Lungs

| | KLRG1+ | KLRG1- |
|---|---|---|
| 6d | ** | ns |
| 8d | ns | ns |
| 10d | * | ns |
| 15d | ns | ns |
| 30d | *** | ns |

**Table 3-3. Statistical comparisons for Figure 3-6**

An unpaired two-tailed Student's t test was used to compare the numbers of OTI-WT and OTI-TKO after transfer and IAV infection based on expression of KLRG1 (ns = not significant;* $P < 0.05$; ** $P < 0.01$; *** $P < 0.005$). Red lettering indicates larger numbers of mutant CTLs and blue lettering indicates larger numbers of WT CTLs.

Table 3-4

OTI-SKO vs. OTI-WT

MLNs

| | DN | CD103+ | CD69+CD103+ | CD69+ | Total |
|---|---|---|---|---|---|
| 6d | ns | ns | ns | ns | ns |
| 8d | ns | ns | ns | ns | ns |
| 10d | ns | ns | ns | ns | ns |
| 15d | * | ns | ns | ns | ns |
| 30d | * | * | ns | ns | ns |

Spleens

| | DN | CD103+ | CD69+CD103+ | CD69+ | Total |
|---|---|---|---|---|---|
| 6d | ns | ** | * | ns | ns |
| 8d | ns | ** | * | ns | ns |
| 10d | * | ** | ** | * | ns |
| 15d | ** | *** | *** | ** | ns |
| 30d | *** | ** | ** | ** | ns |

Lungs

| | DN | CD103+ | CD69+CD103+ | CD69+ | Total |
|---|---|---|---|---|---|
| 6d | ns | * | * | ns | ns |
| 8d | ns | ns | ns | ns | ns |
| 10d | ns | ns | ns | ns | ns |
| 15d | *** | ** | ns | ns | ns |
| 30d | *** | *** | ns | * | * |

**Table 3-4. Statistical comparisons for Figure 3-7.**

An unpaired two-tailed Student's t test was used to compare the numbers of OTI-WT and OTI-SKO after transfer and IAV infection based on expression of CD69 and CD103 (ns = not significant;* $P < 0.05$; ** $P < 0.01$; *** $P < 0.005$). Red lettering indicates larger numbers of mutant CTLs and blue lettering indicates larger numbers of WT CTLs.

Table 3-5

OTI-TKO vs. OTI-WT

| | DN | CD103+ | CD62L+CD103+ | CD62L+ | Total |
|---|---|---|---|---|---|
| ILN | ns | ** | ns | ns | ns |
| MLN | ns | * | * | ns | ns |
| Spleen | ns | ** | * | ns | ns |
| Lung | ** | *** | ns | ns | ** |

OTI-SKO vs. OTI-WT

| | DN | CD103+ | CD62L+CD103+ | CD62L+ | Total |
|---|---|---|---|---|---|
| ILN | * | ns | ns | * | * |
| MLN | ns | ns | ns | * | ns |
| Spleen | *** | ** | * | ** | ns |
| Lung | ** | * | ns | *** | * |

**Table 3-5. Statistical comparisons for Figure 3-9.**

An unpaired two-tailed Student's t test was used to compare the numbers of transferred OTI-WT OTI-TKO and OTI-SKO cells after X31-OVA infection based on expression of CD103 and CD62L (ns = not significant;* P < 0.05; ** P <0.01; *** P < 0.005). Red lettering indicates larger numbers of mutant CTLs and blue lettering indicates larger numbers of WT CTLs.

# CHAPTER IV

# MECHANISMS OF SMAD4 SIGNALING IN CD8 T CELLS

**Abstract**

The data in the previous chapter show that Smad4 can regulate differentiation of effector and memory CD8 T cells independently of the TGFβ receptor. To further define the signaling pathways, and downstream target genes, we compared the global transcriptional profile of wild type and Smad4-deficient CTLs during IAV infection, using RNA-sequencing and bioinformatics for comparative analysis. The data show that Smad4-deficiency caused major changes in the transcriptional program of early $T_{EFF}$ (EE) cells, including dysregulated expression of several genes that are involved in cell migration and proliferation. In chapter III we showed that late proliferation and terminal differentiation of $T_{EFF}$ cell were suppressed by TGFβ, but were dependent on Smad4. Since cell proliferation is linked to increased energetic demands, we use a Seahorse flux analyzer to compare cellular metabolism in mutant and wild type CTLs during IAV infection. *Ex vivo* analysis showed that CTLs lacking the TGFβ receptor were capable of prolonged glycolysis during the $T_{EFF}$ response. However this effect was not seen in EE cells lacking Smad4, which showed signs of enhanced mitochondrial biogenesis. Previous studies have shown that pro-inflammatory cytokines provide a third signal during CD8 T cell differentiation and promote terminal differentiation of $T_{EFF}$ cells. The RNA-sequencing suggested that CTLs lacking Smad4 express the IL-12 receptor at reduced levels, and we found that the cells did not signal via STAT4 efficiently during *in vitro* stimulation with recombinant cytokine. We also found that the transcriptional regulator Eomesodermin was expressed at reduced levels in the Smad4-deficient cells, whereas CTLs lacking the TGFβ receptor expressed Eomesodermin at high levels. Together these data indicate that regulation of the CTL response via Smad4 involves a cooperative response with IL-12 and some T-box transcription factors.

## Introduction

Our results in Chapter 3 demonstrate that Smad4 deletion led to significantly altered effector and memory CD8 T cell differentiation independently of the TGFβ receptor. CD8 T cell responses are mainly governed by signaling from the T cell receptor (TCR) (signal 1), co-stimulatory molecules (signal 2) and pro inflammatory cytokines (signal 3) (112). All three signals are present during infection *in vivo*, and antigen-specific CTLs integrate the strength and duration of these signals to regulate their transcriptional profiles. We previously showed that deletion of TGFβRII, but not Smad4, led to late proliferation and terminal differentiation of $T_{EFF}$ cells (51). Since cell proliferation is usually supported by increased metabolism (113;114), we used RNA-sequencing to investigate whether TGFβ or Smad4 regulate the expression levels of genes that are involved in cellular metabolism and migration.

## Major metabolic changes during T cell activation.

The metabolic requirements of CD8 T cells change during the response to infection and reflect remodeling of diverse metabolic pathways (Figure 4-1). Naïve CD8 T cells rely on fatty acid oxidation (FAO), or oxidative phosphorylation (OXPHOS) of glucose-derived pyruvate in the mitochondria for energy generation. This process begins in the cytosol, when glucose is converted to pyruvate (Figure 4-1, Green box) and enters the mitochondria. In resting cells, pyruvate is converted to acetyl coenzyme A (CoA) and oxidized in the tricarboxylic acid (TCA) cycle to generate NADPH, which fuels ATP production via the electron transport chain (Figure 4-1, yellow box)(115). Upon activation, CTLs switch to aerobic glycolysis when glucose is fermented into lactate despite the presence of sufficient oxygen (116). Glycolysis only produces 2 molecules of adenosine triphosphate (ATP) per glucose, while 36 molecules of ATP are generated from one molecule of glucose by OXPHOS. This switch is required to generate the metabolic intermediates that are used to increase biomass during cell proliferation and cytokine

production, and also helps maintain the redox (NAD+/NADH) balance in activated CTLs (117). Glycolysis produces glycose-6-phosphate, which supports nucleotide synthesis via the pentose phosphate pathway, and 3-phosphoglycerate (3-PG) which can serve as the substrate for serine biosynthesis (116;117). Resting cells use the TCA cycle to convert acetyl-CoA and oxaloacetate to citrate and generate substrates for the electron transport chain. In contrast, activated cells shuttle citrate back to the cytosol, where it is converted back Acetyl-CoA and used as a substrate for de novo lipid synthesis (Figure 4-1, blue box). Acetyl-CoA carboxylase (ACCs) catalyzes the first step of fatty acid synthesis (FAS) to generate malonyl-CoA, which is a potent suppressor of FAO (118;119). Recent studies have shown that T cells can adapt to low availability of glucose by using glutamine for OXPHOS in the mitochondria (120). While $T_{EFF}$ cells survive and proliferate in the absence of glucose, cytokine expression is critically dependent on the availability of glucose and anabolic metabolism (117;120). After the contraction of the $T_{EFF}$ response, memory CD8 T cells switch back to OXPHOS (121;122). Unlike naïve T cells which are metabolically quiescent and $T_{EFF}$ cells which are metabolically active, memory CD8 T cells are considered to be “metabolically primed” (114). Memory cells have enhanced mitochondria mass and increased spare respiratory capacity, which not only supports long-term survival but also provides a bioenergetic advantage for rapid ATP production upon re-exposure to antigen (123;124). Interestingly, memory T cells retain the machinery for glycolysis and lipid synthesis, which are is not present in naïve CD8 T cells. A recent study showed that memory CD8 T cells cannot adsorb free fatty acids very efficiently, and thus use extracellular glucose to fuel FAO and OXPHOS. During this process lipids are synthesized by lysosomal acid lipase (LAL)-mediated lipolysis of triglyceride (TAG) (124). The glycerol channel aquaporin 9 (AOP 9), which is induced by IL-7, is required for glycerol import into memory CD8 T cells and subsequent synthesis of TAG (125).

**Signaling pathways that regulate T cell metabolism**

The metabolic profiles of antigen-specific CD8 T cells are regulated by environmental signals during infection (126). Early after activation, the metabolic switch to enhanced glycolysis is mediated by signals from the TCR, costimulation via CD28 and growth factors such as IL-2 or other pro-inflammatory cytokines. These signals *upregulate c-Myc expression and stabilize hypoxia-induced factor 1α (HIF-1α), which are key regulators of the glycolytic switch* (116;127). These signals also significantly enhance the activity of mammalian target of rapamycin (mTOR) complexes via the PI3K/Akt pathway, which plays a key role in differentiation of $T_{EFF}$ cells. Studies have shown that inhibiting mTOR using rapamycin, or activating AMPK with metformin, enhances the generation of memory CD8 T cells (128;129). On the other hand, deficiencies in TSC1/2 (upstream inhibitor of mTOR), LKB1 (upstream activator of AMPK) or AMPKα1 leads to sustained glycolytic activity and defective development of memory cells (130-132). During memory generation, AMP-activated protein kinase (AMPK) is activated in response to decreased cellular energy (i.e. increased AMP/ATP ratio), to promote FAO and suppress glycolysis (132), while IL-15 is essential for the homeostasis of memory CD8 T cells and enhanced mitochondrial biogenesis (123).

**Transcriptional control of CD8 T cell differentiation**

Environmental signals govern the expression levels of several key transcription factors that determine the fate of $T_{EFF}$ cells (112;133). Some pairs of transcription factors function in a reciprocal way during CD8 T cell differentiation. Examples include the T-box transcription factor T-bet, which coordinates its actions with the downstream transcription factor Zeb2 (134;135) thus creating a gradient effect on the numbers of terminally-differentiated $T_{EFF}$ cells (29). T-bet is positively regulated by pro-inflammatory cytokines such as IL-12, which links inflammation with expansion and terminal differentiation (28). In contrast, Eomesodermin (Eomes), which is

homologous to T-bet in the DNA-binding domain, facilitates long-term persistence of memory T cells (136). Another example of a counter-regulatory pathway involves B lymphocyte-induced maturation protein-1 (Blimp-1) and B-cell lymphoma 6 (Bcl-6). Blimp-1 expression is induced by IL-2 and represses the expression of Bcl-6, thereby promoting effector functions and memory formation (137;138). In addition, two inhibitors of DNA binding proteins (Id2 and Id3) work together, since high expression of Id3 in EE cells preferentially induces long-lived memory cells, while Id2 promotes the survival of terminally differentiated $T_{EFF}$ cells (139). Reciprocal regulation can also occur via STAT3 and STAT4, which promote distinct $T_{EFF}$ cell fates. STAT4 activity is induced by IL-12 and/or type I IFN, to increase T-bet expression and terminal differentiation of $T_{EFF}$ cells (140). In contrast, STAT3 is activated by IL-10 and/or IL-21 to promote memory T cell development by inducing Bcl6, Eomes and the suppressor of cytokine signaling 3 (SOCS3), which in turn dampen the response to IL-12 (141). Meta-analyses of gene-expression profiles demonstrate that the cell-fate decisions of $T_{EFF}$ cells are controlled by a complex transcriptional network, rather than a single 'master regulator' (142;143). Since our data show that the formation of KLRG1+ $T_{EFF}$ cells is reciprocally governed by TGFβ and Smad4, we further examined whether deletion of Smad4 interfered with the pathways that regulate key transcription factors.

**Major goals for chapter 4:**

**Aim 2.1** To identify transcriptional targets of Smad4 signaling in activated CTLs

**Aim 2.2** To examine whether Smad4 is involved in regulation of cellular metabolism after CD8 T cell activation

**Aim 2.3** To determine whether Smad4 regulates the CTL response to IL-12.

## Results

*Transcriptional profiles regulated by Smad4*

Our results in chapter 3 suggest that Smad4 plays a previously unappreciated role in regulation of the CD8 T cell response, which is independent of TGFβ. Therefore we analyzed the gene profiles of activated OTI-WT and OTI-SKO cells by RNA-sequencing to identify the transcription program that is regulated by Smad4. Equal numbers of OTI-WT and OTI-SKO cells were transferred into recipient mice 48h before X31-OVA infection as in our previous experiments. The transferred cells were sorted from the spleens 6dpi for RNA-sequencing (RNA-Seq), a time point when the majority of the OTI-WT and OTI-SKO cells maintained an early effector phenotype ($KLRG1^{lo}CD127^{lo}CD103^{lo}CD44^{hi}$) (Figure 4-2).

RNA-Seq identified 197 genes with differential expression levels of greater that 2-fold between the OTI-SKO and OTI-WT cells (Figure 4-3, Table 4-1). Among these genes 138 genes were upregulated in absence of Smad4 (red) and 59 genes were downregulated (blue). The Ingenuity pathway analysis (IPA) is web-based software that is used for the analysis and interpretation of RNA-Seq data based on the manually curated Ingenuity Knowledge Database (http://www.ingenuity.com/products/ipa). IPA was used to analyze the genes with significantly different expression levels in our RNA-Seq, and showed that 78 genes were associated with 'cellular movement' (Figure 4-4A). These dysregulated genes included adhesion molecules such as integrins and chemokine receptors (Figure 4-4B). As expected, transcription of the *Itgae* gene which encodes CD103 was highly upregulated in the absence of Smad4 ($log_2$=4.18), even though the donor cells were sorted for low CD103 expression early in the response. In contrast, transcription of the *Sell* gene (CD62L) was down-regulated in the OTI-SKO cells by 6dpi ($log_2$=-1.26).

IPA also identified significant changes in the transcription levels of 77 genes that are involved in 'Cell Growth and Proliferation' as well as 84 genes that are involved in 'Cell Death and Survival' including many genes that are involved in signaling downstream of costimulatory molecules (signal 2) and cytokines (signal 3) which are known to play important roles in the proliferation and survival of $T_{EFF}$ cells during infection (Figure 4-4A, Figure 4-4B). The IL-7 receptor (*Il7r* or CD127) was up-regulated in EE cells from OTI-SKO mice ($log_2$=1.15), which is consistent with preferential formation of memory precursors. On the other hand a subunit of the high affinity IL-12 receptor (*Il12rb2*) was downregulated in the OTI-SKO cells ($log_2$=-1.12). Although studies have shown that IL-12 signaling promotes terminal differentiation of KLRG1+ $T_{EFF}$ cells by inducing the expression of the transcription factor T-bet (29), there was very little difference in the transcription levels of T-bet in Smad4-deficient CTLs during IAV infection. In contrast the ligand for CD40 (*cd40lg)* was transcribed at reduced levels in the OTI-SKO cells ($log_2$=-1.09). While CD40L is mostly known for its role in CD4 T cell-mediated help (144); expression is upregulated in activated CD8 T cells and thus promotes IL-12 production from CD8α+ DCs (145). Although our RNA-Seq did not reveal a significant difference in *Klrg1* transcription, a related gene (*Klre1)* which has no known function was significantly downregulated in the OTI-SKO cells (log2= -1.05). The literature also shows low expression of this gene in memory precursors, relative to terminally differentiated $T_{EFF}$ cells (29).

Our RNA-Seq identified changes in the expression levels of multiple transcription factors which are known to regulate the CD8 T cell response (Figure 4-4B). A recent study showed that downregulation of Eomes is essential for the development of CD103+ $T_{RM}$ cells in the skin (146). In another study downregulation of Eomes led to increased expression of the TGFβ receptor, while TGFβ signaling can suppress Eomes expression (146). Furthermore, deletion of Eomes resulted in diminished numbers of $T_{CM}$ cells (147). We found that Eomes was significantly downregulated in the OTI-SKO cells (log2= -1.67), which was consistent with widespread

CD103 expression and deficient development of CD62L+ $T_{CM}$ cells. Other genes that were highly expressed in the OTI-SKO cells included the *Ahr* gene (log2= 1.81) which encodes the ligand for the aryl hydrocarbon receptor (AHR). This pathway is involved in the maintenance of skin $T_{RM}$ cells, as well as skin and intestinal γδ T cells (40;41).

Together the transcriptional changes that were observed in the absence of Smad4 suggest that anti-viral CTLs acquire a transcriptional signature of $T_{RM}$ cells during an early phase of the CTL response to IAV infection. We used gene set enrichment analysis (GSEA) to compare data sets from the literature with the transcriptional changes identified in our RNA-Seq. The reference data set was comprised of genes that were upregulated more than 4-fold in $T_{RM}$ cells that were isolated from the lungs during IAV infection, relative to $T_{CM}$ cells isolated from the spleens of HSV infected mice (62). A comparison between this reference set and our RNA-seq data, showed significant enrichment for the transcriptional profile of OTI-SKO cells (Figure 4-4C). A core signature for $T_{RM}$ cells was recently identified by comparing the transcripts in $T_{RM}$ cells from the skin, gut and lungs with $T_{CM}$ and $T_{EM}$ cells in the spleens (62). Many of the genes that were identified in this study were also dysregulated in our RNA-seq, including *Itgae* and *Eomes* (Figure 4-4D). Since the EE cells from Smad4 KO mice were transcriptionally programmed towards $T_{RM}$ cell development, we postulate that Smad4 regulates memory CD8 T cell differentiation during an early stage of the CTL response.

*Smad4 regulates the transcription of genes involved in cellular metabolism*

Data from autoimmunity and tumor models indicate that Smad4 has a TGFβ receptor-independent role in promoting T cell proliferation by directly regulating c-Myc expression and DNA binding (148). Our RNA-Seq data showed that c-Myc was significantly downregulated in the absence of Smad4 ($log_2$=-1.23) (Figure 4-4B). In contrast, the *myc* oncogene is highly expressed in many types of tumor cells and is upregulated in $T_{EFF}$ cells from normal mice,

causing metabolic reprogramming toward increased glycolysis and glutaminolysis (116). Conditional deletion of c-Myc from $T_{EFF}$ cells abrogated cell growth and proliferation after antigen stimulation (116). The *Tfap4* gene encodes activating enhancer binding protein 4 (AP4), which is a the transcription factor that acts downstream of c-Myc and drives clonal expansion of antigen-specific CTLs (149). Our data showed significantly lower mRNA transcription of *Tfap4* ($log_2$=-1.04) in OTI-SKO cells (Figure 4-4B). Since the RNA-seq data showed low levels of c-Myc and AP4 expression in Smad4-deficient cells, we used using Gene Set Enrichment Analysis (GSEA) to other dysregulated genes in OTI-SKO cells with the transcriptional signature of *in vitro* activated CD8 T cells after conditional deletion of c-Myc (149). This study showed that many genes which were upregulated more than 4-fold in c-Myc-deficient CD8 T cells (146), were also significantly enriched in the OTI-SKO cells, relative to OTI-WT cells (Figure 4-5A). Relevant to this thesis, the *Itgae* gene (CD103) was the most upregulated gene in the c-Myc-deficient CTLs, as compared to WT cells (149).

Considering the important role of c-Myc in metabolic reprogramming during T cell activation (112), we examined the RNA-seq data for dysregulation of genes that are involved in cellular metabolism (Figure 4-5B). We found that the gene for the peroxisome proliferator-activated receptor gamma (PPARγ), which is a key regulator of lipid metabolism and glucose homeostasis (150), was upregulated ($log_2$=1.66) in the OTI-SKO cells. In addition, *Nr1h3* ($log_2$=1.15) which encodes the liver X receptor α chain (LXRα) and is involved in cholesterol transport was upregulated. In normal cells, expression of *Nr1h3* is suppressed during T cell activation to favor of cholesterol synthesis (151). We also found that Slc2a3, which encodes the glucose transporter Glut3, was downregulated in OTI-SKO cells ($log_2$=-0.84), while Glut1 was expressed at normal levels. Similarly *Pdk1* which encodes pyruvate dehydrogenase kinase 1 (PDHK1), was downregulated ($log_2$=-0.79). PDHK1 plays a key role in CD4 T cell differentiation by inhibiting the activity of pyruvate dehydrogenases and therefore controls glucose entry into

the TCA cycle (152). Finally, transcription of fatty acid synthase (*Fasn*), a key enzyme of fatty acid synthesis, was moderately downregulated in OTI-SKO cells ($log_2$=-0.72). Together these results support the hypothesis that Smad4 deletion alters the metabolic profile of anti-viral CTLs during the $T_{EFF}$ response.

*TGFβ may regulate shift from glycolysis to OXPHOS in memory precursors*

Extensive research has shown that cell proliferation requires increased energy for biosynthesis of membrane components and cellular organelles (122). As TGFβRII and Smad4 differentially regulate late proliferation in $T_{EFF}$ cells, we further examined the mutant CTLs for defects in cellular metabolism using a Seahorse® flux analyzer (150).

For this study EE cells ($KLRG1^{lo}CD127^{lo}$) were purified from the spleens of IAV infected mice at various time points after infections and memory precursors (MPECs, $KLRG1^{lo}CD127^{hi}$) were isolated 8dpi. The purified cells were plated in 96 well plates and a glycolysis Stress Test® was used to examine their glycolytic capacity directly *ex vivo* (153). During glycolysis cells extrude protons causing acidification of the culture media, which can be measured as extracellular acidification rate (ECAR). Glucose was injected at the beginning of the test to increase ECAR and establish a baseline for glycolysis under resting conditions. Next Oligomycin treatment was used to inhibit ATP synthesis in the mitochondria, which leads to a further increase in ECAR as the cells accelerate ATP production. The ECAR measured under 'stress conditions' indicates the maximum glycolytic capacity of the cells, while the difference between the maximal and basal ECAR is used to define the glycolytic reserve of the cells. At the end of the test, 2-DG is used to shut down glycolysis by inhibiting hexokinase activity, thereby causing a significant decrease in ECAR.

The glycolysis Stress Test did not reveal any significant differences in the glycolysis rate of EE cells isolated from OTI-WT and OTI-TKO mice during the expansion (3.5 and 6dpi) or the peak

of the $T_{EFF}$ response (8dpi) (Figure 4-6A). In contrast, memory precursors that lacked the TGFβ receptor showed significantly higher ECAR under both basal and stress conditions than WT cells and maintained a higher glycolytic reserve 8dpi (Figure 4-6B), which is consistent with their capacity for prolonged proliferation, as shown in chapter III. In contrast, Smad4 deficiency did not alter the glycolytic capacity of $T_{EFF}$ cells at any time point (Figure 4-6). These data suggest that TGFβ may regulate the switch from glycolysis back to OXPHOS during the transition to memory formation.

*TGFβ and Smad4 may reciprocally regulate mitochondrial respiration*

We next performed a Mito Stress Test® to evaluate OXPHOS in $T_{EFF}$ cells lacking the TGFβ receptor or Smad4. For this test basal oxygen consumption rate (OCR) is used to measure OXPHOS activity in mitochondria under resting conditions. After treatment with Oligomycin a decrease in OCR reflects the mitochondrial respiration that is associated with ATP production. Maximal OCR is determined using Carbonyl cyanide-4 (trifluoromethoxy) phenylhydrazone (FCCP) to disrupts the mitochondrial membrane potential and stimulate the electron transport chain (ETC) to operate at maximum capacity. The increase from basal OCR to maximal OCR is defined as spare respiratory capacity (SRC). High SRC is associated with enhanced cell survival and persistence, which are determined by substrate delivery to the mitochondria, as well as the activity of the enzymes associated with OXPHOS (154). A third injection of Rotenone and Antimycin inhibits Complex I and Complex III activities in the ETC and shuts down OXPOHOS in mitochondria. The remaining OCR is a result of non-mitochondrial respiration.

There was no difference in the basal respiration for EE cells from OTI-WT and OTI-TKO mice during IAV infection (Figure 4-7A, Figure 4-8). However the maximal OCR and SRCs were decreased 3.5dpi (Figure 4-8). As SRC is important for CD8 T cell memory development (123),

the TGFβ receptor may use this pathway to impair memory formation and favor the generation of KLRG1+ $T_{EFF}$ cells.

In similar experiments, EE cells from OTI-SKO mice displayed significantly higher basal and maximal OCRs than wild type cells (Figure 4-7A, Figure 4-8), which could indicate enhanced mitochondrial biogenesis and preferential use of OXPHOS for energy production. Analysis of EE cells during the expansion phase of the $T_{EFF}$ response (6dpi) did not reveal any difference in energy consumption. The maximal OCR for EE cells that were isolated at the peak of the CTL response (8dpi) was slightly higher for the OTI-SKO than WT cells, which may indicate faster conversion from glycolysis back to OXPHOS. Smad4-deletion did not significantly affect the SRC of the CTLs, which indicates that Smad4 deletion did not alter substrate delivery and enzyme activity in mitochondria under stressed condition (Figure 4-8). Overall the data indicate that Smad4 may suppress mitochondria biogenesis after T cell activation.

*TGFβ or Smad4 deletion does not alter mitochondrial fuel usage*

Glucose, fatty acids, and amino acids can all be used as substrates for OXPHOS in the mitochondria. Recent studies showed that SRC in memory CD8 T cells is fueled by fatty acid oxidation (FAO) (123;124). To examine whether $T_{EFF}$ cells from OTI-TKO or OTI-SKO mice rely on FAO for SRC, we performed a Mito stress test® in the presence of Etomoxir to inhibit carnitine palmitoyl transferase 1α (CPT1α) activity, which is the rate-limiting enzyme for FAO (155). During this assay inhibition of FAO abrogated the SRC and decreased the OCR to basal levels in both wild type and mutant cells (Figure 4-9A). Treatment with Etomoxir also decreased the basal OCR regardless of whether the cells expressed the TGFβ receptor or Smad4 (Figure 4-9B). Therefore use of FAO to fuel OXPHOS during both basal and stress states was not altered by TGFβRII or Smad4 deletion.

We used another inhibitor, BPTES, to shut down glutamine oxidation in the mitochondria by inhibiting glutaminase GLS1 activity (156). This inhibitor did not affect either the basal or maximal OCRs of $T_{EFF}$ cells (Figure 4-9B). It is possible that other glutaminases compensate for inhibition of GLS1, as glutamine depletion in media decreased the OCR and OCR/ECAR ratios for all three cell types under basal conditions (Figure 4-9C). These results are consistent with the role of glutaminolysis in fueling OXPHOS in $T_{EFF}$ cells (120).

Lastly, UK5099 blocks the transport of glucose-derived pyruvate into the mitochondria (157). This inhibitor had no impact on the basal OCR and abrogated the SRC for all three types of cells (Figure 4-9B). Consistently, the literature shows that memory CD8 T cells generated *in vitro* are depend on extracellular glucose to support FAO through intrinsic lipid synthesis and lipolysis (124). We found that deprivation of glucose during cell culture resulted in a higher ratio of OCR/ECAR ratio for all three types of cells (Figure 4-9C). Consistently, a recent study showed that AMPK pathway can upregulate glutamine oxidation in $T_{EFF}$ cells in response to low glucose availability (120). In summary, ex-vivo analysis of $T_{EFF}$ cells showed that all three types of cells were able to adapt to different substrates for OXPHOS, which suggests that these processes are not regulated by TGFβRII or Smad4.

*Smad4 may regulate terminal differentiation of $T_{EFF}$ cells by IL12 signaling and T-bet expression*

To further understand how Smad4 and TGFb influence the phenotype and proliferative capacity of activated CTLs, we investigated whether the OTI-TKO and OTI-SKO cells were responsive to cytokine stimulation. Our RNA-Seq data indicated that the β2 subunit of the IL-12 receptor (*IL12rb2*) was downregulated more than 2 fold in EE cells from OTI-SKO mice, as compared to OTI-WT cells (Figure 4-3B). IL-12 is a pro-inflammatory cytokine which promotes terminal differentiation of $T_{EFF}$ cells by upregulating T-bet (29). A gradient of T-bet is induced by TCR signaling and amplified by IL-12 to promote the formation of KLRG1+ $T_{EFF}$ cells, while low T-bet

expression leads to development of memory precursors (28). One mechanism by which IL-12 regulates T-bet expression is via mTOR complex 1 (mTORC1) signaling. Studies have shown that IL-12 uses both PI3K/Akt pathway and STAT4 phosphorylation to enhance mTORC1 activity during TCR stimulation with costimulatory signals. mTORC1 and mTORC2-dependent phosphorylation of Akt further leads to inactivation of the transcription factor Foxo1 which suppresses T-bet (158;159).

We used phospho-flow analysis to determine whether TGFβRII or Smad4 regulates the CD8 T cell response by altering IL-12 signaling. We isolated CTLs from the spleens 6dpi and found that the STAT4 was phosphorylated at slightly higher levels in OTI-TKO cells than WT CTLs during IL-12 stimulation *in vitro* (Figure 4-10A). Although there was no difference in T-bet expression before the peak of the CTL response, the OTI-TKO cells expressed T-bet at slightly higher levels than OTI-WT cells during the memory phase of infection (Figure 4-11A, Figure 4-11B).

We also isolated OTI-SKO cells from the spleens 6dpi, for use in similar experiments. In contrast to the OTI-TKO cells, we found that Stat4 was phosphorylated at significantly lower levels in OTI-SKO cells than control cells after *in vitro* stimulation with IL-12 (Figure 4-10A). We also used phosphorylation of S6 to assess signaling via the PI3K/Akt/mTORC1 pathway (160). Ex-vivo analysis showed reduced Phosphorylation of S6 in OTI-SKO $T_{EFF}$ cells, as compared to WT cells (Figure 4-10C), which is consistent with reduced mTORC1 activity. These results support our hypothesis that IL-12 signaling is compromised in the absence of Smad4. Since we found no difference in phosphorylation of STAT5 after IL-2 stimulation *in vitro* (Figure 4-10B), the defects appear to be specific for the IL-12 signaling pathway. Although IL-12 is known to promote terminal differentiation of $T_{EFF}$ cells by upregulating T-bet (29), our experiments with OTI-SKO cells revealed only minor differences in T-bet expression during IAV infection (Figure 4-11). Based on this result, we postulate that Smad4 may control additional regulatory

molecules involved in terminal differentiation of $T_{EFF}$ cells, which leads to reduced numbers of KLRG1+ $T_{EFF}$ cells in absence of Smad4.

*Smad4 and TGFβ cooperate to regulate $T_{RM}$ and $T_{CM}$ development*

Previous studies have shown that downregulation of T-bet and Eomes is essential for the development of CD103+ $T_{RM}$ cells in the lungs and skin (146;161). These T-box transcription factors can suppress expression of the TGFβ receptor and downstream signaling pathways (146). Conversely, signals from the TGFβ receptor can reduce expression of both transcription factors in activated CTLs (146). In our studies, OTI-WT cells only upregulated CD103 in the lungs, where Eomes was expressed at low levels (Figure 4-12). The OTI-TKO cells expressed Eomes at higher levels than OTI-WT cells at all time points analyzed (Figure 4-12A, Figure 4-12B), and also expressed T-bet at slightly higher levels than the control cells 15dpi (Figure 4-11), which may explain the deficient development of CD103+ $T_{RM}$ cells in the absence of TGFβ receptor (Figure 4-12C). In contrast, OTI-SKO cells expressed Eomes at low levels at all time points analyzed (Figure 4-12A, Figure 4-12B), and T-bet expression was also moderately reduced in OTI-SKO cells (Figure 4-11). Reduced levels of these T-box transcription factor may lead to widespread expression of CD103 on OTI-SKO cells (Figure 4-12C), and there was no difference in Eomes expression between the CD103+ and CD103- OTI-SKO cell subsets (Figure 4-12C).

Previous studies have also shown that Eomes promotes the formation of CD62L+ $T_{CM}$ cells (147). Consistent with this concept, some OTI-WT cells expressed CD62L in local lymph nodes which corresponded with high Eomes expression (Figure 4-12D). We found that a higher proportion of the OTI-TKO cells re-expressed CD62L in the lymphoid organs 15dpi as compared to WT cells and corresponded with high Eomes expression (Figure 4-12D). In contrast, low Eomes expression in the OTI-SKO cells was associated with decreased numbers of CD62L+

$T_{CM}$ cells in the resting lymph nodes (Figure 4-12D). Based on these data we postulate that Smad4 and TGFβ may counter-regulate memory formation by adjusting the ratio of T-bet and Eomes.

## Discussion

The data in this chapter explore the mechanisms by which Smad4 regulates effector and memory CD8 T cell differentiation. Our RNA-Seq data showed that several phenotypic markers were transcriptionally altered in undifferentiated EE cells lacking Smad4, including CD103, CD127 and CD62L. In addition, GSEA suggests that the transcription signature for $T_{RM}$ cells was enriched in SKO CTLs before 6dpi. We postulate that Smad4 installs a unique transcriptional profile in $T_{EFF}$ cells during an early phase of the CTL response.

The literature shows that rapidly proliferating $T_{EFF}$ cells are fueled by enhanced glycolysis (116). We were not able to detect any significant difference in glycolysis between EE cells from OTI-WT and OTI-TKO mice at any time point during IAV infection. However, memory precursor cells lacking the TGFβ receptor showed signs of prolonged glycolysis 8dpi, while the WT cells reverted to OXPHOS. The EE cells from the OTI-TKO mice also had limited spare respiratory capacity, which is crucial for the development and persistence of memory CD8 T cells (123). It is possible that inefficient induction or maintenance of SRC favors terminal differentiation of $T_{EFF}$ cells, over memory precursor formation by OTI-TKO cells. Based on these data we postulate that TGFβ inhibits terminal differentiation of $T_{EFF}$ cells by curtailing glycolysis and promoting SRC in developing memory CD8 T cells.

Our RNA-Seq data showed low expression of c-Myc and its downstream target AP4 in the SKO CTLs analyzed 6dpi. Despite the fact that c-Myc and AP4 play crucial roles in initiating and sustaining the glycolytic activity of $T_{EFF}$ cells, the OTI-SKO cells did not show any deficiency in the Glycolytic Stress Test. The metabolic state of $T_{EFF}$ cells is regulated by several factors (114), that could compensate for low c-Myc and AP4 expression. Consistently, we did not find significant differences in the transcription levels of enzymes that are important for glycolysis. The OTI-SKO CTLs were also capable of proliferating at similar a rate to OTI-WT cells during

IAV infection. We found some evidence that Smad4 deletion-promotes mitochondria biogenesis, since that OTI-SKO $T_{EFF}$ cells consumed more oxygen under both basal and stress conditions during tests performed 3.5dpi. Studies have shown that CD8 T cells undergo a metabolic switch from OXPHOS to glycolysis upon activation, while cells the survive the contraction of the $T_{EFF}$ response switch back to OXPHOS during memory development (115;122). There was no difference in OXPHOS during the expansion phase of infection, but the OTI-SKO cells displayed higher maximal OCR at the peak of the response than WT cells. Overall these data suggest that Smad4 may regulate the balance between OXPHOS and glycolysis by favoring mitochondria respiration.

Although the TGFβ receptor and Smad4 mutations altered OXPHOS, there were no differences in the types of fuels that could be utilized for mitochondrial respiration. The OTI-SKO, OTI-TKO and OTI-WT cells had a similar capacity to generate energy from glucose, fatty acids and amino acids during deprivation of individual nutrients. Consistently, our RNA-Seq data did not indicate substantial changes in the pathways that are involved in utilization of these substrates. It is possible that the process of harvesting and sorting of $T_{EFF}$ cells altered their metabolic state, or that the in vitro assays did not accurately mimic the nutrient environment *in vivo*.

The IL-12 receptor is composed of two subunits (β1 and β2). The IL-12Rβ2 subunit is part of a high affinity receptor which is transcriptionally regulated, while the low affinity IL-12Rβ1 receptor is constitutively expressed (162). Since the RNA-sequencing data indicated reduced transcription of the *Il12rb2* gene in OTI-SKO cells 6dpi, we postulate that low expression of the high affinity IL-12 receptor contributed low numbers of KLRG1+ $T_{EFF}$ cells during infection. Consistently, phospho-flow analysis showed decreased STAT4 phosphorylation and mTORC1 signaling in OTI-SKO cells during IL-12 stimulation. Since IAV infection does not induce large numbers of KLRG1+ CTLs, we performed similar experiments with mice that were infected with recombinant *Listeria Monocytogene* expressing the OVA epitope (LM-OVA), which is a

pathogen that induces high amounts of IL-12 and KLRG1+ $T_{EFF}$ cells during infection (163). The OTI-SKO cells did not produce very many KLRG1+ $T_{EFF}$ cells during LM-OVA infection (data not shown). When the CTLs were examined directly *ex vivo*, the level of phosphorylated S6 was significantly decreased early after activation (d2.5) and during the expansion phase of infection (d5). Furthermore the OTI-SKO cells expressed T-bet at reduced levels during activation (d2.5) and the memory phase of infection (d15) (data not shown). These data support the idea that Smad4 supports terminal differentiation of $T_{EFF}$ cells by enhancing or maintaining IL-12 signaling and T-bet expression. Further experiments will confirm that *Il12rb2* is expressed at low levels in SKO CTLs by qPCR and flow cytometry. However it remains unclear how Smad4 regulates IL-12 receptor expression.

Studies have shown that TGFβ can reduce T-bet expression in pulmonary and skin $T_{RM}$ cells (146;161). We found slightly enhanced expression of T-bet in the absence of TGFβRII during the memory phase of infection with IAV. Our data indicate that TGFβ and Smad4 are both involved in regulating the balance between $T_{RM}$ and $T_{CM}$ cells, possibly by regulating Eomes and T-bet expression. We postulate that high expressions of Eomes and T-bet render the TKO CTLs incapable of acquiring a CD103+ phenotype, but promote the formation of CD62L+ $T_{CM}$ cells. In contrast, low expression of T-bet and Eomes in Smad4 deficient cells may be responsible for widespread CD103 expression in the spleens and lymphoid tissues after IAV infection.

Previous studies indicate that T-bet and Eomes are reciprocally regulated in $T_{EFF}$ cells (158). Upon CD8 T cell activation, Eomes expression is induced via a Runx3-dependent process (164), and expression can be amplified by IL-2 (165). Since Eomes is a target gene of Foxo1, expression levels can be suppressed by IL-12 signaling via the PI3K/Akt/mTOR pathway (54). In our studies the TKO and SKO cells responded to IL-2 stimulation *in vitro* and phosphorylated STAT5 normally. Still, it remains to be explored whether another signal is involved in regulating Eomes expression in TKO and SKO CTLs. Also, T-bet and Eomes cooperate to regulate

effector functions by inducing the expression of IFNγ, granzyme B and perforin, and CD8 T cells lacking both T-bet and Eomes differentiated into IL17-producing CTLs (164). While IFNγ and TNF production in response to peptide stimulation *in vitro* was unaltered by TGFβRII or Smad4 deletion, further study is needed to determine the production of other effector molecules and cytokines, and the effector function of these CTLs by killing assay.

In summary, this chapter shows that Smad4 establishes a unique transcription profile in $T_{EFF}$ cells at early stage of the CD8 T cell response. While Smad4 and TGFβ may be involved in the balance between OXPHOS and glycolysis, deletion of these genes did not affect the usage of different nutrient substrates. Importantly, our data indicate that Smad4 acts upstream of two master transcription factors, T-bet and Eomes, to regulate effector and memory differentiation.

Figure 4-1

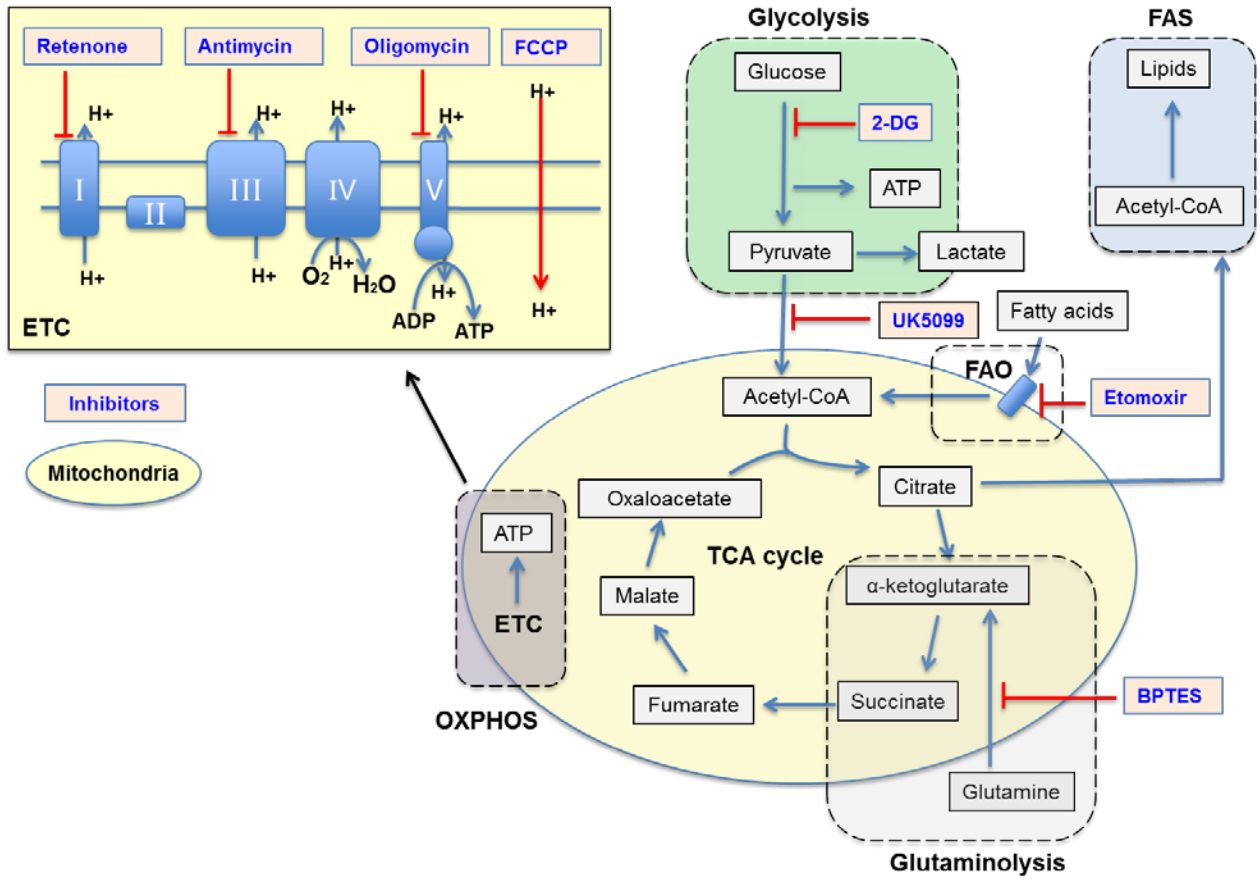
Retenone
Antimycin
Oligomycin
FCCP
H+
I
II
III
IV
V
O2
H2O
ADP
ATP
ETC
Inhibitors
Mitochondria
Glycolysis
Glucose
2-DG
ATP
Pyruvate
Lactate
FAS
Lipids
Acetyl-CoA
UK5099
Fatty acids
FAO
Etomoxir
Acetyl-CoA
Citrate
Oxaloacetate
TCA cycle
α-ketoglutarate
Malate
Fumarate
Succinate
BPTES
Glutamine
Glutaminolysis
ATP
ETC
OXPHOS

**Figure 4-1. Metabolic pathways in CD8 T cells**

Naïve CD8 T cells use fatty acid oxidation (FAO), or oxidative phosphorylation (OXPHOS) of glucose-derived pyruvate in mitochondria, to generate energy. During this process acetyl CoA is oxidized in the tricarboxylic acid (TCA) cycle to generate NADPH, which fuels ATP production via the electron transport chain (ETC). Upon activation, CD8 T cells undergo a metabolic switch characterized by enhanced glycolysis, during which glucose is fermented into lactate despite of the presence of sufficient oxygen. Activated T cells also upregulate OXPHOS of glutamine in mitochondria, and downregulate FAO in favor of fatty acid synthesis (FAS). These metabolic changes are essential for biomass synthesis, which supports cell growth, extensive proliferation and effector functions of $T_{EFF}$ cells. After the peak of the response, development of memory CD8 T cells involves conversion of cellular metabolism back to a catabolic state that primarily relies on FAO and OXPHOS. We have examined the role of individual pathways in CD8 T cell metabolism using the pharmaceutical inhibitors shown in blue.

Figure 4-2

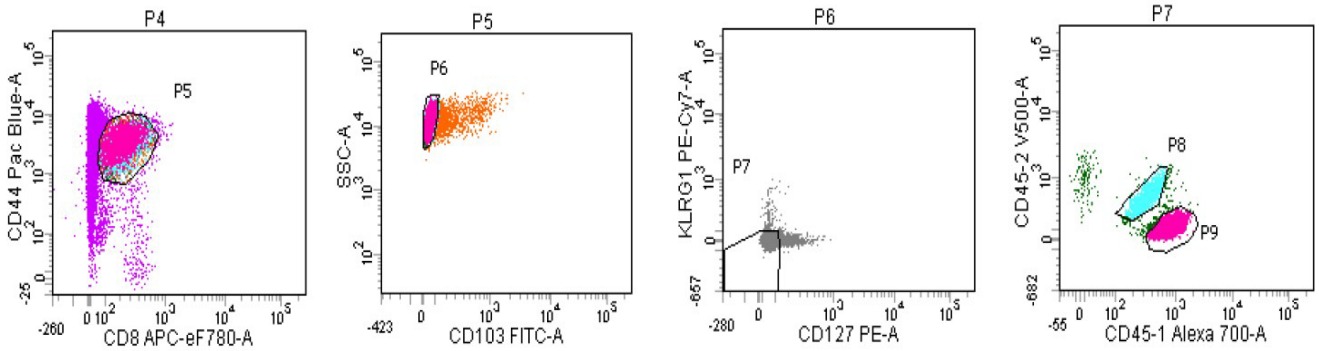
P4
P5
CD44 Pac Blue-A
CD8 APC-eF780-A
P5
P6
SSC-A
CD103 FITC-A
P6
P7
KLRG1 PE-Cy7-A
CD127 PE-A
P7
P8
P9
CD45-2 V500-A
CD45-1 Alexa 700-A

**Figure 4-2. Sorting strategy for RNA-Sequencing**

C57BL/6 mice received mixed populations of congenically marked naïve OTI-WT and OTI SKO cells 48hrs before X31-OVA infection. Transferred cells were recovered from pools of three spleens 6dpi (total 9 mice) and divided into subsets using KLRG1, CD127, CD103 and CD44 expression.

Figure 4-3

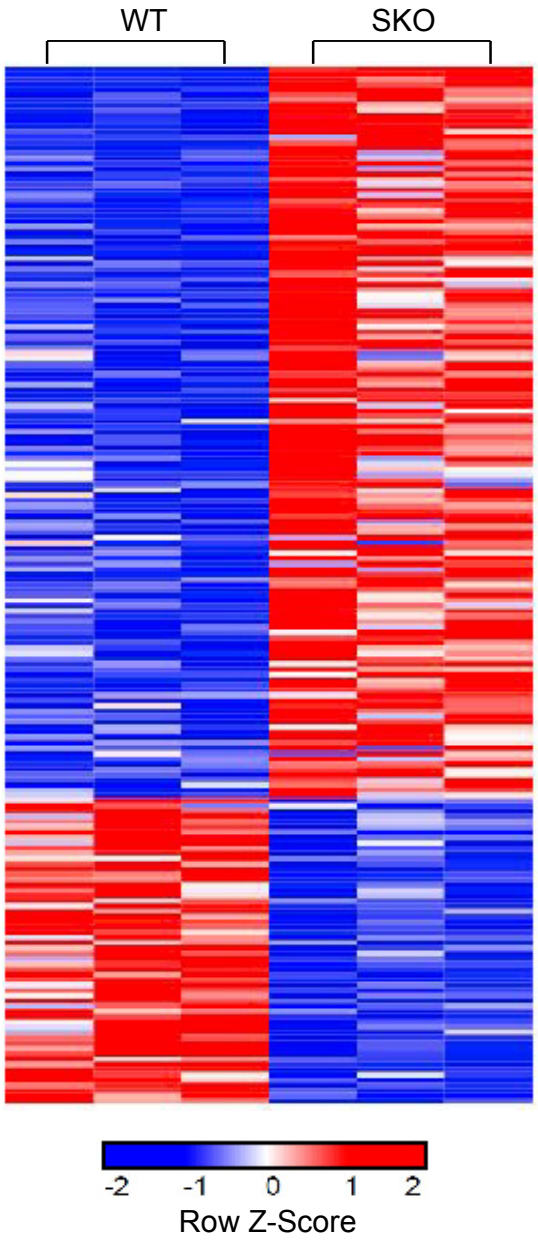

**Figure 4-3. Altered gene expression in Smad4-deficient CTLs**

RNA was extracted from KLRG1$^{lo}$ CD127$^{lo}$ CD103$^{lo}$ CD44$^{hi}$ OTI-WT and OTI-SKO cells for RNA-Sequencing. The heatmap shows changes in gene expression greater than two fold ($Log_2$ fold change >1 or <-1, $p<0.05$, false discovery rate<0.05). Comparative values are calculated as fragments per kilobase of transcript per million mapped reads (FPKM), standardized by row Z-score ($z=(x-\mu)/\sigma$) and plotted on a color scale. Red indicates high expression and blue indicates low expression in OTI-SKO cells relative to OTI-WT cells.

Figure 4-4

A.

Molecular and Cellular Functions

| Name | P-value range | Molecular# |
|---|---|---|
| Cellular Movement | 5.03E-04 - 1.08E-21 | 50 |
| Cellular Development | 6.14E-04 - 1.08E-21 | 69 |
| Cellular Growth and Proliferation | 6.14E-04 - 1.08E-21 | 77 |
| Cell-to-Cell Signaling and Interaction | 5.03E-04 - 1.08E-21 | 51 |
| Cell Death and Survival | 5.40E-04 - 1.08E-21 | 84 |

B.

Cell migration and interaction

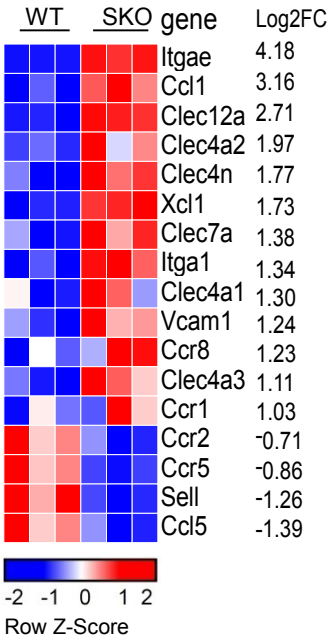


Cytokines and costimulation

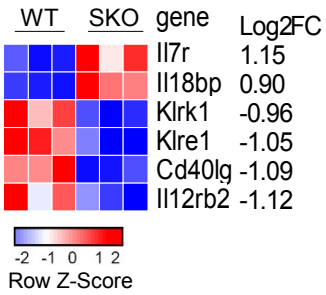


Transcription factors

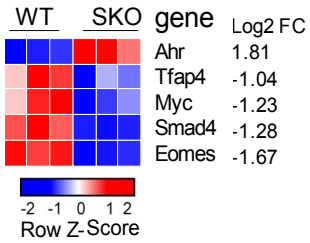


C.

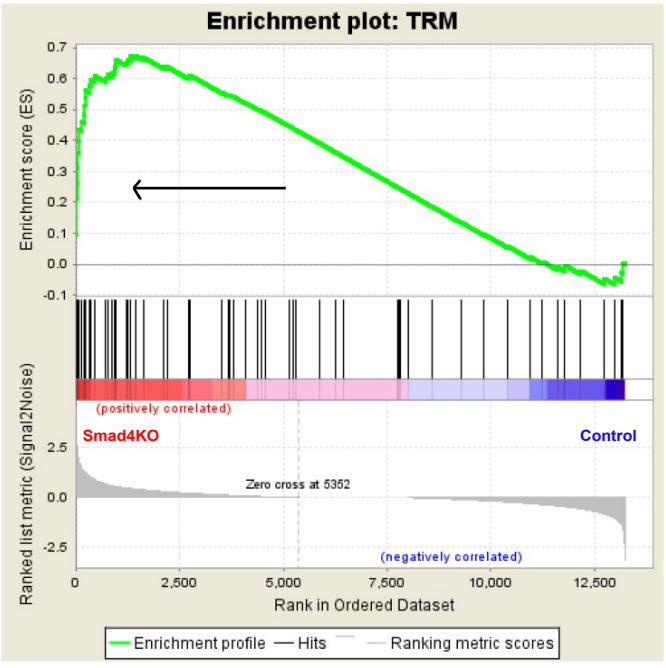


D.

| Gene | Log2FC |
|---|---|
| Itgae | 4.18 |
| Skil | 1.96 |
| Xcl1 | 1.73 |
| Hpgd | 1.59 |
| Itga1 | 1.34 |
| Inpp4b | 0.75 |
| Qpct | 0.64 |
| Klre1 | -1.05 |
| Eomes | -1.67 |

**Figure 4-4. Smad4-deficiency changes the transcriptional profile of $T_{EFF}$ cells during the early phase of the CTL response.**

**(A)** Ingenuity Pathway Analysis was used to assess the function roles of genes with transcriptional changes greater than two fold ($Log_2$ fold change >1 or <-1, $p<0.05$, false discovery rate<0.05). The list shows the top 5 molecular and cellular functions with significant transcriptional changes between the OTI-WT and OTI-SKO cells.

**(B)** Differentially expressed genes were grouped based on their functions. Expression values are plotted by Z-scores with red indicating high expression and blue indicating low expression in the OTI-SKO cells.

**(C)** Gene Set Enrichment Analysis (GSEA) was used to compare genes that were differentially expressed in OTI-WT and OTI-SKO cells with a reference set from the literature. The reference set is composed of genes identified by comparing $T_{RM}$ cells in IAV infected lungs with circulating $T_{CM}$ cells after HSV infection 30dpi ($Log_2$ fold change >2 or <-2).

**(D)** Genes with significantly differential expression in RNA-Seq were compared with a previously defined core signature of genes shared by skin, gut and lung $T_{RM}$ cells. Genes that exhibited a similar regulation pattern in our RNA-Seq and the published $T_{RM}$ signature are listed.

**Figure 4-5**

**A.**

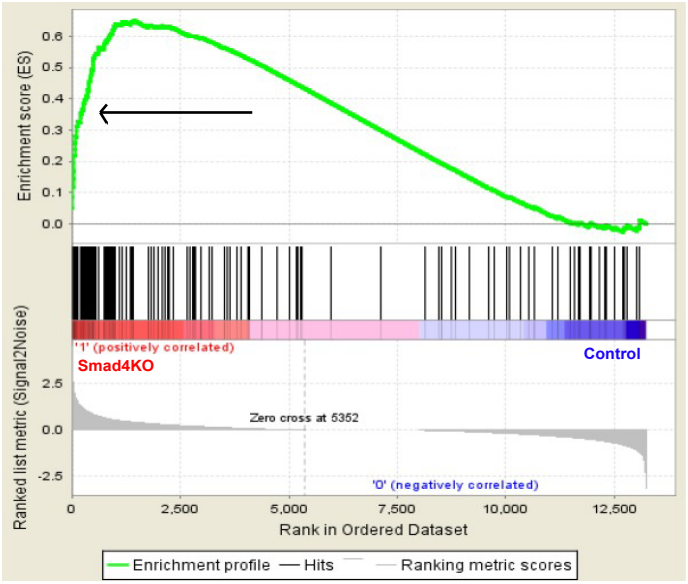


**B.** Cellular metabolism

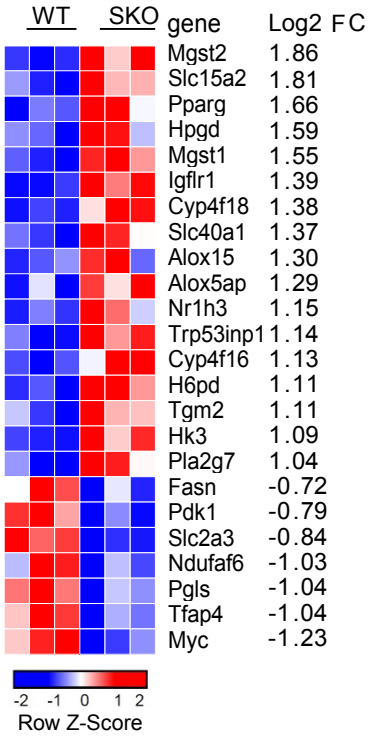

**Figure 4-5. Smad4 regulates the transcription of genes involved in cellular metabolism**

**(A)** Gene Set Enrichment Analysis was used to compare the transcriptional profile of OTI-SKO cells with a transcriptional signature of myc-deficient $T_{EFF}$ cells from the literature. The genes in the reference set were upregulated more than 4-fold in ERT-Cre $myc^{flox/flox}$ CD8 T cells 3 days after *in vitro* activation. c-Myc was deleted by tamoxifen on day 1 after activation.

**(B)** The heat map shows genes with differential expression between OTI-SKO and OTI-WT cells that are involved in cellular metabolism, with red indicating high expression and blue indicating low expression in OTI-SKO cells.

Figure 4-6

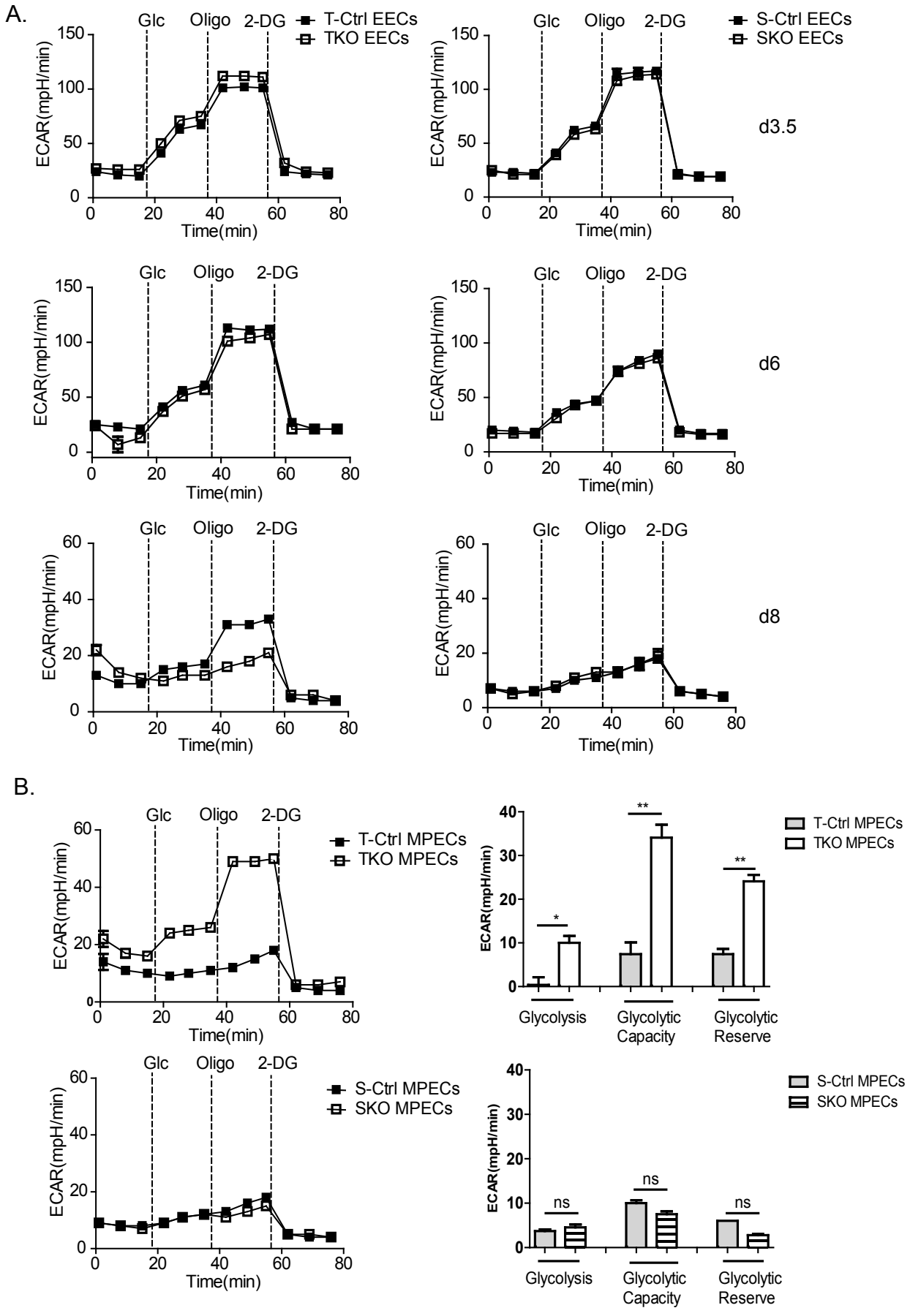
A.
Glc
Oligo
2-DG
T-Ctrl EECs
TKO EECs
S-Ctrl EECs
SKO EECs
ECAR(mpH/min)
Time(min)
d3.5
d6
d8
B.
T-Ctrl MPECs
TKO MPECs
S-Ctrl MPECs
SKO MPECs
Glycolysis
Glycolytic Capacity
Glycolytic Reserve
ns

**Figure 4-6. TGFβ may decrease glycolysis in memory precursors**

C57BL/6 mice received mixed populations of congenically marked naïve OTI-WT and OTI-TKO cells, or OTI-WT and OTI-SKO cells 48hrs before X31-OVA infection. Early effector cells (EECs) and memory precursor effector cells (MPECs) were isolated from lymphoid tissues at indicated time points based on KLRG1 and CD127 expression. The cells were plated at $2x10^5$ cells per well (3-4 wells/group) for analysis using the Glycolysis Stress Test and a XF-96 Extracellular Flux Analyzer.

**(A)** Extracellular acidification rates (ECAR) for early effector cells from OTI-WT, OTI-TKO and OTI-SKO mice during treatment with Glucose (Glc, 10mM); Oligomycin (Oligo, 4μM); 2-Deoxy-D–glucose (2-DG, 50mM).

**(B)** Extracellular acidification rates (ECAR) for MPEC cells from OTI-WT (grey), OTI-TKO (white) and OTI-SKO (hatched) mice 8dpi. Bar graphs show basal glycolysis, maximum glycolytic capacity, and glycolytic. Means ± SD. *$p < 0.05$, **$p < 0.01$.

Figure 4-7

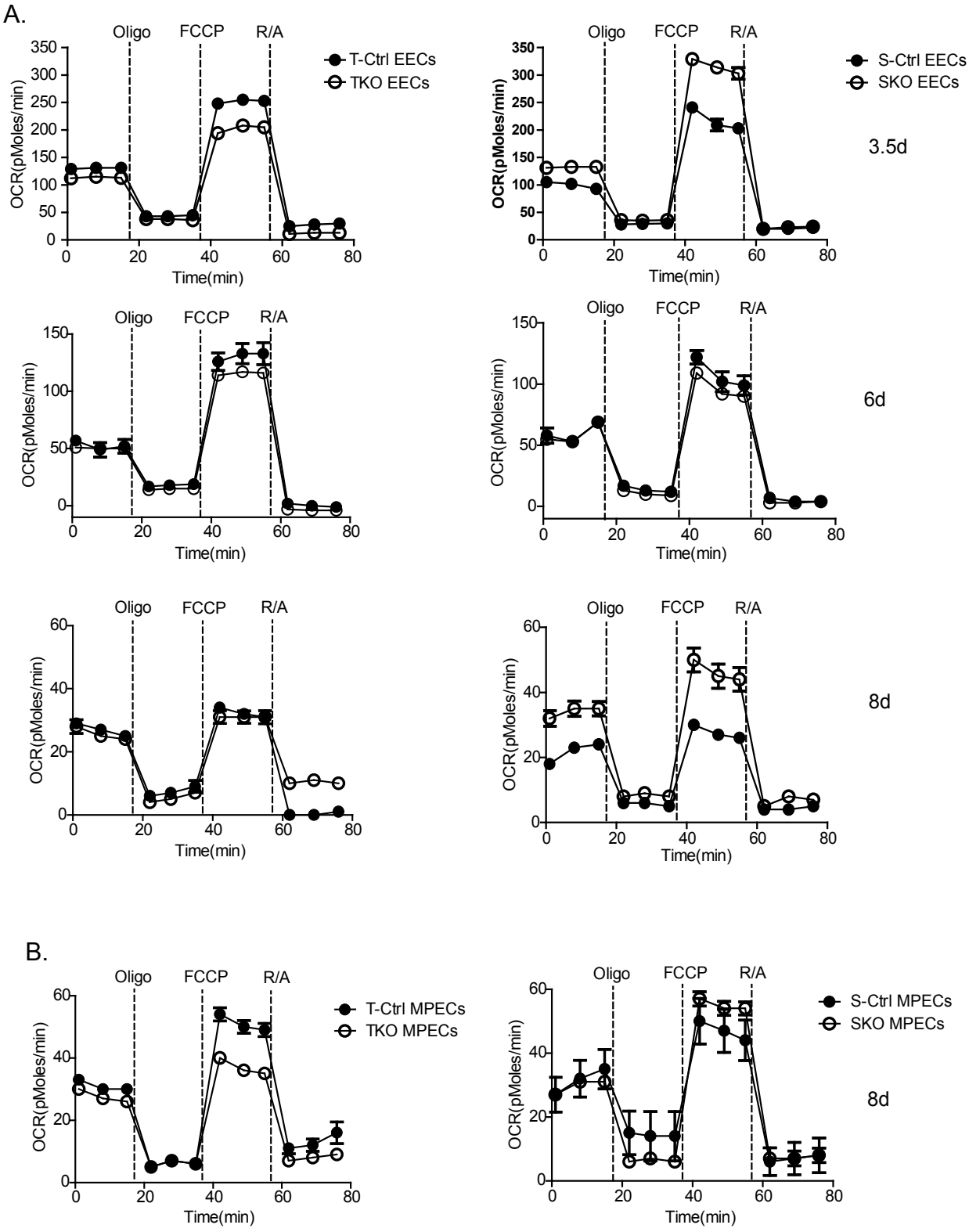


Statistic comparisons of Figure 4-6 are shown in Figure 4-8

**Figure 4-7. Smad4 may regulate mitochondrial respiration in activated CTLs**

C57BL/6 mice received mixed populations of congenically marked naïve OTI-WT and OTI-TKO cells, or OTI-WT and OTI-SKO cells 48hrs before X31-OVA infection. Early effector cells (EECs) and memory precursor effector cells (MPECs) were isolated from lymphoid tissues at indicated time points based on KLRG1 and CD127 expression. The cells were plated at $2x10^5$ cells per well (3-4 wells/group) for analysis using the Mito Stress Test and a XF-96 Extracellular Flux Analyzer

**(A)** Oxygen consumption by early effector cells from OTI-WT, OTI-TKO and OTI-SKO mice. during treatment Oligomycin (Oligo, 4μM), Carbonyl cyanide-4 (trifluoromethoxy) phenylhydrazone (FCCP, 0.5μM), and Retenone/Antimycin (R/A, 0.5μM).

**(B)** Oxygen consumption by MPEC cells from OTI-WT (grey), OTI-TKO (white) and OTI-SKO (hatched) mice 8dpi.

Figure 4-8

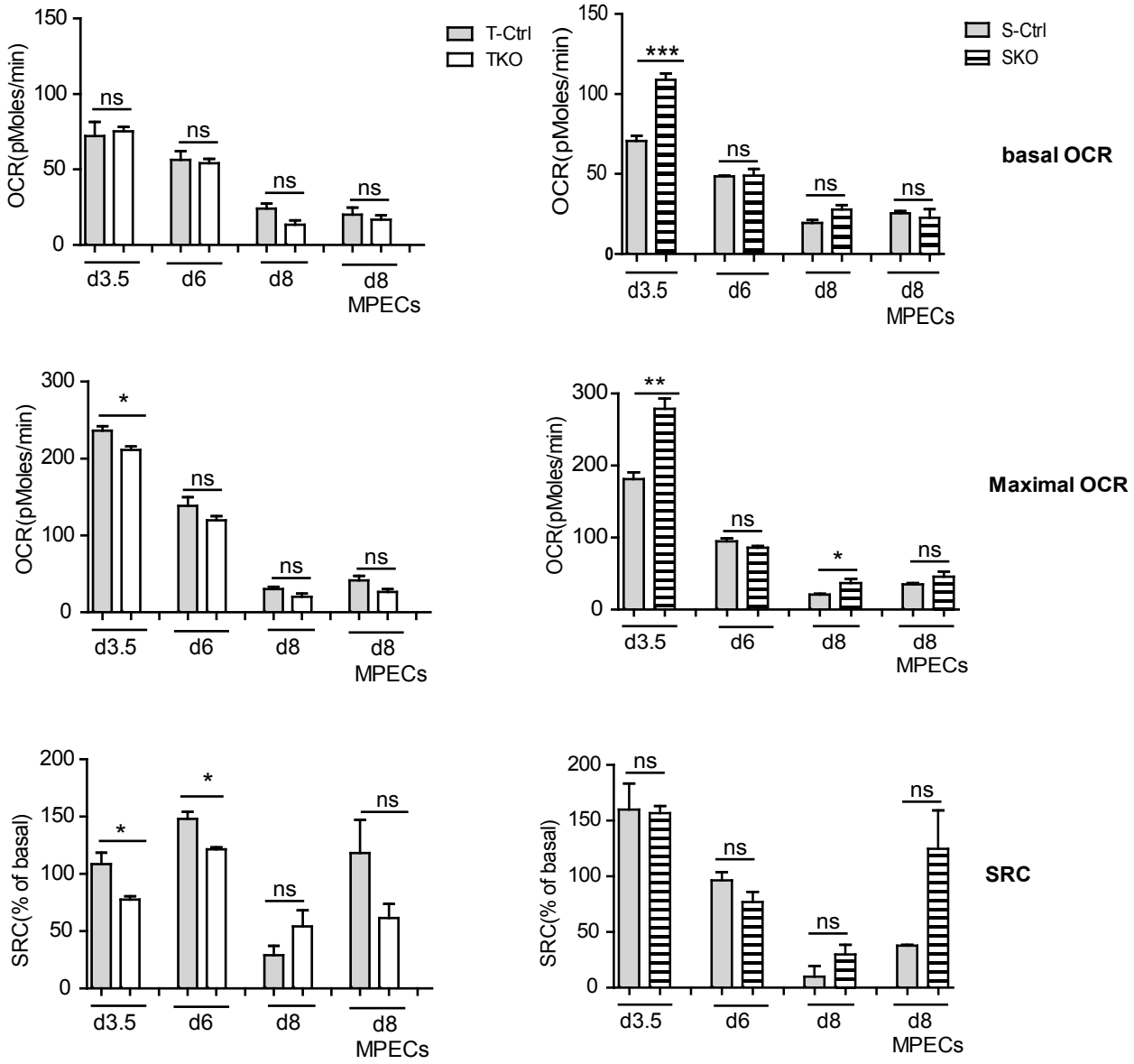
T-Ctrl
TKO
S-Ctrl
SKO
basal OCR
Maximal OCR
SRC
OCR(pMoles/min)
SRC(% of basal)
d3.5
d6
d8
d8 MPECs
ns
*
**
***

**Figure 4-8. TGFβ increases spare respiratory capacity while Smad4 may suppress OXPHOS**

Basal oxygen consumption rate (OCR), maximum OCR, and spare respiratory capacity (SRC) for OTI-WT (grey shading), OTI-TKO (white), OTI-SKO (hatched) cells during Mito Stress Test. Values were calculated using the data shown in **Figure 4-6**. Means ± SD. *p <0.05, **p < 0.01, ***p<0.005.

Figure 4-9

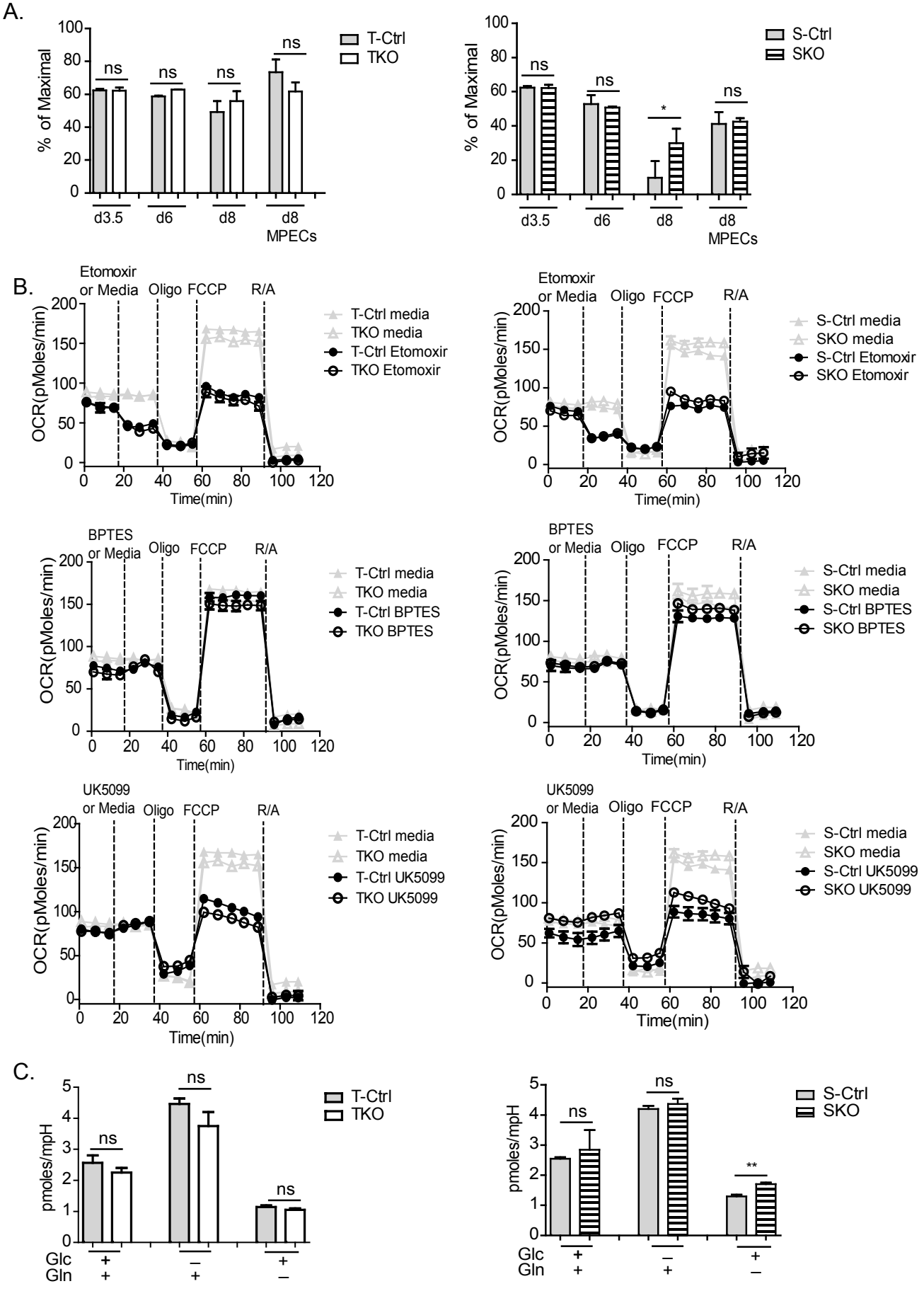
A.
% of Maximal
T-Ctrl
TKO
S-Ctrl
SKO
ns
*
d3.5
d6
d8
d8 MPECs
B.
Etomoxir or Media
BPTES or Media
UK5099 or Media
Oligo
FCCP
R/A
OCR(pMoles/min)
Time(min)
T-Ctrl media
TKO media
T-Ctrl Etomoxir
TKO Etomoxir
S-Ctrl media
SKO media
S-Ctrl Etomoxir
SKO Etomoxir
T-Ctrl BPTES
TKO BPTES
S-Ctrl BPTES
SKO BPTES
T-Ctrl UK5099
TKO UK5099
S-Ctrl UK5099
SKO UK5099
C.
pmoles/mpH
Glc
Gln

**Figure 4-9. TGFβ or Smad4 deletion does not alter mitochondrial fuel usage**

C57BL/6 mice received mixed populations of congenically marked naïve OTI-WT and OTI-TKO cells, or OTI-WT and OTI-SKO cells 48hrs before X31-OVA infection. Early effector cells (EECs) and memory precursor effector cells (MPECs) were isolated from lymphoid tissues at the indicated time points based on KLRG1 and CD127 expression. The cells were plated at $2x10^5$ cells per well (3-4 wells/group) for analysis using the Mito Stress Kit and a XF-96 Extracellular Flux Analyzer.

**(A)** Oxygen consumption rate by EECs and MPEC during treatment with Oligomycin (4μM), FCCP (0.5μM), Etomoxir (200mM) and Retenone/Antimycin (0.5μM). OXPHOS from fatty acid oxidation (FAO) was determined by the percentage of maximal OCR decreased in response to Etomoxir. *p <0.05.

**(B)** OXPHOS by EECs from OTI-TKO (left panel) and OTI-SKO (right panel) mice. Cells were analyzed 6dpi in media (grey color) or inhibitors (black color). 200μM Etomoxir (inhibitor of fatty acid oxidation), 50μM BPTES (inhibitor of glutaminolysis), and 50μM UK5099 (inhibitor of glucose-derived pyruvate transport) were used before the injection of Oligomycin.

**(C)** Bar graphs show the ratios for basal OCR versus ECAR by EECs from OTI-WT (grey shading), OTI-TKO (white), OTI-SKO (hatched) mice. Cells were analyzed 6dpi in the presence (+) or absence (-) of glucose (Glc, 25mM) or glutamine (Gln, 2mM). Means ± SD. **p < 0.01.

Figure 4-10

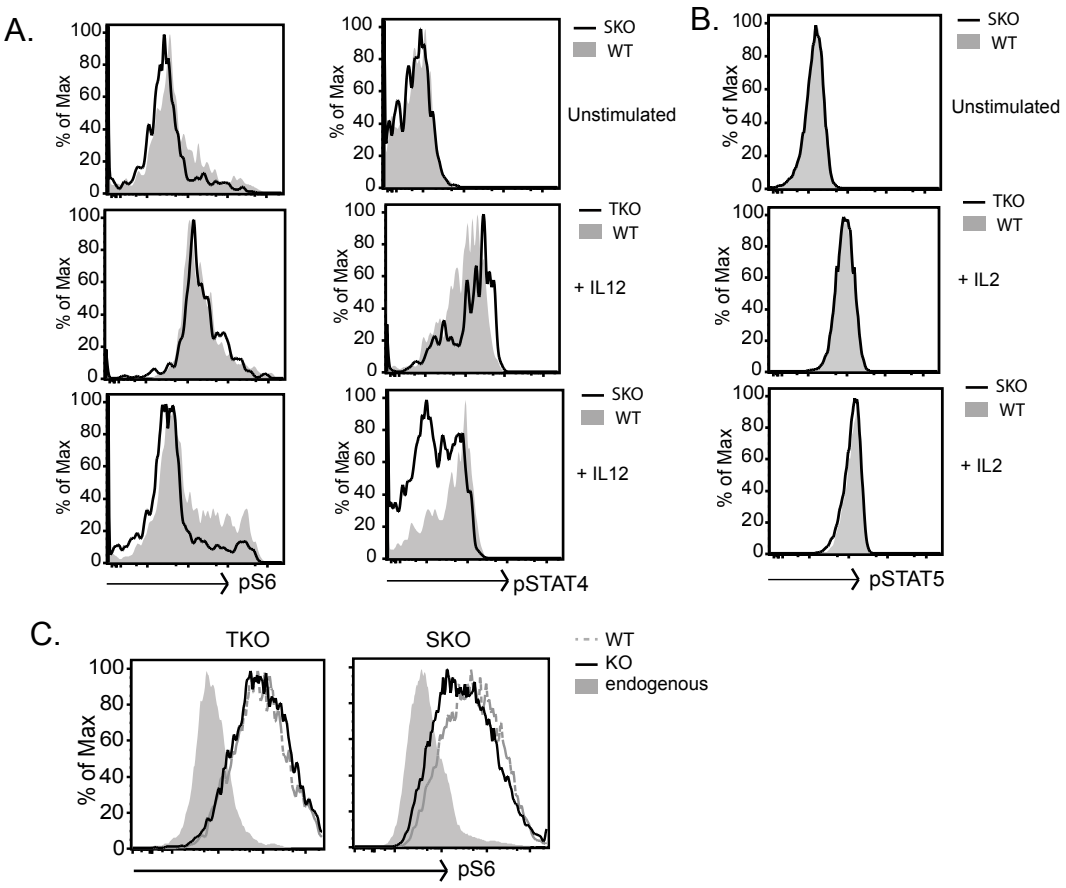
A.
% of Max
pS6
pSTAT4
SKO
WT
TKO
Unstimulated
+ IL12
B.
pSTAT5
+ IL2
C.
TKO
SKO
KO
endogenous

**Figure 4-10. Smad4 deletion led to reduced IL-12 signaling**

Congenically marked cells from OTI-WT and OTI-TKO cells, or OTI-WT and OTI-SKO mice were sorted for low CD44 expression and transferred into C57BL/6 mice before X31-OVA infection. Representative graphs were shown with 3-4 mice/group.

**(A-B)** Splenocytes were harvested 6dpi and rested in cell culture media for 2-3 hours. The cells were then stimulated with **(A)** 2ng/ml IL-12 for 1 hour or **(B)** 5ng/ml IL-2 for 30 minutes, or left unstimulated as control. Phosphorylation of S6, STAT4 and STAT5 were determined by phospho-flow on gated OTI-WT (grey shading), OTI-TKO or OTI-SKO cells (solid line).

**(C)** Phosphorylation of S6 in gated OTI-WT (grey dashed line), OTI-TKO or OTI-SKO (solid line) and endogenous cells (grey shading) were determined *ex vivo* 6 dpi.

Figure 4-11

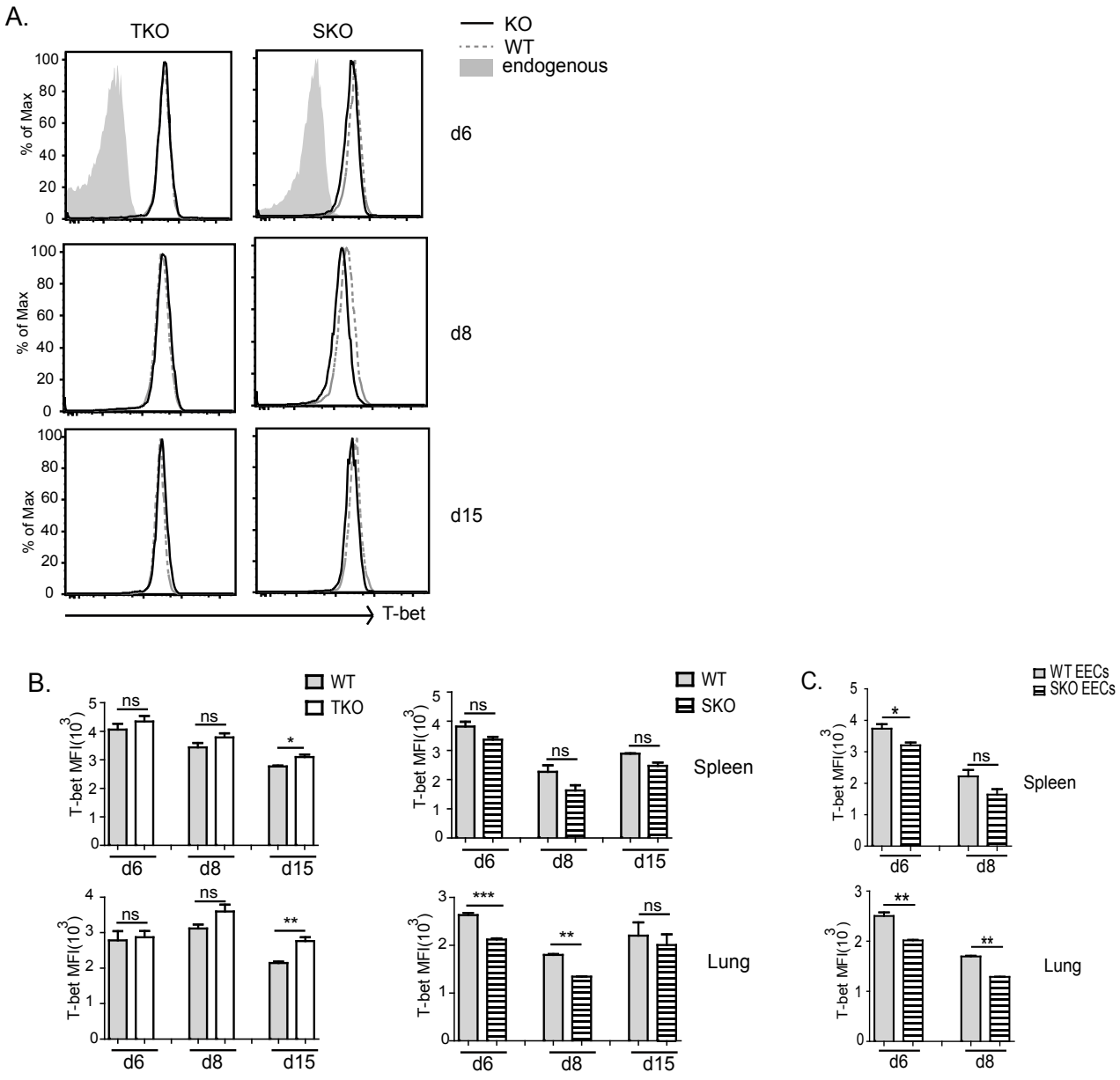
A.
TKO
SKO
KO
WT
endogenous
% of Max
d6
d8
d15
T-bet
B.
WT
TKO
SKO
T-bet MFI(10^3)
ns
*
**
***
Spleen
Lung
d6
d8
d15
C.
WT EECs
SKO EECs

**Figure 4-11. Smad4 promotes T-bet expression in $T_{EFF}$ cells**

Congenically marked OTI-WT and OTI-TKO cells, or OTI-WT and OTI-SKO cells were sorted for low CD44 expression and transferred into C57BL/6 mice before X31-OVA infection. Bar graphs show means 3-4 mice/group ± SD. *p<0.05, **p < 0.01, ***p<0.005. Two independent experiments yielded similar results.

**(A)** T-bet expression in OTI-WT (grey dashed line), OTI-TKO or OTI-SKO (solid line) and endogenous cells (grey shading) in spleens and lungs.

**(B)** Mean fluorescence intensity for T-bet staining in OTI-WT (grey shading), OTI-TKO (white), and OTI-SKO (hatched) cells.

**(C)** Mean fluorescence intensity of T-bet staining in $KLRG1^{lo}CD127^{lo}$ early effector cell (EEC) subsets of OTI-WT (grey shading) and OTI-SKO cells (hatched).

Figure 4-12

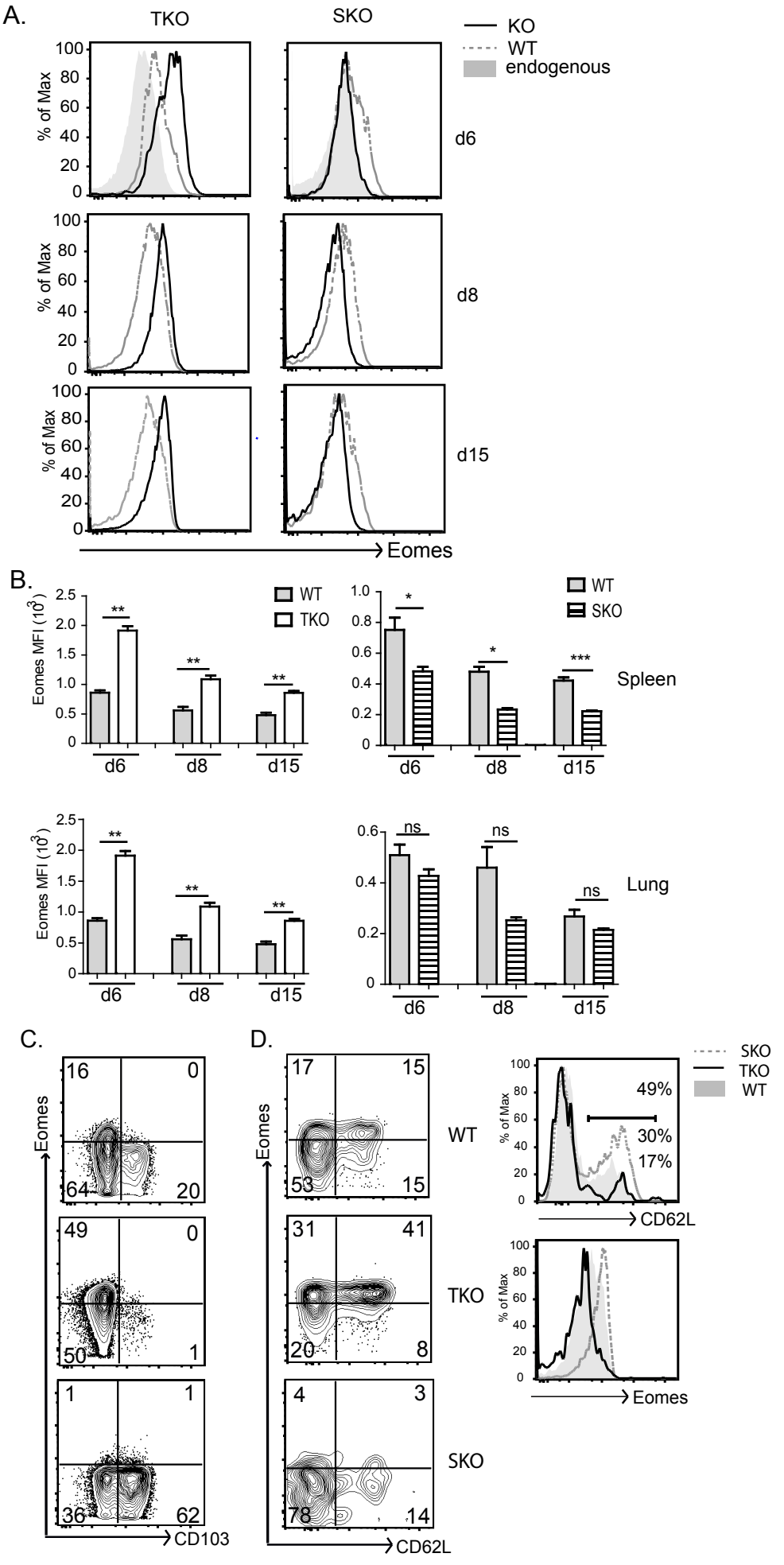
A.
TKO
SKO
KO
WT
endogenous
% of Max
d6
d8
d15
Eomes
B.
WT
TKO
SKO
Eomes MFI (10^3)
Spleen
Lung
ns
C.
Eomes
CD103
D.
CD62L
49%
30%
17%

**Figure 4-12. TGFβ and Smad4 reciprocally balance $T_{RM}$ and $T_{CM}$ cell development by regulating the level of Eomes**

Congenically marked OTI-WT and OTI-TKO cells, or OTI-WT and OTI-SKO cells were sorted for low CD44 expression and transferred into C57BL/6 mice before X31-OVA infection. Two independent experiments with 3-4 mice/group yielded similar results.

**(A)** Eomes expression in OTI-WT (grey dashed line), OTI-TKO or OTI-SKO (solid line) and endogenous cells (grey shading) in spleens and lungs at indicated time points after infection.

**(B)** Mean fluorescence intensity for Eomes staining in OTI-WT (grey shading), OTI-TKO (white), and OTI-SKO (hatched) cell populations. Bar graphs show means ± SD. *$p<0.05$, **$p < 0.01$, ***$p<0.005$.

**(C)** Contour plots show Eomes and CD103 expression on OTI-WT, OTI-TKO and OTI-SKO cells in the inguinal lymph nodes 15dpi.

**(D)** Contour plots show Eomes and CD62L expression by OTI-WT (grey shading), OTI-TKO (solid line) and OTI-SKO (grey dashed line) cells in inguinal lymph nodes 15dpi.

**Table 4-1**

| gene id | WT FPKM avg | SKO FPKM avg | logFC SKO vs WT | P values | FDR values |
|---|---|---|---|---|---|
| Apol9b | 0.473957 | 13.9909 | 4.88359 | 0.00005 | 0.00106695 |
| Itgae | 0.559934 | 10.1293 | 4.17714 | 0.00005 | 0.00106695 |
| Xlr3b | 0.169004 | 2.5016 | 3.88772 | 0.00005 | 0.00106695 |
| Ldlrad4 | 0.857605 | 12.6805 | 3.88616 | 0.00005 | 0.00106695 |
| Lrig1 | 0.129343 | 1.25309 | 3.27621 | 0.00105 | 0.0132538 |
| Ccl1 | 0.425493 | 3.80449 | 3.16049 | 0.0026 | 0.0266737 |
| Osgin1 | 0.434457 | 3.23384 | 2.89596 | 0.00005 | 0.00106695 |
| Ntrk3 | 0.161671 | 1.19818 | 2.88971 | 0.00005 | 0.00106695 |
| Snrpn | 0.103321 | 0.710952 | 2.78262 | 0.0014 | 0.0166164 |
| Pmepa1 | 0.415701 | 2.84695 | 2.7758 | 0.00005 | 0.00106695 |
| Smoc1 | 0.15181 | 1.0007 | 2.72067 | 0.00005 | 0.00106695 |
| Clec12a | 0.800612 | 5.25632 | 2.71488 | 0.00005 | 0.00106695 |
| Chit1 | 0.139254 | 0.842951 | 2.59773 | 0.0006 | 0.00844667 |
| Stra6 | 0.285184 | 1.53616 | 2.42937 | 0.00005 | 0.00106695 |
| B4galnt4 | 0.294419 | 1.42384 | 2.27384 | 0.00005 | 0.00106695 |
| Pde9a | 0.266168 | 1.26349 | 2.24701 | 0.00005 | 0.00106695 |
| Ms4a1 | 0.440085 | 1.94388 | 2.14309 | 0.00005 | 0.00106695 |
| Ly6d | 1.27098 | 5.57013 | 2.13177 | 0.00005 | 0.00106695 |
| Ifitm2 | 73.2209 | 315.195 | 2.10592 | 0.00005 | 0.00106695 |
| Cd79a | 0.94739 | 4.00567 | 2.08001 | 0.00005 | 0.00106695 |
| Trim16 | 0.529912 | 2.22827 | 2.0721 | 0.00005 | 0.00106695 |
| Cabp4 | 0.167867 | 0.671713 | 2.00053 | 0.00355 | 0.0338821 |
| Clec4a2 | 0.150902 | 0.590796 | 1.96905 | 0.00025 | 0.00420232 |
| Skil | 4.27655 | 16.6768 | 1.96332 | 0.00005 | 0.00106695 |
| Cd19 | 0.278619 | 1.08009 | 1.95478 | 0.00005 | 0.00106695 |
| Cd300e | 0.244483 | 0.922832 | 1.91633 | 0.00015 | 0.0027444 |
| Wdfy1 | 2.40211 | 8.9192 | 1.89261 | 0.00005 | 0.00106695 |
| Mgst2 | 13.4696 | 48.9486 | 1.86156 | 0.00005 | 0.00106695 |
| Nt5e | 4.84586 | 17.5741 | 1.85863 | 0.00005 | 0.00106695 |
| Ahr | 0.546005 | 1.91558 | 1.8108 | 0.00005 | 0.00106695 |
| Slc15a2 | 0.171012 | 0.59773 | 1.8054 | 0.00005 | 0.00106695 |
| Ifitm1 | 359.535 | 1239.3 | 1.78532 | 0.00005 | 0.00106695 |
| Gpr34 | 0.47902 | 1.64181 | 1.77713 | 0.00005 | 0.00106695 |
| Clec4n | 1.12165 | 3.83041 | 1.77188 | 0.00005 | 0.00106695 |
| Xcl1 | 56.5929 | 187.945 | 1.73161 | 0.00005 | 0.00106695 |
| Ncf4 | 104.251 | 338.283 | 1.69817 | 0.00005 | 0.00106695 |
| Adamdec1 | 0.1811 | 0.575544 | 1.66814 | 0.0005 | 0.00728161 |
| Pparg | 0.190734 | 0.602245 | 1.65879 | 0.00165 | 0.0190483 |
| Aif1 | 1.52525 | 4.71307 | 1.62762 | 0.00005 | 0.00106695 |
| Smpd5 | 2.91887 | 8.98112 | 1.62148 | 0.00005 | 0.00106695 |

**Table 4-1**

| gene id | WT FPKM avg | SKO FPKM avg | logFC SKO vs WT | P values | FDR values |
|---|---|---|---|---|---|
| Nostrin | 0.225849 | 0.694589 | 1.6208 | 0.00185 | 0.0207659 |
| Hpgd | 0.42501 | 1.27747 | 1.58772 | 0.00005 | 0.00106695 |
| Isg20 | 21.0853 | 62.9184 | 1.57725 | 0.00005 | 0.00106695 |
| Tsc22d1 | 2.65905 | 7.80252 | 1.55303 | 0.00005 | 0.00106695 |
| Siglece | 0.399534 | 1.1695 | 1.54949 | 0.00015 | 0.0027444 |
| Ly86 | 0.944492 | 2.75718 | 1.54558 | 0.00005 | 0.00106695 |
| Mgst1 | 1.32724 | 3.87377 | 1.54531 | 0.00005 | 0.00106695 |
| Trf | 2.54745 | 7.2591 | 1.51074 | 0.00005 | 0.00106695 |
| Zfp1 | 3.12285 | 8.88687 | 1.50881 | 0.00005 | 0.00106695 |
| Ubd | 1.48628 | 4.15867 | 1.48442 | 0.00005 | 0.00106695 |
| Tnfsf11 | 0.436528 | 1.20653 | 1.46671 | 0.00005 | 0.00106695 |
| Actn2 | 0.984984 | 2.71515 | 1.46286 | 0.00005 | 0.00106695 |
| Wfdc17 | 3.23602 | 8.90308 | 1.46008 | 0.00005 | 0.00106695 |
| Sirpa | 0.362194 | 0.989893 | 1.45051 | 0.00005 | 0.00106695 |
| Igj | 0.275663 | 0.750231 | 1.44443 | 0.00075 | 0.010136 |
| Mzb1 | 0.630755 | 1.71356 | 1.44185 | 0.00245 | 0.0254178 |
| Cd74 | 21.7353 | 58.5862 | 1.43052 | 0.00005 | 0.00106695 |
| Gm6682 | 3.01385 | 8.06528 | 1.42012 | 0.00005 | 0.00106695 |
| Ski | 2.00806 | 5.33904 | 1.41078 | 0.00005 | 0.00106695 |
| Igflr1 | 16.0449 | 42.1123 | 1.39213 | 0.00005 | 0.00106695 |
| Clec7a | 0.48677 | 1.26657 | 1.37962 | 0.00005 | 0.00106695 |
| Znrf1 | 0.879341 | 2.28715 | 1.37906 | 0.00005 | 0.00106695 |
| Prkcz | 0.674504 | 1.75405 | 1.37879 | 0.00005 | 0.00106695 |
| Cyp4f18 | 1.00359 | 2.60786 | 1.37769 | 0.00005 | 0.00106695 |
| H2-Aa | 10.1775 | 26.3452 | 1.37215 | 0.00005 | 0.00106695 |
| Slc40a1 | 5.01024 | 12.9556 | 1.37062 | 0.00005 | 0.00106695 |
| Cd101 | 0.904812 | 2.32059 | 1.3588 | 0.00005 | 0.00106695 |
| Tdgf1 | 0.247519 | 0.633122 | 1.35495 | 0.00335 | 0.0325245 |
| Smurf2 | 2.21604 | 5.66591 | 1.35432 | 0.00005 | 0.00106695 |
| Cd5l | 2.32932 | 5.93757 | 1.34996 | 0.00005 | 0.00106695 |
| Itga1 | 0.650255 | 1.64982 | 1.34323 | 0.00005 | 0.00106695 |
| Timp2 | 1.25164 | 3.17258 | 1.34183 | 0.00005 | 0.00106695 |
| Spic | 3.44003 | 8.67104 | 1.33378 | 0.00005 | 0.00106695 |
| Treml4 | 1.78477 | 4.49377 | 1.33219 | 0.00005 | 0.00106695 |
| Ctsh | 0.717442 | 1.8064 | 1.33218 | 0.00005 | 0.00106695 |
| AF251705 | 0.495993 | 1.24613 | 1.32906 | 0.00275 | 0.0277078 |
| Fcgr4 | 1.21145 | 3.01882 | 1.31725 | 0.00005 | 0.00106695 |
| Hba-a1,Hba-a2 | 1.79225 | 4.44333 | 1.30987 | 0.0056 | 0.0483077 |
| Clec4a1 | 0.492829 | 1.21622 | 1.30325 | 0.00045 | 0.00673737 |
| Alox15 | 0.241831 | 0.595398 | 1.29985 | 0.00175 | 0.0199303 |

**Table 4-1**

| gene id | WT FPKM avg | SKO FPKM avg | logFC SKO vs WT | P values | FDR values |
|---|---|---|---|---|---|
| Alox5ap | 1.86947 | 4.55591 | 1.28511 | 0.00005 | 0.00106695 |
| Emr4 | 0.290241 | 0.703602 | 1.27751 | 0.00005 | 0.00106695 |
| Pilrb2 | 0.349515 | 0.846674 | 1.27645 | 0.00055 | 0.00790752 |
| Cd302 | 0.660607 | 1.59103 | 1.26809 | 0.0005 | 0.00728161 |
| Adamts6 | 0.304442 | 0.73204 | 1.26576 | 0.00005 | 0.00106695 |
| Gpr25 | 0.738372 | 1.7549 | 1.24897 | 0.00005 | 0.00106695 |
| A930001A20Rik | 1.08039 | 2.56676 | 1.2484 | 0.00005 | 0.00106695 |
| Vcam1 | 3.38238 | 8.00392 | 1.24267 | 0.00005 | 0.00106695 |
| Gngt2 | 28.0047 | 66.1468 | 1.24 | 0.00005 | 0.00106695 |
| Ccr8 | 1.11522 | 2.62516 | 1.23508 | 0.00025 | 0.00420232 |
| Beta-s | 2.47094 | 5.79766 | 1.23041 | 0.0003 | 0.00481139 |
| Cpd | 0.669247 | 1.54902 | 1.21075 | 0.00005 | 0.00106695 |
| Cd14 | 2.0551 | 4.71151 | 1.19698 | 0.00005 | 0.00106695 |
| H2-Ab1 | 4.91075 | 11.2582 | 1.19696 | 0.00005 | 0.00106695 |
| Csf3r | 0.396414 | 0.90815 | 1.19592 | 0.00005 | 0.00106695 |
| Hebp1 | 1.00834 | 2.30729 | 1.19422 | 0.0005 | 0.00728161 |
| Car2 | 49.7481 | 113.292 | 1.18733 | 0.00005 | 0.00106695 |
| Gpr56 | 0.860425 | 1.94781 | 1.17873 | 0.00005 | 0.00106695 |
| Plaur | 1.83661 | 4.14319 | 1.1737 | 0.00005 | 0.00106695 |
| Ifitm3 | 61.9976 | 138.329 | 1.15782 | 0.00005 | 0.00106695 |
| Il7r | 6.82418 | 15.1439 | 1.15001 | 0.00005 | 0.00106695 |
| Cfb | 0.432428 | 0.958073 | 1.14767 | 0.00035 | 0.00544946 |
| Nr1h3 | 0.834216 | 1.84696 | 1.14666 | 0.0002 | 0.00347123 |
| Card6 | 0.434881 | 0.961298 | 1.14436 | 0.00005 | 0.00106695 |
| Zfyve28 | 0.355081 | 0.78432 | 1.1433 | 0.00005 | 0.00106695 |
| Trp53inp1 | 2.24681 | 4.95092 | 1.13982 | 0.00005 | 0.00106695 |
| Apol7e | 2.78206 | 6.10043 | 1.13276 | 0.00005 | 0.00106695 |
| Cyp4f16 | 0.456374 | 0.99817 | 1.12907 | 0.00065 | 0.00903759 |
| Lgals7 | 4.89169 | 10.6196 | 1.11832 | 0.00005 | 0.00106695 |
| H6pd | 1.80681 | 3.92196 | 1.11813 | 0.00005 | 0.00106695 |
| Tgm2 | 0.451958 | 0.977916 | 1.11352 | 0.00025 | 0.00420232 |
| 2410066E13Rik | 0.609879 | 1.31876 | 1.11259 | 0.0011 | 0.013782 |
| Clec4a3 | 0.835719 | 1.79818 | 1.10545 | 0.00045 | 0.00673737 |
| Tgfb3 | 0.283352 | 0.607118 | 1.09938 | 0.00115 | 0.0142673 |
| Fxyd4 | 3.12148 | 6.68394 | 1.09847 | 0.00025 | 0.00420232 |
| Abi3 | 3.97913 | 8.48765 | 1.09291 | 0.00005 | 0.00106695 |
| Hk3 | 0.444541 | 0.947071 | 1.09115 | 0.00055 | 0.00790752 |
| Treml2 | 0.500225 | 1.06124 | 1.08511 | 0.00005 | 0.00106695 |
| Gpr68 | 16.6537 | 35.2195 | 1.08053 | 0.00005 | 0.00106695 |
| Exoc3l | 0.923014 | 1.93958 | 1.07132 | 0.00005 | 0.00106695 |

**Table 4-1**

| gene id | WT FPKM avg | SKO FPKM avg | logFC SKO vs WT | P values | FDR values |
|---|---|---|---|---|---|
| Herc3 | 3.60473 | 7.5183 | 1.06052 | 0.00005 | 0.00106695 |
| 1110032F04Rik | 0.579364 | 1.20566 | 1.05728 | 0.00055 | 0.00790752 |
| Tyrobp | 12.0953 | 25.1601 | 1.05669 | 0.00005 | 0.00106695 |
| Fpr1 | 0.853556 | 1.77127 | 1.05323 | 0.001 | 0.0127818 |
| Slpi | 11.1663 | 23.1621 | 1.05262 | 0.00005 | 0.00106695 |
| Tubb6 | 3.56027 | 7.3718 | 1.05003 | 0.00005 | 0.00106695 |
| Coro2a | 4.82731 | 9.98667 | 1.04878 | 0.00005 | 0.00106695 |
| Pla2g7 | 1.54176 | 3.18522 | 1.04681 | 0.00005 | 0.00106695 |
| Nucb2 | 1.07649 | 2.22055 | 1.04458 | 0.00005 | 0.00106695 |
| Aldh3b1 | 0.406258 | 0.833482 | 1.03675 | 0.00475 | 0.0430644 |
| Ccr1 | 0.368808 | 0.754128 | 1.03194 | 0.00095 | 0.0122509 |
| Bank1 | 0.301958 | 0.617186 | 1.03136 | 0.00135 | 0.0161745 |
| Wdpcp | 0.62804 | 1.28272 | 1.03028 | 0.0003 | 0.00481139 |
| Actg2 | 3.88243 | 7.91998 | 1.02854 | 0.00005 | 0.00106695 |
| Hck | 0.372092 | 0.756215 | 1.02314 | 0.0052 | 0.0459923 |
| Zfp286 | 0.480721 | 0.967483 | 1.00904 | 0.0004 | 0.00611523 |
| Ndrg4 | 0.503973 | 1.01301 | 1.00723 | 0.0003 | 0.00481139 |
| Fcer1g | 13.6225 | 27.3045 | 1.00315 | 0.00005 | 0.00106695 |
| Thnsl2 | 0.593658 | 1.18892 | 1.00194 | 0.0018 | 0.0203625 |
| Ppan | 16.2166 | 8.05833 | -1.00892 | 0.00005 | 0.00106695 |
| Fcgr2b | 1.55503 | 0.769867 | -1.01426 | 0.00085 | 0.0112182 |
| Mon1a | 4.36323 | 2.14101 | -1.0271 | 0.00005 | 0.00106695 |
| Ndufaf6 | 3.63118 | 1.77551 | -1.0322 | 0.00025 | 0.00420232 |
| Pgls | 54.3735 | 26.3605 | -1.04453 | 0.00005 | 0.00106695 |
| Tfap4 | 1.89303 | 0.917472 | -1.04496 | 0.0001 | 0.00194923 |
| Klre1 | 2.38785 | 1.157 | -1.04532 | 0.00135 | 0.0161745 |
| Ncln | 20.7909 | 10.0634 | -1.04684 | 0.00005 | 0.00106695 |
| Cass4 | 0.834876 | 0.403332 | -1.04959 | 0.0003 | 0.00481139 |
| Vcl | 2.12142 | 1.02402 | -1.05078 | 0.00005 | 0.00106695 |
| Egfl7 | 11.146 | 5.37934 | -1.05102 | 0.00005 | 0.00106695 |
| Amacr | 0.926152 | 0.446442 | -1.05278 | 0.0006 | 0.00844667 |
| Prpsap1 | 22.3375 | 10.6551 | -1.06792 | 0.00005 | 0.00106695 |
| Ndrg1 | 7.61007 | 3.61925 | -1.07222 | 0.00005 | 0.00106695 |
| BC035044 | 14.9724 | 7.08461 | -1.07954 | 0.0002 | 0.00347123 |
| Cd40lg | 4.38038 | 2.0546 | -1.0922 | 0.00005 | 0.00106695 |
| Gas7 | 1.42671 | 0.664431 | -1.1025 | 0.00005 | 0.00106695 |
| Snx9 | 1.02742 | 0.478472 | -1.10252 | 0.0013 | 0.0156867 |
| Dusp4 | 4.11041 | 1.90117 | -1.1124 | 0.00005 | 0.00106695 |
| Il12rb2 | 7.46018 | 3.42689 | -1.12231 | 0.00005 | 0.00106695 |
| Fam73b | 1.7871 | 0.818919 | -1.12582 | 0.00005 | 0.00106695 |

**Table 4-1**

| gene id | WT FPKM avg | SKO FPKM avg | logFC SKO vs WT | P values | FDR values |
|---|---|---|---|---|---|
| Bco2 | 0.853014 | 0.388532 | -1.13454 | 0.00195 | 0.0213909 |
| Rbm47 | 1.70923 | 0.776711 | -1.1379 | 0.00005 | 0.00106695 |
| Fam160a2 | 0.579563 | 0.261699 | -1.14706 | 0.00005 | 0.00106695 |
| Med25 | 2.47916 | 1.11462 | -1.15331 | 0.00005 | 0.00106695 |
| Crybb1 | 3.02753 | 1.34356 | -1.17209 | 0.0007 | 0.00957517 |
| Thop1 | 5.10911 | 2.26659 | -1.17255 | 0.00005 | 0.00106695 |
| Wdr95 | 5.74354 | 2.50267 | -1.19848 | 0.00005 | 0.00106695 |
| Myc | 39.7952 | 17.0124 | -1.22601 | 0.00005 | 0.00106695 |
| Ehd2 | 0.850203 | 0.36109 | -1.23545 | 0.00015 | 0.0027444 |
| Irak1bp1 | 0.627635 | 0.264979 | -1.24405 | 0.00345 | 0.0333357 |
| Serpine2 | 1.15618 | 0.486288 | -1.24948 | 0.00025 | 0.00420232 |
| Map1s | 4.23466 | 1.76697 | -1.26097 | 0.00005 | 0.00106695 |
| Sell | 35.8891 | 14.9705 | -1.26142 | 0.00005 | 0.00106695 |
| Smad4 | 4.68181 | 1.9306 | -1.27801 | 0.00005 | 0.00106695 |
| Ydjc | 4.37975 | 1.78581 | -1.29427 | 0.00005 | 0.00106695 |
| Trim46 | 1.05721 | 0.413773 | -1.35335 | 0.00005 | 0.00106695 |
| Tfeb | 2.46188 | 0.962091 | -1.35551 | 0.00005 | 0.00106695 |
| Tnfrsf25 | 0.889051 | 0.346203 | -1.36065 | 0.0023 | 0.0243349 |
| Cblc | 0.746897 | 0.284538 | -1.39229 | 0.00275 | 0.0277078 |
| Ccl5 | 2161.53 | 822.098 | -1.39467 | 0.00005 | 0.00106695 |
| Gimap7 | 133.178 | 50.3793 | -1.40245 | 0.00005 | 0.00106695 |
| Lamb3 | 1.53786 | 0.576776 | -1.41484 | 0.00005 | 0.00106695 |
| Hmga1 | 162.24 | 59.9278 | -1.43683 | 0.00005 | 0.00106695 |
| Hist1h4m | 5.83564 | 2.15347 | -1.43823 | 0.0024 | 0.0250529 |
| Ndfip1 | 67.6603 | 24.967 | -1.43829 | 0.00005 | 0.00106695 |
| Hpdl | 1.96099 | 0.696275 | -1.49386 | 0.00005 | 0.00106695 |
| Chchd10 | 16.1001 | 5.71545 | -1.49413 | 0.00005 | 0.00106695 |
| H2-Q10 | 37.4232 | 13.2812 | -1.49455 | 0.00005 | 0.00106695 |
| Serpinb9b | 6.84584 | 2.2889 | -1.58058 | 0.00005 | 0.00106695 |
| Arl4d | 3.34451 | 1.09684 | -1.60844 | 0.00005 | 0.00106695 |
| Eomes | 4.89641 | 1.53838 | -1.67031 | 0.00005 | 0.00106695 |
| Ltb4r1 | 0.807339 | 0.251671 | -1.68163 | 0.00315 | 0.0309684 |
| Prr7 | 1.10655 | 0.337841 | -1.71165 | 0.0032 | 0.0313687 |
| Parm1 | 1.57757 | 0.362293 | -2.12247 | 0.00005 | 0.00106695 |
| Ociad2 | 2.99943 | 0.501212 | -2.5812 | 0.00005 | 0.00106695 |
| Art2b | 5.79599 | 0.907782 | -2.67464 | 0.00005 | 0.00106695 |
| Art2a-ps | 0.798092 | 0.12206 | -2.70896 | 0.00515 | 0.0456696 |

**Table 4-1. Genes with significantly differential expression in absence of Smad4**

Congenically marked OTI-WT and OTI-SKO cells were sorted for low CD44 expression and transferred into C57BL/6 mice 48hrs before infection with X31-OVA. Transferred cells lacking KLRG1, CD127 and CD103 expression were isolated from pools of three spleens 6dpi (total 9 mice) and used for RNA-Sequencing. All genes with transcriptional changes greater than two folds ($Log_2$ fold change >1 or <-1, $p<0.05$, false discovery rate (FDR) <0.05) are listed.

# CHAPTER V

# DISCUSSION AND CONCLUSION

*CD8 T cell differentiation are regulated by TGFβ and Smad4*

In this thesis we have shown that the expression levels of multiple homing receptors are altered in the absence of TGFβRII or Smad4, which thus changed the distribution of CTLs *in vivo*. While the kinetics of the CD8 T cell response was unaltered by Smad4 deficiency, as shown by normal expansion and contraction, terminal differentiation of KLRG1+ $T_{EFF}$ cells was greatly reduced when Smad4 was absent. Upon activation Smad4-deficient (SKO) CTLs expressed activation markers similarly to WT cells, yet downregulated CD127 slower than WT cells. They also re-expressed CD127 at higher frequency and very few cells acquired a KLRG1+ phenotype. When Smad4 was expressed some KLRG1+ WT $T_{EFF}$ cells were found in the lungs at 8dpi by confocal microscopy. In normal animals KLRG1+ CTLs have strong lytic activity and facilitate viral clearance from the lungs (166). Low numbers of KLRG1+ cells may explain why the SKO mice underwent more severe weight loss during primary IAV infection and recovered slower than the WT group. To test this hypothesis viral titer can be compared on different time points after primary infection. The production of IFNγ and TNF was not affected by Smad4 deletion. However, these cytokines, while contributing to IAV pathogenesis, are not required for viral clearance (167;168). We will further whether Smad4 regulates effector functions by examining other molecules such as granzyme B and perforin.

Deletion of Smad4 also resulted in widespread expression of CD103 not only in the lungs, but also in the spleens and lymph nodes where WT CTLs do not express CD103. This odd population of CD103+ SKO CTLs in the circulation did not re-express CD62L, which is required for T cell migration across HEVs and entry into resting lymph nodes (169). Consequently, only small numbers of SKO cells were found in the resting lymph nodes and expressed CCR7, which was sufficient for inefficient migration into the ILN. On the other hand, normal numbers of CD103+CD69+ pulmonary $T_{RM}$ cells developed in absence of Smad4. No difference in protection between WT and SKO mice was observed during secondary infection, which is

consistent with the important role of $T_{RM}$ cells in heterosubtypic immunity (61). Confocal imaging will be used to further examine whether Smad4 deficiency alters the localization of antigen-specific CD8 T cells after re-challenge.

TGFβRII deficiency also did not significantly alter the kinetics of the CD8 T cell response after IAV infection. In contrast to SKO CTLs, $T_{EFF}$ cell differentiation was skewed towards the formation of the KLRG1+ subset. This observation is consistent with the literature, as blocking TGFβ signaling also led to the accumulation of $T_{EFF}$ cells with a terminally differentiated phenotype (KLRG1+) after *Listeria Monocytogene* infection (86). WT and TKO mice underwent similar weight loss during primary infection, which suggest that they can control IAV infection as effectively as WT mice.

Previous studies also show that TGFβ is essential for the generation/maintenance of CD103+CD69+ $T_{RM}$ cells in various tissues (63-66). Consistently, while WT antigen-specific CD8 T cells upregulated CD103 in the lungs during the memory phase of infection, CD103 and CD69 were absence from TGFβRII-deficient (TKO) CTLs in the lungs even at 60dpi, which indicates a deficiency in $T_{RM}$ cell development. Confocal microscopy confirmed that OTI-TKO cells did not locate in the walls of the airways. The long-lived KLRG1+ $T_{EFF}$ cells were mostly found in blood vessels. Development of circulating memory CD8 T cells was not impaired by TGFβRII deletion. In fact, increased numbers of CD62L+ $T_{CM}$ cells were observed in the resting lymph nodes. A previous study from our lab shows that $T_{RM}$ cells remain poised in the lungs to provide frontline defenses during the earliest phase of re-infection. Early viral control resulted in less recruitment of circulating memory CD8 T cells and less inflammation in the reinfected lungs (61). During secondary infection the TKO mice recovered slightly slower than WT mice. The absence of $T_{RM}$ cells may have resulted in delayed viral clearance, and increased migration of nascent $2^{nd}$ $T_{EFF}$ cells to the lungs in these mice. Viral titer will be determined by plaque assay or qPCR, and pathology in the lungs will be examined by Hematoxylin and eosin (H&E) staining.

The effect of Smad4 on terminal differentiation and memory formation appeared to be independent of TGFβRII, as CTLs that were deficient of both Smad4 and TGFβRII (STDKO) showed similar phenotypes as SKO cells. The STDKO mice also behaved similarly to SKO mice in protection studies, and recovered from primary infection with delayed kinetics. Our model suggests that an unknown ligand (we refer to as Smad4 ligand) signals through Smad4 to promote formation of KLRG1+ $T_{EFF}$ cells. This pathway, which also suppresses CD103 and is required for CD62L expression on $T_{CM}$ cells, may be counter-regulated by TGFβ via a mechanism that may involve competition for Smad4. Further study is required to identify the Smad4 ligand. A recent study shows that conditional deletion of TGFβRII on memory CD8 T cells results in upregulation of KLRG1, which may be driven by basal inflammation from commensal microbiota (170). Therefore it is possible that Smad4 ligand can also be induced by commensal microbiota, and continuous counter-regulation by TGFβ is required to avoid KLRG1 expression. For the purpose of effective and safe vaccination against IAV infection, an ideal CTL response should elicit low numbers of KLRG1+ $T_{EFF}$ cells, which can be pathogenic, while generating sufficient numbers of $T_{RM}$ cells in lungs. Therefore pharmaceutical inhibition of Smad4 may serve to facilitate the development of a new IAV vaccine by optimizing and sustaining cell-mediated immunity.

*Smad4 may regulate $T_{EFF}$ cell generation via IL-12 signaling*

IL-12 is an important inflammatory cytokine in the CD8 T cell response, which is known to promote terminal differentiation of $T_{EFF}$ cells (29). IL-12 signaling enhances mTORC1 activity through the PI3K/Akt pathway and STAT4 phosphorylation (158). Early exposure to IL-12 can also sustain expression of the expression of high-affinity IL-2 receptor, CD25, and prolong cell proliferation during the late phase of the CD8 T cell response, which is associated with terminal differentiation of $T_{EFF}$ cells (51).

While no difference in cell proliferation was observed at early time points, the TKO cells showed increased BrdU incorporation at and after the peak of the CTL response. It is possible that CTLs lacking TGFβRII are more sensitive to low concentrations of costimulatory molecules, or cytokines that induce cell proliferation during the late phase of infection. The IL-12 receptor is known to be downregulated by TGFβ on CD4 T cells (171). Though IL-12 stimulation *in vitro* resulted in a slightly higher level of phosphorylated STAT4 in OTI-TKO cells at 6dpi, no difference was observed in mTORC1 activity, as shown by the phosphorylation level of S6. We also did not observe a difference in CD25 expression, or responsiveness to IL-2 stimulation *in vitro* between the OTI-TKO and OTI-WT cells. We will use qPCR to compare the transcription levels of IL-12 receptor, as well as other costimulatory molecules and cytokine receptors. Responsiveness to other cytokines can also be examined through *in vitro* stimulation and phospho-flow. At early time points, when there was no significant difference in cell survival and proliferation, lack of TGFβRII resulted in faster downregulation of CD127 at d3.5, and at 6dpi. At this time there were already higher frequencies of KLRG1+ cells and lower frequencies of memory precursors among the TKO cell population. So we also need to consider the possibility that prolonged proliferation may not be the only mechanism leading to the accumulation of KLRG1+ $T_{EFF}$ cells among TKO CTLs.

Our RNA-Seq showed that the *Il12rb2* gene, which encodes the IL-12 receptor β2 chain, was downregulated in the OTI-SKO cells. Indeed, IL-12 stimulation *in vitro* resulted in lower level of phosphorylated STAT4 and S6 in OTI-SKO cells at 6dpi. OTI-SKO cells also showed reduced S6 phosphorylation directly *ex vivo* at 6dpi. These results suggest that Smad4 deletion results in weaker transduction of IL-12 signaling *in vitro* and *in vivo*. Additional qPCR and flow cytometry are needed to confirm decreased expression of the IL-12 receptor on SKO CTLs as compared to WT cells. Also, it remains unclear how Smad4 regulates IL-12 receptor expression. As *il12rb2* is known to be downregulated by TGFβ on CD4 T cells (171), it is possible that the unknown

‘Smad4 ligand‘ may induce *Il12rb2* transcription, while TGFβ suppresses transcription by competing away Smad4 with phosphorylated Smad2/3.

*Transcription factors are regulated by Smad4 and TGFβ*

IL-12 is known to promote terminal differentiation of $T_{EFF}$ cells by upregulating the transcription factor, T-bet (29). Despite of the accumulation of KLRG1+ $T_{EFF}$ cells in absence of TGFβRII, no difference in T-bet expression was observed between TKO and WT CTLs during the acute phase of CD8 T cell response. We will use qPCR and intracellular flow cytometry to further examine the expression levels of other important transcription factors known to promote KLRG1+ $T_{EFF}$ cell formation, including Blimp-1, Id2 and Zeb2 (134;135;138;172).

On the other hand, while OTI-SKO cells showed reduced responsiveness to IL-12 stimulation *in vitro*, we only found a small reduction of T-bet in SKO CTLs after IAV infection. Nevertheless, OTI-SKO cells expressed significantly reduced levels of T-bet from 2.5dpi with LM-OVA infection. This may reflect a difference in the inflammatory environment during the two types of infection. The literature shows that LM infection can generate high concentrations of IL-12 and large numbers of KLRG1+ $T_{EFF}$ cells (163), while relatively few KLRG1+ $T_{EFF}$ cells can be found during IAV infection. It is possible that IAV infection induces low amounts of IL-12, or the Smad4 ligand which may be required for IL-12 receptor expression, which leads to relatively low IL-12-induced T-bet expression in WT cells. It is possible that TCR signaling can compensate for reduced IL-12 signaling in SKO CTLs and induce T-bet expression to a similar level as the WT cells. Also, in our model high concentrations of TGFβ are activated by the IAV neuraminidase, which may reduce IL-12 receptor expression on the WT cells and therefore minimize the difference in T-bet expression between WT and SKO CTLs. We could test these possibilities *in vitro* by modulating the concentration of antigen, IL-12 and TGFβ. Nevertheless, considering the key role of T-bet in promoting KLRG1+ $T_{EFF}$ cell generation (29), decreased T-bet expression

may explain why SKO CTLs preferentially differentiated into memory precursors. To further prove this hypothesis, we will transduce OTI-SKO cells with a retrovirus expressing T-bet, and examine whether enforced expression of T-bet restores terminal differentiation in absence of Smad4.

Recent studies show that proper development of $T_{RM}$ cells in lungs and skin requires downregulation of T-bet and Eomes (146;161). TGFβ signaling, which is enhanced by such downregulation, can further suppress the expression of these two transcription factors (146). Consistently, we found that while T-bet expression was unaltered in $T_{EFF}$ cells until the peak of the response, memory CD8 T cells lacking TGFβRII retained a significantly higher level of T-bet than the WT counterpart. Also, a lack of TGFβ signal in these cells resulted in increased induction and maintenance of Eomes throughout the CD8 T cell response. As enforced expression of these two transcription factors abrogated formation of $T_{RM}$ cells in skin (146), high level of T-bet and Eomes maintained by TKO CTLs may lead to their deficiency in $T_{RM}$ cell development. This hypothesis can be tested by knocking down Eomes and T-bet in TKO CTLs with retroviruses expressing small interfering RNA (siRNA).

On the other hand, Eomes and T-bet were both expressed at lower levels in SKO CTLs. Though WT CTLs in the lungs expressing CD103 had lower Eomes and T-bet expression than the CD103- counterparts, both CD103+ and CD103- SKO CTLs expressed low levels of these two transcription factors. To answer the question whether Smad4 suppresses CD103 expression via these two transcription factors, using retrovirus expressing T-bet or Eomes, we will examine whether enforced expression of these two transcription factors can reverse the widespread expression of CD103 in lymphoid tissues in absence of Smad4. A recent study showed that T-bet can directly bind to the regulatory region of the CD103 gene (161). It would be interesting to examine whether Eomes also directly regulates CD103 expression. Also, it remained unclear as how Smad4 promotes Eomes expression. Eomes expression is known to be amplified by IL-2

(165), yet we did not observe difference in phosphorylated STAT5 after IL-2 stimulation *in vitro* in OTI-SKO cells at 6dpi.

As Eomes deficiency can diminish $T_{CM}$ cell population (147), enhanced Eomes expression in the OTI-TKO cells may also explain why higher frequencies of these cells expressed CD62L at memory phase in lymphoid organs, and were found at increased numbers than WT cells in resting lymph nodes at 30dpi by confocal microscopy. On the other hand, low level of Eomes in the SKO CTLs may render these cells unable to develop into CD62L+ $T_{CM}$ cells. Therefore, while Eomes did not control the differentiation of KLRG1+ and CD127+ effector subsets (147), altered expression of Eomes may be associated with the balance between CD103+ $T_{RM}$ and CD62L+ $T_{CM}$ cell development. It would be interesting to examine whether enforced expression of Eomes can rescue the impaired development of $T_{CM}$ cells among SKO cell population.

*Metabolic profiles of CTLs are altered by TGFβ and Smad4*

Enhanced glycolysis is generally associated with a higher proliferative capacity and terminal differentiation of $T_{EFF}$ cells (116;123). Nevertheless, here we did not observe a significant difference in the glycolytic stress test between TKO and WT early effector cells analyzed directly *ex vivo*. Nevertheless, TGFβRII deficiency resulted in decreased spare respiratory capacity (SRC), which is a unique property of memory CD8 T cells generated *in vitro* (123), and consistent with the fact that lower frequencies of memory precursors were observed among the TKO population. Moreover, the TKO $T_{EFF}$ cells that had acquired a CD127+ memory precursor phenotype seemed to be 'addicted' to glycolysis and deficient in conversation back to mitochondria respiration, as shown by enhanced glycolytic activity and reduced OXPHOS as compared to WT CTLs. We still need to consider the possibility that these cells may behave differently *in vivo* and the *in vitro* environment. Therefore sorted cells can be treated with TGFβ before the metabolic tests to determine whether the presence of TGFβ alters glycolysis or

OXPHOS activity. Also, previous studies with *in vitro* activated CD8 T cells showed that SRC is a unique feature of IL-15-derived memory CD8 T cells, while IL-2-derived effector CD8 T cells are highly glycolytic and do not maintain SRC (123;124). In our experiments $T_{EFF}$ cells isolated from recipient mice at different time points were all metabolically similar to *in vitro* memory CD8 T cells in the mito stress test (123;124). One possible explanation is that, compared to *in vivo* generated CTLs, CD8 T cells activated *in vitro* may receive much stronger signals from anti-CD3/CD28 antibodies and a high concentration of IL-2 in culture, which can be tested by a titration of these stimulations. Also, the concentrations of nutrients were much higher in cell culture media than *in vivo* settings. For example, the concentration of glucose used in these *in vitro* studies were 25 mM, while the level of glucose is around 5mM in lymphoid tissues, and the availability of nutrients may be further reduced at the infection site (114). Therefore *in vitro* generated $T_{EFF}$ cells may appear to be more glycolytic than the $T_{EFF}$ cells analyzed *ex vivo* in our study.

We did not observe any difference in mitochondrial fuel usage between the TKO and WT CTLs. In both types of cells, fatty acid oxidation supported OXPHOS at both basal and under stress condition. While OCR was not altered by BPTES-mediated glutominolysis inhibition, the influx of glucose-derived pyruvate into the TCA cycle was necessary to support maximal OCR and SRC. Consistently, recent studies have shown that memory CD8 T cells generated *in vitro* did not import exogenous fatty acids, but actively used extracellular glucose to synthesize lipids which fueled FAO through intrinsic lipolysis and maintained OXPHOS and SRC (124).

On the other hand, RNA-Seq revealed downregulation in transcription of c-Myc and its target gene AP4 in SKO early effector cells (EECs). In addition, a recent study suggests that Smad4 may promote cell proliferation by directly regulating c-Myc expression (148). Despite the key roles of c-Myc and AP4 in enhancing and maintaining glycolytic metabolism upon T cell activation, no difference in glycolytic activity was observed between SKO and WT EECs at

various time points. On the other hand, SKO EECs showed enhanced basal and maximal OCR at 3.5dpi, which may suggest enhanced mitochondria biogenesis in absence of Smad4. To test this hypothesis, cells could be stained with mitochondria-specific dyes to compare mitochondria mass and membrane potential by flow cytometry and confocal microscopy. The difference in OXPHOS was not observed between WT and SKO EECs at 6dpi. The absence of Smad4 also did not alter mitochondria fuel usage at this time point. Consistently, RNA-Seq did not reveal significant change in the expression levels of key genes involved in OXPHOS, such as carnitine palmitoyltransferase 1α (CPT1α) or mitochondrial transcription factor A (TFAM). At 8dpi, however, SKO EECs again showed higher OCR under stressed conditions, which may suggest faster conversion back to OXPHOS. These data suggests Smad4 deletion may influence the balance between OXPHOS and glycolysis at these metabolic switch points. Further studies are needed to examine whether the expression level or activity of key enzymes that are involved in OXPHOS and glycolysis are altered by the absence of Smad4 at these two time points.

In conclusion, in this thesis we have demonstrated the distinctive roles of TGFβ and its downstream molecule, Smad4, in effector and memory CD8 T cell differentiation after IAV infection (Figure 5-1). A novel pathway, which we believe is triggered by an unknown Smad4 ligand, can promote terminal differentiation and acquisition of the KLRG1+ phenotype. The mechanism may involve enhanced IL-12 signaling and T-bet expression, and possibly also inhibiting OXPHOS activity. Smad4-mediated generation of the KLRG1+ $T_{EFF}$ cell subset may promote viral clearance during primary infection, yet is not required for protection during the recall response. Our data suggest that Smad4 acts as a suppressor of CD103 during $T_{RM}$ cell development and promotes conversion of $T_{EFF}$ cells to CD62L+ $T_{CM}$ cells, through enhanced Eomes and T-bet expression. On the other hand, TGFβ, possibly by preventing Smad4 from activating its target genes with phosphorylated Smad2/3, inhibits KLRG1+ $T_{EFF}$ cell in favor of memory precursor formation, and may also promote a metabolic switch from glycolysis back to

mitochondria respiration. Also, by downregulating Eomes and T-bet TGFβ signal is essential for the generation/maintenance of pulmonary $T_{RM}$ cells, which play a key role in heterosubtypic immunity. These data provide a better understanding on the signaling pathways governing the generation of different subsets of antigen-specific CD8 T cells participating in cell-mediated immunity against IAVs, and may facilitate the development of IAV vaccine with long-lasting protection.

**Figure 5-1**

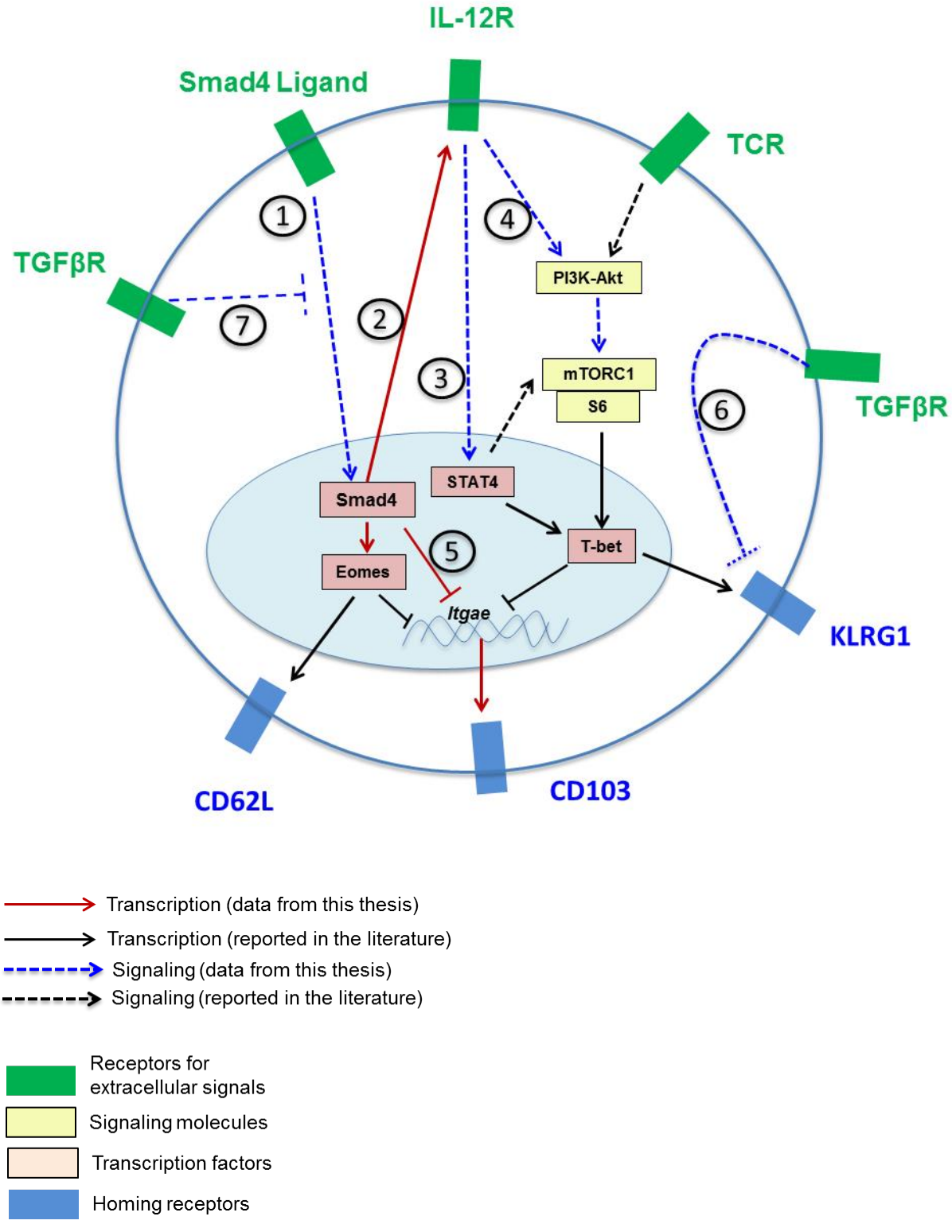
IL-12R
Smad4 Ligand
TCR
TGFβR
1
2
3
4
5
6
7
PI3K-Akt
mTORC1
S6
STAT4
Smad4
T-bet
Eomes
Itgae
TGFβR
KLRG1
CD62L
CD103
Transcription (data from this thesis)
Transcription (reported in the literature)
Signaling (data from this thesis)
Signaling (reported in the literature)
Receptors for extracellular signals
Signaling molecules
Transcription factors
Homing receptors

**Figure 5-1. Model summarizing the roles of TGFβ and Smad4 in effector and memory CD8 T cell differentiation**

**(1)** An unknown receptor uses a novel Smad4-dependent signaling pathway to promote CD8 T cell proliferation and $T_{EFF}$ differentiation. **(2)** The transcriptional targets of this signaling pathway include the IL-12 receptor, which can signal through **(3)** STAT4 or **(4)** the PI3K/Akt/mTOR pathway to promote T-bet expression during terminal differentiation of KLRG1+ $T_{EFF}$ cells. **(5)** Smad4 is a repressor of the *Itgae* gene (CD103) during development of $T_{RM}$ cells, and promotes re-expression of the sell gene (CD62L) on $T_{CM}$ cells by a mechanism that may involve Eomes. **(6)** TGFβ suppresses terminal differentiation of KLRG1+ $T_{EFF}$ cells and **(7)** promotes re-expression of CD103 on $T_{RM}$ cells by a mechanism may involve competition within the Smad signaling cascade.

Reference List


1. Molinari NA, Ortega-Sanchez IR, Messonnier ML, Thompson WW, Wortley PM, Weintraub E, Bridges CB. The annual impact of seasonal influenza in the US: Measuring disease burden and costs. Vaccine 2007 Jun 28;25(27):5086-96

2. Foppa IM, Cheng PY, Reynolds SB, Shay DK, Carias C, Bresee JS, Kim IK, Gambhir M, Fry AM. Deaths averted by influenza vaccination in the U.S. during the seasons 2005/06 through 2013/14. Vaccine 2015 Jun 12;33(26):3003-9

3. Gasparini R, Amicizia D, Lai PL, Panatto D. Clinical and socioeconomic impact of seasonal and pandemic influenza in adults and the elderly. Human Vaccines & Immunotherapeutics 2012 Jan 1;8(1):21-8

4. Neumann G, Noda T, Kawaoka Y. Emergence and pandemic potential of swine-origin H1N1 influenza virus. Nature 2009 Jun 18;459(7249):931-9

5. Simonsen L, Reichert TA, Viboud C, Blackwelder WC, Taylor RJ, Miller MA. IMpact of influenza vaccination on seasonal mortality in the us elderly population. Archives of Internal Medicine 2005 Feb 14;165(3):265-72

6. Kash JC, Taubenberger JK. Infectious Disease Theme Issue: The Role of Viral, Host, and Secondary Bacterial Factors in Influenza Pathogenesis. The American Journal of Pathology 2015 Jun;185(6):1528-36

7. Kuiken T, Taubenberger JK. Pathology of human influenza revisited. Vaccine 2008 Sep 12;26, Supplement 4:D59-D66

8. Kuiken T, Riteau B, Fouchier RAM, Rimmelzwaan GF. Pathogenesis of influenza virus infections: the good, the bad and the ugly. Current Opinion in Virology 2012 Jun;2(3):276-86

9. Marcelin G, Aldridge JR, Duan S, Ghoneim HE, Rehg J, Marjuki H, Boon ACM, McCullers JA, Webby RJ. Fatal Outcome of Pandemic H1N1 2009 Influenza Virus Infection Is Associated with Immunopathology and Impaired Lung Repair, Not Enhanced Viral Burden, in Pregnant Mice. Journal of Virology 2011 Nov 1;85(21):11208-19

10. Ballinger MN, Standiford TJ. Postinfluenza Bacterial Pneumonia: Host Defenses Gone Awry. Journal of Interferon & Cytokine Research 2010 Aug 20;30(9):643-52

11. Bouvier NM, Palese P. The Biology of Influenza Viruses. Vaccine 2008 Sep 12;26(Suppl 4):D49-D53

12. Subbarao K, Joseph T. Scientific barriers to developing vaccines against avian influenza viruses. Nat Rev Immunol 2007 Apr;7(4):267-78

13. Skehel JJ, Wiley DC. Receptor Binding and Membrane Fusion in Virus Entry: The Influenza Hemagglutinin: The Influenza Hemagglutinin. Annu.Rev.Biochem. 2000 Jun 1;69(1):531-69

14. Cross KJ, Burleigh LM, Steinhauer DA. Mechanisms of cell entry by influenza virus. Expert Reviews in Molecular Medicine 2001;3(21):1-18

15. Steinhauer DA. Role of Hemagglutinin Cleavage for the Pathogenicity of Influenza Virus. Virology 1999 May 25;258(1):1-20

16. Rossman JS, Lamb RA. Influenza virus assembly and budding. Virology 2011 Mar 15;411(2):229-36

17. Wagner R, Wolff T, Herwig A, Pleschka S, Klenk HD. Interdependence of Hemagglutinin Glycosylation and Neuraminidase as Regulators of Influenza Virus Growth: a Study by Reverse Genetics. J Virol 2000 Jul 15;74(14):6316-23

18. Cox RJ, Brokstad KA, Ogra P. Influenza Virus: Immunity and Vaccination Strategies. Comparison of the Immune Response to Inactivated and Live, Attenuated Influenza Vaccines. Scandinavian Journal of Immunology 2004 Jan 1;59(1):1-15

19. Tong S, Zhu X, Li Y, Shi M, Zhang J, Bourgeois M, Yang H, Chen X, Recuenco S, Gomez J, et al. New World Bats Harbor Diverse Influenza A Viruses. PLoS Pathog 2013 Oct 10;9(10):e1003657

20. Askonas BA, Taylor PM, Esquivel FERN. Cytotoxic T Cells in Influenza Infection. Annals of the New York Academy of Sciences 1988 Aug 1;532(1):230-7

21. Stanekova Z, Vareckova E. Conserved epitopes of influenza A virus inducing protective immunity and their prospects for universal vaccine development. Virol J 2010 Nov 30;7:351

22. Nguyen HH, Moldoveanu Z, Novak MJ, van Ginkel FW, Ban E, Kiyono H, McGhee JR, Mestecky J. Heterosubtypic Immunity to Lethal Influenza A Virus Infection Is Associated with Virus-Specific CD8+Cytotoxic T Lymphocyte Responses Induced in Mucosa-Associated Tissues. Virology 1999 Feb 1;254(1):50-60

23. Kreijtz JHCM, Bodewes R, van Amerongen G, Kuiken T, Fouchier RAM, Osterhaus ADME, Rimmelzwaan GF. Primary influenza A virus infection induces cross-protective immunity against a lethal infection with a heterosubtypic virus strain in mice. Vaccine 2007 Jan 8;25(4):612-20

24. Guermonprez P, Valladeau J, Zitvogel L, Thery C, Amigorena S. Antigen Presentation and T Cell Stimulation by Dendritic Cells. Annu.Rev.Immunol. 2002 Apr 1;20(1):621-67

25. Cui W, Kaech SM. Generation of effector CD8+ T cells and their conversion to memory T cells. Immunological Reviews 2010 Jul 1;236(1):151-66

26. Kaech SM, Wherry EJ. Heterogeneity and Cell-Fate Decisions in Effector and Memory CD8+ T Cell Differentiation during Viral Infection. Immunity 2007 Sep 21;27(3):393-405

27. Newell EW, Sigal N, Bendall SC, Nolan GP, Davis MM. Cytometry by Time-of-Flight Shows Combinatorial Cytokine Expression and Virus-Specific Cell Niches within a Continuum of CD8+ T Cell Phenotypes. Immunity 2012 Jan 27;36(1):142-52

28. Kaech SM, Tan JT, Wherry EJ, Konieczny BT, Surh CD, Ahmed R. Selective expression of the interleukin 7 receptor identifies effector CD8 T cells that give rise to long-lived memory cells. Nat Immunol 2003 Dec;4(12):1191-8

29. Joshi NS, Cui W, Chandele A, Lee HK, Urso DR, Hagman J, Gapin L, Kaech SM. Inflammation Directs Memory Precursor and Short-Lived Effector CD8+ T Cell Fates via the Graded Expression of T-bet Transcription Factor. Immunity 2007 Aug 24;27(2):281-95

30. Grandemann C, Schwartzkopff S, Koschella M, Schweier O, Peters C, Voehringer D, Pircher H. The NK receptor KLRG1 is dispensable for virus-induced NK and CD8+ T-cell differentiation and function in vivo. Eur.J.Immunol. 2010 May 1;40(5):1303-14

31. Hand TW, Cui W, Jung YW, Sefik E, Joshi NS, Chandele A, Liu Y, Kaech SM. Differential effects of STAT5 and PI3K/AKT signaling on effector and memory CD8 T-cell survival. Proceedings of the National Academy of Sciences 2010 Sep 21;107(38):16601-6

32. Gerlach C, van Heijst JWJ, Swart E, Sie D, Armstrong N, Kerkhoven RM, Zehn D, Bevan MJ, Schepers K, Schumacher TNM. One naive T cell, multiple fates in CD8+ T cell differentiation. The Journal of Experimental Medicine 2010 Jun 7;207(6):1235-46

33. Buchholz VR, Flossdorf M, Hensel I, Kretschmer L, Weissbrich B, Graf P, Verschoor A, Schiemann M, Hofer T, Busch DH. Disparate Individual Fates Compose Robust CD8+ T Cell Immunity. Science 2013 May 3;340(6132):630-5

34. Gerlach C, Rohr JC, Peria Ll, van Rooij N, van Heijst JWJ, Velds A, Urbanus J, Naik SH, Jacobs H, Beltman JB, et al. Heterogeneous Differentiation Patterns of Individual CD8+ T Cells. Science 2013 May 3;340(6132):635-9

35. Plumlee C, Sheridan BS, Cicek BB, Lefrancois L. Environmental Cues Dictate the Fate of Individual CD8+ T Cells Responding to Infection. Immunity 2013 Aug 22;39(2):347-56

36. Wherry EJ, Puorro KA, Porgador A, Eisenlohr LC. The Induction of Virus-Specific CTL as a Function of Increasing Epitope Expression: Responses Rise Steadily Until Excessively High Levels of Epitope Are Attained. The Journal of Immunology 1999 Oct 1;163(7):3735-45

37. Henrickson SE, Perro M, Loughhead SM, Senman B, Stutte S, Quigley M, Alexe G, Iannacone M, Flynn MP, Omid S, et al. Antigen Availability Determines CD8+ T Cell-Dendritic Cell Interaction Kinetics and Memory Fate Decisions. Immunity 2013 Sep 19;39(3):496-507

38. Badovinac VP, Haring JS, Harty JT. Initial T Cell Receptor Transgenic Cell Precursor Frequency Dictates Critical Aspects of the CD8+ T Cell Response to Infection. Immunity 2007 Jun 22;26(6):827-41

39. Obar JJ, Khanna KM, Lefrancois L. Endogenous Naive CD8+ T Cell Precursor Frequency Regulates Primary and Memory Responses to Infection. Immunity 2008 Jun 13;28(6):859-69

40. D'Souza WN, Hedrick SM. Cutting Edge: Latecomer CD8 T Cells Are Imprinted with a Unique Differentiation Program. The Journal of Immunology 2006 Jul 15;177(2):777-81

41. Sharpe AH. Mechanisms of Costimulation. Immunol Rev 2009 May;229(1):5-11

42. Chen L, Flies DB. Molecular mechanisms of T cell co-stimulation and co-inhibition. Nat Rev Immunol 2013 Apr;13(4):227-42

43. Williams MA, Bevan MJ. Effector and Memory CTL Differentiation. Annu.Rev.Immunol. 2007 Mar 21;25(1):171-92

44. Hendriks J, Xiao Y, Rossen JWA, van der Sluijs KF, Sugamura K, Ishii N, Borst J. During Viral Infection of the Respiratory Tract, CD27, 4-1BB, and OX40 Collectively Determine Formation of CD8+ Memory T Cells and Their Capacity for Secondary Expansion. The Journal of Immunology 2005 Aug 1;175(3):1665-76

45. Moraes TJ, Lin GHY, Wen T, Watts TH. Incorporation of 4-1BB ligand into an adenovirus vaccine vector increases the number of functional antigen-specific CD8 T cells and enhances the duration of protection against influenza-induced respiratory disease. Vaccine 2011 Aug 26;29(37):6301-12

46. Ballesteros-Tato A, Lean B, Lee BO, Lund FE, Randall TD. Epitope-Specific Regulation of Memory Programming by Differential Duration of Antigen Presentation to Influenza-Specific CD8+ T Cells. Immunity 2014 Jul 17;41(1):127-40

47. Haring JS, Badovinac VP, Harty JT. Inflaming the CD8+ T Cell Response. Immunity 2006 Jul;25(1):19-29

48. Morishima N, Owaki T, Asakawa M, Kamiya S, Mizuguchi J, Yoshimoto T. Augmentation of Effector CD8+ T Cell Generation with Enhanced Granzyme B Expression by IL-27. The Journal of Immunology 2005 Aug 1;175(3):1686-93

49. Ben-Sasson SZ, Hogg A, Hu-Li J, Wingfield P, Chen X, Crank M, Caucheteux S, Ratner-Hurevich M, Berzofsky JA, Nir-Paz R, et al. IL-1 enhances expansion, effector function, tissue localization, and memory response of antigen-specific CD8 T cells. The Journal of Experimental Medicine 2013 Mar 11;210(3):491-502

50. Kalia V, Sarkar S, Subramaniam S, Haining WN, Smith KA, Ahmed R. Prolonged Interleukin-2RÎ± Expression on Virus-Specific CD8+ T Cells Favors Terminal-Effector Differentiation In Vivo. Immunity 2010 Jan 29;32(1):91-103

51. Starbeck-Miller GR, Xue HH, Harty JT. IL-12 and type I interferon prolong the division of activated CD8 T cells by maintaining high-affinity IL-2 signaling in vivo. The Journal of Experimental Medicine 2014 Jan 13;211(1):105-20

52. Kurtulus S, Tripathi P, Moreno-Fernandez ME, Sholl A, Katz JD, Grimes HL, Hildeman DA. Bcl-2 Allows Effector and Memory CD8+ T Cells To Tolerate Higher Expression of Bim. The Journal of Immunology 2011 May 15;186(10):5729-37

53. Wensveen FM, Klarenbeek PL, van Gisbergen KPJM, Pascutti MF, Derks IAM, van Schaik BDC, ten Brinke A, de Vries N, Cekinovic D, Jonjic S, et al. Pro-Apoptotic

Protein Noxa Regulates Memory T Cell Population Size and Protects against Lethal Immunopathology. The Journal of Immunology 2013 Feb 1;190(3):1180-91

54. Harty JT, Badovinac VP. Shaping and reshaping CD8+ T-cell memory. Nat Rev Immunol 2008 Feb;8(2):107-19

55. Sallusto F, Lenig D, Forster R, Lipp M, Lanzavecchia A. Two subsets of memory T lymphocytes with distinct homing potentials and effector functions. Nature 1999 Oct 14;401(6754):708-12

56. Obar JJ, Lefrancois L. Early Signals during CD8+ T Cell Priming Regulate the Generation of Central Memory Cells. The Journal of Immunology 2010 Jul 1;185(1):263-72

57. Wherry EJ, Teichgraber V, Becker TC, Masopust D, Kaech SM, Antia R, von Andrian UH, Ahmed R. Lineage relationship and protective immunity of memory CD8 T cell subsets. Nat Immunol 2003 Mar;4(3):225-34

58. Graef P, Buchholz VR, Stemberger C, Flossdorf M, Henkel L, Schiemann M, Drexler I, Hofer T, Riddell SR, Busch DH. Serial Transfer of Single-Cell-Derived Immunocompetence Reveals Stemness of CD8+ Central Memory T Cells. Immunity 2014 Jul 17;41(1):116-26

59. Cauley LS, Lefrancois L. Guarding the perimeter: protection of the mucosa by tissue-resident memory T cells. Mucosal Immunol 2013 Jan;6(1):14-23

60. Schenkel JM, Masopust D. Tissue-Resident Memory T Cells. Immunity 2014 Dec 18;41(6):886-97

61. Wu T, Hu Y, Lee YT, Bouchard KR, Benechet A, Khanna K, Cauley LS. Lung-resident memory CD8 T cells ($T_{RM}$) are indispensable for optimal cross-protection against pulmonary virus infection. Journal of Leukocyte Biology 2014 Feb 1;95(2):215-24

62. Mackay LK, Rahimpour A, Ma JZ, Collins N, Stock AT, Hafon ML, Vega-Ramos J, Lauzurica P, Mueller SN, Stefanovic T, et al. The developmental pathway for CD103+CD8+ tissue-resident memory T cells of skin. Nat Immunol 2013 Dec;14(12):1294-301

63. Lee YT, Suarez-Ramirez JE, Wu T, Redman JM, Bouchard K, Hadley GA, Cauley LS. Environmental and Antigen Receptor-Derived Signals Support Sustained Surveillance of the Lungs by Pathogen-Specific Cytotoxic T Lymphocytes. Journal of Virology 2011 May 1;85(9):4085-94

64. Zhang N, Bevan MJ. Transforming Growth Factor-Î² Signaling Controls the Formation and Maintenance of Gut-Resident Memory T Cells by Regulating Migration and Retention. Immunity 2013 Oct 17;39(4):687-96

65. El-Asady R, Yuan R, Liu K, Wang D, Gress RE, Lucas PJ, Drachenberg CB, Hadley GA. TGF-β-dependent CD103 expression by CD8+ T cells promotes selective destruction of the host intestinal epithelium during graft-versus-host disease. The Journal of Experimental Medicine 2005 May 16;201(10):1647-57

66. Sheridan BS, Pham QM, Lee YT, Cauley LS, Puddington L, Lefrancois L. Oral Infection Drives a Distinct Population of Intestinal Resident Memory CD8+ T Cells with Enhanced Protective Function. Immunity 2014 May 15;40(5):747-57

67. Kim TS, Hufford MM, Sun J, Fu YX, Braciale TJ. Antigen persistence and the control of local T cell memory by migrant respiratory dendritic cells after acute virus infection. The Journal of Experimental Medicine 2010 Jun 7;207(6):1161-72

68. Mackay LK, Stock AT, Ma JZ, Jones CM, Kent SJ, Mueller SN, Heath WR, Carbone FR, Gebhardt T. Long-lived epithelial immunity by tissue-resident memory T (TRM) cells in the absence of persisting local antigen presentation. Proceedings of the National Academy of Sciences 2012 May 1;109(18):7037-42

69. Casey KA, Fraser KA, Schenkel JM, Moran A, Abt MC, Beura LK, Lucas PJ, Artis D, Wherry EJ, Hogquist K, et al. Antigen-Independent Differentiation and Maintenance of Effector-like Resident Memory T Cells in Tissues. The Journal of Immunology 2012 May 15;188(10):4866-75

70. Skon CN, Lee JY, Anderson KG, Masopust D, Hogquist KA, Jameson SC. Transcriptional downregulation of S1pr1 is required for the establishment of resident memory CD8+ T cells. Nat Immunol 2013 Dec;14(12):1285-93

71. Schenkel JM, Fraser KA, Vezys V, Masopust D. Sensing and alarm function of resident memory CD8+ T cells. Nat Immunol 2013 May;14(5):509-13

72. Ariotti S, Hogenbirk MA, Dijkgraaf FE, Visser LL, Hoekstra ME, Song JY, Jacobs H, Haanen JB, Schumacher TN. Skin-resident memory CD8+ T cells trigger a state of tissue-wide pathogen alert. Science 2014 Oct 3;346(6205):101-5

73. Schenkel JM, Fraser KA, Beura LK, Pauken KE, Vezys V, Masopust D. Resident memory CD8 T cells trigger protective innate and adaptive immune responses. Science 2014 Oct 3;346(6205):98-101

74. Wang Q, Strong J, Killeen N. Homeostatic Competition Among T Cells Revealed by Conditional Inactivation of the Mouse Cd4 Gene. The Journal of Experimental Medicine 2001 Dec 17;194(12):1721-30

75. Hogquist KA, Jameson SC, Heath WR, Howard JL, Bevan MJ, Carbone FR. T cell receptor antagonist peptides induce positive selection. Cell 1994;76(1):17-27

76. Li MO, Wan YY, Sanjabi S, Robertson AK, Flavell RA. Transforming Growth Factor-β Regulation of Immune Responses. Annu.Rev.Immunol. 2006 Mar 21;24(1):99-146

77. Taylor AW. Review of the activation of TGF-Î² in immunity. Journal of Leukocyte Biology 2009 Jan 1;85(1):29-33

78. Schultz-Cherry S, Hinshaw VS. Influenza virus neuraminidase activates latent transforming growth factor beta. Journal of Virology 1996 Dec 1;70(12):8624-9

79. Carlson CM, Turpin EA, Moser LA, O'Brien KB, Cline TD, Jones JC, Tumpey TM, Katz JM, Kelley LA, Gauldie J, et al. Transforming Growth Factor-β: Activation by

Neuraminidase and Role in Highly Pathogenic H5N1 Influenza Pathogenesis. PLoS Pathog 2010 Oct 7;6(10):e1001136

80. Li MO, Flavell RA. TGF-β: A Master of All T Cell Trades. Cell 2008 Aug 8;134(3):392-404

81. Park SR, Lee JH, Kim PH. Smad3 and Smad4 mediate transforming growth factor-β1-induced IgA expression in murine B lymphocytes. Eur.J.Immunol. 2001 Jun 1;31(6):1706-15

82. Ichiyama K, Sekiya T, Inoue N, Tamiya T, Kashiwagi I, Kimura A, Morita R, Muto G, Shichita T, Takahashi R, et al. Transcription Factor Smad-Independent T Helper 17 Cell Induction by Transforming-Growth Factor-β Is Mediated by Suppression of Eomesodermin. Immunity 2011 May 27;34(5):741-54

83. Chen W, Jin W, Hardegen N, Lei Kj, Li L, Marinos N, McGrady G, Wahl SM. Conversion of Peripheral CD4+CD25- Naive T Cells to CD4+CD25+ Regulatory T Cells by TGF-β Induction of Transcription Factor Foxp3. The Journal of Experimental Medicine 2003 Dec 15;198(12):1875-86

84. Li MO, Sanjabi S, Flavell RA. Transforming Growth Factor-β Controls Development, Homeostasis, and Tolerance of T Cells by Regulatory T Cell-Dependent and -Independent Mechanisms. Immunity 2006 Sep;25(3):455-71

85. Zhang N, Bevan MJ. TGF-β signaling to T cells inhibits autoimmunity during lymphopenia-driven proliferation. Nat Immunol 2012 Jul;13(7):667-73

86. Sanjabi S, Mosaheb MM, Flavell RA. Opposing Effects of TGF-β and IL-15 Cytokines Control the Number of Short-Lived Effector CD8+ T Cells. Immunity 2009 Jul 17;31(1):131-44

87. Derynck R, Zhang YE. Smad-dependent and Smad-independent pathways in TGF-β family signalling. Nature 2003 Oct 9;425(6958):577-84

88. Shi Y, Massague J. Mechanisms of TGF-β Signaling from Cell Membrane to the Nucleus. Cell 2003 Jun 13;113(6):685-700

89. Massague J, Seoane J, Wotton D. Smad transcription factors. Genes & Development 2005 Dec 1;19(23):2783-810

90. Fink SP, Mikkola D, Willson JKV, Markowitz S. TGF-[beta]-induced nuclear localization of Smad2 and Smad3 in Smad4 null cancer cell lines. Oncogene 0 AD;22(9):1317-23

91. He W, Dorn DC, Erdjument-Bromage H, Tempst P, Moore MAS, Massaguq J. Hematopoiesis Controlled by Distinct TIF1γ and Smad4 Branches of the TGFβ Pathway. Cell 125(5):929-941. 2006.

92. Doisne JM, Bartholin L, Yan KP, Garcia ClN, Duarte N, Le Luduec JBt, Vincent D, Cyprian F, Horvat B, Martel S, et al. iNKT cell development is orchestrated by different branches of TGF-β signaling. The Journal of Experimental Medicine 2009 Jun 8;206(6):1365-78

93. Dupont S, Mamidi A, Cordenonsi M, Montagner M, Zacchigna L, Adorno M, Martello G, Stinchfield MJ, Soligo S, Morsut L, et al. FAM/USP9x, a Deubiquitinating Enzyme Essential for TGFÎ² Signaling, Controls Smad4 Monoubiquitination. Cell 2009 Jan 9;136(1):123-35

94. Zhang YE. Non-Smad pathways in TGF-β signaling. Cell Res 2009 Jan;19(1):128-39

95. Gui T, Sun Y, Shimokado A, Muragaki Y. The Roles of Mitogen-Activated Protein Kinase Pathways in TGF-β-Induced Epithelial-Mesenchymal Transition. J Signal Transduct 2012 Jan 29;2012:289243

96. Lee MK, Pardoux C, Hall MC, Lee PS, Warburton D, Qing J, Smith SM, Derynck R. TGF-β activates Erk MAP kinase signalling through direct phosphorylation of ShcA. EMBO J 2007 Sep 5;26(17):3957-67

97. Sorrentino A, Thakur N, Grimsby S, Marcusson A, von Bulow V, Schuster N, Zhang S, Heldin CH, Landstrom M. The type I TGF-β receptor engages TRAF6 to activate TAK1 in a receptor kinase-independent manner. Nat Cell Biol 2008 Oct;10(10):1199-207

98. Yamashita M, Fatyol K, Jin C, Wang X, Liu Z, Zhang YE. TRAF6 Mediates Smad-Independent Activation of JNK and p38 by TGF-β. Molecular Cell 2008 Sep 26;31(6):918-24

99. Yi JY, Shin I, Arteaga CL. Type I Transforming Growth Factor β Receptor Binds to and Activates Phosphatidylinositol 3-Kinase. Journal of Biological Chemistry 2005 Mar 18;280(11):10870-6

100. Lamouille S, Derynck R. Cell size and invasion in TGF-β-induced epithelial to mesenchymal transition is regulated by activation of the mTOR pathway. The Journal of Cell Biology 2007 Jul 30;178(3):437-51

101. Zhang L, Zhou F, ten Dijke P. Signaling interplay between transforming growth factor-β receptor and PI3K/AKT pathways in cancer. Trends in Biochemical Sciences 2013 Dec;38(12):612-20

102. Edlund S, Landstrom Mn, Heldin CH, Aspenstrom P. Transforming Growth Factor-β induced Mobilization of Actin Cytoskeleton Requires Signaling by Small GTPases Cdc42 and RhoA. Mol Biol Cell 2002 Mar 9;13(3):902-14

103. Hu Y, Lee YT, Kaech SM, Garvy B, Cauley LS. Smad4 Promotes Differentiation of Effector and Circulating Memory CD8 T Cells but Is Dispensable for Tissue-Resident Memory CD8 T Cells. The Journal of Immunology 2015 Mar 1;194(5):2407-14

104. Ely KH, Cookenham T, Roberts AD, Woodland DL. Memory T Cell Populations in the Lung Airways Are Maintained by Continual Recruitment. The Journal of Immunology 2006 Jan 1;176(1):537-43

105. Anderson KG, Sung H, Skon CN, Lefrancois L, Deisinger A, Vezys V, Masopust D. Cutting Edge: Intravascular Staining Redefines Lung CD8 T Cell Responses. The Journal of Immunology 2012 Sep 15;189(6):2702-6

106. Knudson CJ, Weiss KA, Hartwig SM, Varga SM. The Pulmonary Localization of Virus-Specific T Lymphocytes Is Governed by the Tissue Tropism of Infection. Journal of Virology 2014 Aug 15;88(16):9010-6

107. Kim BG, Li C, Qiao W, Mamura M, Kasperczak B, Anver M, Wolfraim L, Hong S, Mushinski E, Potter M, et al. Smad4 signalling in T cells is required for suppression of gastrointestinal cancer. Nature 2006 Jun 22;441(7096):1015-9

108. Kunkel EJ, Ramos CL, Steeber DA, Maller W, Wagner N, Tedder TF, Ley K. The Roles of L-Selectin, β7 Integrins, and P-Selectin in Leukocyte Rolling and Adhesion in High Endothelial Venules of Peyer's Patches. The Journal of Immunology 1998 Sep 1;161(5):2449-56

109. Gu AD, Wang Y, Lin L, Zhang SS, Wan YY. Requirements of transcription factor Smad-dependent and -independent TGF-β signaling to control discrete T-cell functions. Proceedings of the National Academy of Sciences 2012 Jan 17;109(3):905-10

110. Moustakas A, Souchelnytskyi S, Heldin CH. Smad regulation in TGF-β signal transduction. Journal of Cell Science 2001 Dec 15;114(24):4359-69

111. Miller DS, Kok T, Li P. The virus inoculum volume influences outcome of influenza A infection in mice. Laboratory Animals 2013 Jan 1;47(1):74-7

112. Kaech SM, Cui W. Transcriptional control of effector and memory CD8+ T cell differentiation. Nat Rev Immunol 2012 Nov;12(11):749-61

113. Wang R, Green DR. Metabolic checkpoints in activated T cells. Nat Immunol 2012 Oct;13(10):907-15

114. Pearce EL, Poffenberger MC, Chang CH, Jones RG. Fueling Immunity: Insights into Metabolism and Lymphocyte Function. Science 2013 Oct 11;342(6155)

115. Pearce EL, Pearce EJ. Metabolic Pathways in Immune Cell Activation and Quiescence. Immunity 2013 Apr 18;38(4):633-43

116. Wang R, Dillon CP, Shi LZ, Milasta S, Carter R, Finkelstein D, McCormick LL, Fitzgerald P, Chi H, Munger J, et al. The Transcription Factor Myc Controls Metabolic Reprogramming upon T Lymphocyte Activation. Immunity 2011 Dec 23;35(6):871-82

117. Chang CH, Curtis JD, Maggi J, Faubert B, Villarino AV, O'Sullivan D, Huang SCC, van der Windt GJ, Blagih J, Qiu J, et al. Posttranscriptional Control of T Cell Effector Function by Aerobic Glycolysis. Cell 2013 Jun 6;153(6):1239-51

118. Bauer DE, Hatzivassiliou G, Zhao F, Andreadis C, Thompson CB. ATP citrate lyase is an important component of cell growth and transformation. Oncogene 2005 Jun 13;24(41):6314-22

119. DeBerardinis RJ, Lum JJ, Hatzivassiliou G, Thompson CB. The Biology of Cancer: Metabolic Reprogramming Fuels Cell Growth and Proliferation. Cell Metabolism 2008 Jan;7(1):11-20

120. Blagih J, Coulombe Fo, Vincent EE, Dupuy F, Galicia-Vazquez G, Yurchenko E, Raissi TC, van der Windt GJ, Viollet B, Pearce EL, et al. The Energy Sensor AMPK Regulates T Cell Metabolic Adaptation and Effector Responses InÂ Vivo. Immunity 2015 Jan 20;42(1):41-54

121. Ganeshan K, Chawla A. Metabolic Regulation of Immune Responses. Annu.Rev.Immunol. 2014 Mar 21;32(1):609-34

122. Buck MD, O'Sullivan D, Pearce EL. T cell metabolism drives immunity. The Journal of Experimental Medicine 2015 Aug 24;212(9):1345-60

123. van der Windt GJ, Everts B, Chang CH, Curtis JD, Freitas TC, Amiel E, Pearce EJ, Pearce EL. Mitochondrial Respiratory Capacity Is a Critical Regulator of CD8+ T Cell Memory Development. Immunity 2012 Jan 27;36(1):68-78

124. O'Sullivan D, van der Windt GJ, Huang SCC, Curtis JD, Chang CH, Buck MD, Qiu J, Smith AM, Lam WY, DiPlato LM, et al. Memory CD8+ T Cells Use Cell-Intrinsic Lipolysis to Support the Metabolic Programming Necessary for Development. Immunity 2014 Jul 17;41(1):75-88

125. Cui G, Staron MM, Gray SM, Ho PC, Amezquita RA, Wu J, Kaech SM. IL-7-Induced Glycerol Transport and TAG Synthesis Promotes Memory CD8+ T Cell Longevity. Cell 2015 May 7;161(4):750-61

126. Pollizzi KN, Powell JD. Integrating canonical and metabolic signalling programmes in the regulation of T cell responses. Nat Rev Immunol 2014 Jul;14(7):435-46

127. Finlay DK, Rosenzweig E, Sinclair LV, Feijoo-Carnero C, Hukelmann JL, Rolf J, Panteleyev AA, Okkenhaug K, Cantrell DA. PDK1 regulation of mTOR and hypoxia-inducible factor 1 integrate metabolism and migration of CD8+ T cells. The Journal of Experimental Medicine 2012 Dec 17;209(13):2441-53

128. Araki K, Turner AP, Shaffer VO, Gangappa S, Keller SA, Bachmann MF, Larsen CP, Ahmed R. mTOR regulates memory CD8 T-cell differentiation. Nature 2009 Jul 2;460(7251):108-12

129. Pearce EL, Walsh MC, Cejas PJ, Harms GM, Shen H, Wang LS, Jones RG, Choi Y. Enhancing CD8 T-cell memory by modulating fatty acid metabolism. Nature 2009 Jul 2;460(7251):103-7

130. Shrestha S, Yang K, Wei J, Karmaus PWF, Neale G, Chi H. Tsc1 promotes the differentiation of memory CD8+ T cells via orchestrating the transcriptional and metabolic programs. Proceedings of the National Academy of Sciences 2014 Oct 14;111(41):14858-63

131. MacIver NJ, Blagih J, Saucillo DC, Tonelli L, Griss T, Rathmell JC, Jones RG. The Liver Kinase B1 Is a Central Regulator of T Cell Development, Activation, and Metabolism. The Journal of Immunology 2011 Oct 15;187(8):4187-98

132. Rolf J, Zarrouk M, Finlay DK, Foretz M, Viollet B, Cantrell DA. AMPKα1: A glucose sensor that controls CD8 T-cell memory. Eur.J.Immunol. 2013 Apr 1;43(4):889-96

133. Chang JT, Wherry EJ, Goldrath AW. Molecular regulation of effector and memory T cell differentiation. Nat Immunol 2014 Dec;15(12):1104-15

134. Dominguez CX, Amezquita RA, Guan T, Marshall HD, Joshi NS, Kleinstein SH, Kaech SM. The transcription factors ZEB2 and T-bet cooperate to program cytotoxic T cell terminal differentiation in response to LCMV viral infection. The Journal of Experimental Medicine 2015 Nov 16;212(12):2041-56

135. Omilusik KD, Best JA, Yu B, Goossens S, Weidemann A, Nguyen JV, Seuntjens E, Stryjewska A, Zweier C, Roychoudhuri R, et al. Transcriptional repressor ZEB2 promotes terminal differentiation of CD8+ effector and memory T cell populations during infection. The Journal of Experimental Medicine 2015 Nov 16;212(12):2027-39

136. Intlekofer AM, Takemoto N, Wherry EJ, Longworth SA, Northrup JT, Palanivel VR, Mullen AC, Gasink CR, Kaech SM, Miller JD, et al. Effector and memory CD8+ T cell fate coupled by T-bet and eomesodermin. Nat Immunol 2005 Dec;6(12):1236-44

137. Kallies A, Xin A, Belz GT, Nutt SL. Blimp-1 Transcription Factor Is Required for the Differentiation of Effector CD8+ T Cells and Memory Responses. Immunity 2009 Aug 21;31(2):283-95

138. Rutishauser RL, Martins GiA, Kalachikov S, Chandele A, Parish IA, Meffre E, Jacob J, Calame K, Kaech SM. Transcriptional Repressor Blimp-1 Promotes CD8+ T Cell Terminal Differentiation and Represses the Acquisition of Central Memory T Cell Properties. Immunity 2009 Aug 21;31(2):296-308

139. Ji Y, Pos Z, Rao M, Klebanoff CA, Yu Z, Sukumar M, Reger RN, Palmer DC, Borman ZA, Muranski P, et al. Repression of the DNA-binding inhibitor Id3 by Blimp-1 limits the formation of memory CD8+ T cells. Nat Immunol 2011 Dec;12(12):1230-7

140. Li Q, Eppolito C, Odunsi K, Shrikant PA. IL-12-Programmed Long-Term CD8+ T Cell Responses Require STAT4. The Journal of Immunology 2006 Dec 1;177(11):7618-25

141. Cui W, Liu Y, Weinstein JS, Craft J, Kaech SM. An Interleukin-21- Interleukin-10-STAT3 Pathway Is Critical for Functional Maturation of Memory CD8+ T Cells. Immunity 2011 Nov 23;35(5):792-805

142. Best JA, Blair DA, Knell J, Yang E, Mayya V, Doedens A, Dustin ML, Goldrath AW. Transcriptional insights into the CD8+ T cell response to infection and memory T cell formation. Nat Immunol 2013 Apr;14(4):404-12

143. Arsenio J, Kakaradov B, Metz PJ, Kim SH, Yeo GW, Chang JT. Early specification of CD8+ T lymphocyte fates during adaptive immunity revealed by single-cell gene-expression analyses. Nat Immunol 2014 Apr;15(4):365-72

144. Ballesteros-Tato A, Lean B, Lund FE, Randall TD. CD4+ T helper cells use CD154-CD40 interactions to counteract T reg cell-mediated suppression of CD8+ T cell responses to influenza. The Journal of Experimental Medicine 2013 Jul 29;210(8):1591-601

145. Wong KL, Lew FC, MacAry PA, Kemeny DM. CD40L-expressing CD8 T cells prime CD8α+ DC for IL-12p70 production. Eur.J.Immunol. 2008 Aug 1;38(8):2251-62

146. Mackay LK, Wynne-Jones E, Freestone D, Pellicci DG, Mielke LA, Newman DM, Braun A, Masson F, Kallies A, Belz GT, et al. T-box Transcription Factors Combine with the Cytokines TGF-β and IL-15 to Control Tissue-Resident Memory T Cell Fate. Immunity 2015 Dec 15;43(6):1101-11

147. Banerjee A, Gordon SM, Intlekofer AM, Paley MA, Mooney EC, Lindsten T, Wherry EJ, Reiner SL. Cutting Edge: The Transcription Factor Eomesodermin Enables CD8+ T Cells To Compete for the Memory Cell Niche. The Journal of Immunology 2010 Nov 1;185(9):4988-92

148. Gu AD, Zhang S, Wang Y, Xiong H, Curtis TA, Wan YY. A Critical Role for Transcription Factor Smad4 in T Cell Function that Is Independent of Transforming Growth Factor β Receptor Signaling. Immunity 2015 Jan 20;42(1):68-79

149. Chou C, Pinto AK, Curtis JD, Persaud SP, Cella M, Lin CC, Edelson BT, Allen PM, Colonna M, Pearce EL, et al. c-Myc-induced transcription factor AP4 is required for host protection mediated by CD8+ T cells. Nat Immunol 2014 Sep;15(9):884-93

150. Je-Min C, and Alfred LMB. The Nuclear Receptor PPARs as Important Regulators of T-Cell Functions and Autoimmune Diseases. Mol.Cells 2012 Mar;33(3):217-22

151. Bensinger SJ, Bradley MN, Joseph SB, Zelcer N, Janssen EM, Hausner MA, Shih R, Parks JS, Edwards PA, Jamieson BD, et al. LXR Signaling Couples Sterol Metabolism to Proliferation in the Acquired Immune Response. Cell 2008 Jul 11;134(1):97-111

152. Gerriets VA, Kishton RJ, Nichols AG, Macintyre AN, Inoue M, Ilkayeva O, Winter PS, Liu X, Priyadharshini B, Slawinska ME, et al. Metabolic programming and PDHK1 control CD4+ T cell subsets and inflammation. J Clin Invest125(1):194-207

153. Ferrick DA, Neilson A, Beeson C. Advances in measuring cellular bioenergetics using extracellular flux. Drug Discovery Today 2008 Mar;13(56):268-74

154. Nicholls DG. Spare respiratory capacity, oxidative stress and excitotoxicity. Biochemical Society Transactions 2009 Dec 1;37(6):1385-8

155. Lopaschuk GD, Wall SR, Olley PM, Davies NJ. Etomoxir, a carnitine palmitoyltransferase I inhibitor, protects hearts from fatty acid-induced ischemic injury independent of changes in long chain acylcarnitine. Circulation Research 1988 Dec 1;63(6):1036-43

156. Robinson MM, Mcbryant SJ, Tsukamoto T, Rojas C, Ferraris DV, Hamilton SK, Hansen JC, Curthoys NP. Novel mechanism of inhibition of rat kidney-type glutaminase by bis-2-(5-phenylacetamido-1,2,4-thiadiazol-2-yl)ethyl sulfide (BPTES). Biochemical Journal 2007 Sep 15;406(3):407-14

157. Brailsford MA, Thompson AG, Kaderbhai N, Beechey RB. Pyruvate metabolism in castor-bean mitochondria. Biochemical Journal 1986 Oct 15;239(2):355-61

158. Rao RR, Li Q, Odunsi K, Shrikant PA. The mTOR Kinase Determines Effector versus Memory CD8+ T Cell Fate by Regulating the Expression of Transcription Factors T-bet and Eomesodermin. Immunity 2010 Jan 29;32(1):67-78

159. Rao RR, Li Q, Bupp MR, Shrikant PA. Transcription Factor Foxo1 Represses T-bet-Mediated Effector Functions and Promotes Memory CD8+ T Cell Differentiation. Immunity 2012 Mar 23;36(3):374-87

160. Hay N, Sonenberg N. Upstream and downstream of mTOR. Genes & Development 2004 Aug 15;18(16):1926-45

161. Laidlaw BJ, Zhang N, Marshall HD, Staron MM, Guan T, Hu Y, Cauley LS, Craft J, Kaech SM. CD4+ T Cell Help Guides Formation of CD103+ Lung-Resident Memory CD8+ T Cells during Influenza Viral Infection. Immunity 2014 Oct 16;41(4):633-45

162. Vignali DAA, Kuchroo VK. IL-12 family cytokines: immunological playmakers. Nat Immunol 2012 Aug;13(8):722-8

163. Plumlee C, Obar JJ, Colpitts SL, Jellison ER, Haining WN, Lefrancois L, Khanna KM. Early Effector CD8 T Cells Display Plasticity in Populating the Short-Lived Effector and Memory-Precursor Pools Following Bacterial or Viral Infection. Scientific Reports 2015 Jul 20;5:12264

164. Cruz-Guilloty F, Pipkin ME, Djuretic IM, Levanon D, Lotem J, Lichtenheld MG, Groner Y, Rao A. Runx3 and T-box proteins cooperate to establish the transcriptional program of effector CTLs. The Journal of Experimental Medicine 2009 Jan 16;206(1):51-9

165. Grange M, Verdeil Gg, Arnoux F, Griffon Al, Spicuglia S, Maurizio J, Buferne M, Schmitt-Verhulst AM, Auphan-Anezin N. Active STAT5 Regulates T-bet and Eomesodermin Expression in CD8 T Cells and Imprints a T-bet-Dependent Tc1 Program with Repressed IL-6/TGF-β1 Signaling. The Journal of Immunology 2013 Oct 1;191(7):3712-24

166. Ye F, Turner J, FlaÃ±o E. Contribution of Pulmonary KLRG1high and KLRG1low CD8 T Cells to Effector and Memory Responses during Influenza Virus Infection. The Journal of Immunology 2012 Dec 1;189(11):5206-11

167. Graham MB, Dalton DK, Giltinan D, Braciale VL, Stewart TA, Braciale TJ. Response to influenza infection in mice with a targeted disruption in the interferon gamma gene. The Journal of Experimental Medicine 1993 Nov 1;178(5):1725-32

168. Xu L, Yoon H, Zhao MQ, Liu J, Ramana CV, Enelow RI. Cutting Edge: Pulmonary Immunopathology Mediated by Antigen-Specific Expression of TNF-α by Antiviral CD8+ T Cells. The Journal of Immunology 2004 Jul 15;173(2):721-5

169. von Andrian UH, Mempel TR. Homing and cellular traffic in lymph nodes. Nat Rev Immunol 2003 Nov;3(11):867-78

170. Ma C, Zhang N. Transforming growth factor-β signaling is constantly shaping memory T-cell population. Proceedings of the National Academy of Sciences 2015 Sep 1;112(35):11013-7

171. Gorham JD, Guler ML, Fenoglio D, Gubler U, Murphy KM. Low Dose TGF-β Attenuates IL-12 Responsiveness in Murine Th Cells. The Journal of Immunology 1998 Aug 15;161(4):1664-70

172. Yang CY, Best JA, Knell J, Yang E, Sheridan AD, Jesionek AK, Li HS, Rivera RR, Lind KC, D'Cruz LM, et al. The transcriptional regulators Id2 and Id3 control the formation of distinct memory CD8+ T cell subsets. Nat Immunol 2011 Dec;12(12):1221-9